Effect of Substitution on Electronic Structure, Magnetic and Mechanical Properties of Ni, Pt and Mn-based Heusler Alloys

By

Tufan Roy

(PHYS03201204009)

Raja Ramanna Centre for Advanced Technology, Indore

A thesis submitted to the

Board of Studies in Physical Sciences

In partial fulfillment of requirements

For the Degree of

DOCTOR OF PHILOSOPHY

of

HOMI BHABHA NATIONAL INSTITUTE

August, 2017

Homi Bhabha National Institute[1]

Recommendations of the Viva Voce Committee

As members of the Viva Voce Committee, we certify that we have read the dissertation prepared by Tufan Roy entitled "Effect of substitution on Electronic Structure, Magnetic and Mechanical Properties of Ni, Pt and Mn-based Heusler Alloys" and recommend that it may be accepted as fulfilling the thesis requirement for the award of Degree of Doctor of Philosophy.

Chairman - Prof. Arup Banerjee Arup Banerjee	**Date:** 05/01/2018
Guide / Convener - Prof. Aparna Chakrabarti Aparna Chakrabarti	**Date:** 5.1.2018
Examiner - Prof. Priya Mahadevan Priya Mahadevan	**Date:** 5 Jan 2018
Member 1- Prof. Vinit Kumar Vinit Kumar	**Date:** 5.1.18
Member 2- Prof. M. P. Singh Manraj	**Date:** 5-1-18
Member 3- Prof. H. Ghosh Haranath Ghosh	**Date:** 05.01.18
Member 4- Prof. Satya Bulusu B.S.S	**Date:**
Member 5- Prof. Ashok Arya Ashok	**Date:** 05/01/2018

Final approval and acceptance of this thesis is contingent upon the candidate's submission of the final copies of the thesis to HBNI.

I/We hereby certify that I/we have read this thesis prepared under my/our direction and recommend that it may be accepted as fulfilling the thesis requirement.

Date: 5.1.2018

Place: RRCAT

Aparna Chakrabarti
Prof. Aparna Chakrabarti

STATEMENT BY AUTHOR

This dissertation has been submitted in partial fulfilment of requirements for an advanced degree at Homi Bhabha National Institute (HBNI) and is deposited in the Library to be made available to borrowers under rules of the HBNI.

Brief quotations from this dissertation are allowable without special permission, provided that accurate acknowledgement of source is made. Requests for permission for extended quotation from or reproduction of this manuscript in whole or in part may be granted by the Competent Authority of HBNI when in his or her judgement the proposed use of the material is in the interests of scholarship. In all other instances, however, permission must be obtained from the author.

Tufan Roy

DECLARATION

I, hereby declare that the investigation presented in the thesis has been carried out by me. The work is original and has not been submitted earlier as a whole or in part for a degree/diploma at this or any other Institution/University.

Tufan Roy

List of Publications

In Journals (Included in the thesis)

1. *Ab initio* studies of effect of copper substitution on the electronic and magnetic properties of Ni_2MnGa and Mn_2NiGa
   Aparna Chakrabarti, Mario Siewert, **Tufan Roy**, Krishnakanta Mondal, Arup Banerjee, Markus E. Gruner, Peter Entel
   *Physical Review B, **88**, 174416 (2013)*

2. Effect of substitution on elastic stability, electronic structure and magnetic property of Ni-Mn based Heusler alloys: An *ab initio* comparison
   Tufan Roy, Markus E. Gruner, Peter Entel, Aparna Chakrabarti
   *Journal of Alloys and Compounds, **632**, 822 (2015)*

3. Possibility of martensite transition in Pt-Y-Ga (Y=Cr, Mn, and Fe) system: An *ab-initio* calculation of the bulk mechanical, electronic and magnetic properties
   Tufan Roy, Aparna Chakrabarti
   *Journal of Magnetism and Magnetic Materials, **401**, 929 (2016)*

4. Probing the possibility of coexistence of martensite transition and half-metallicity in Ni and Co-based full-Heusler alloys: An *ab initio* calculation
   Tufan Roy, Dhanshree Pandey, Aparna Chakrabarti
   *Physical Review B, **93**, 184102 (2016)*

5. *Ab initio* studies on electronic, magnetic and mechanical properties of X_2PtGa (X=Cr, Mn, Fe, Co) Heusler Alloys
   Tufan Roy, Aparna Chakrabarti
   *Journal of Magnetism and Magnetic Materials, **423**, 395 (2017)*

6. *Ab initio* study of effect of Co substitution on the magnetic properties of Ni and Pt-based Heusler Alloys
   Tufan Roy, Aparna Chakrabarti
   *Physics Letter A, **381**, 1449 (2017)*

7. Magnetic interactions and electronic structure of $Pt_2Mn_{1-x}Y_xGa$ (Y = Cr and Fe) system : An *ab-initio* calculation
   Tufan Roy, Aparna Chakrabarti
   *Pramana - Journal of Physics, **89**, 6 (2017)*

In Conferences

8. Study of effect of copper-substitution at Ga site in some Ga-based Heusler alloys from first-principles calculations
   Tufan Roy, Aparna Chakrabarti
   DAE-SSPS-2014, VIT, Vellore, December, 2014
   *AIP Conference Proceedings, **1665**, 090036 (2015)*

9. Study of effect of copper-substitution on bulk mechanical, electronic and magnetic properties in some Ga-based Heusler alloys from first-principles calculations
   Tufan Roy, Aparna Chakrabarti
   CTCMP 2015, National Institute of Science Education and Research (NISER), Bhubaneswar, February, 2015

10. The effect of Cu-substitution at Mn site on mechanical stability, electronic structure and magnetic properties of Ni_2MnGa, Pd_2MnGa and Pt_2MnGa
    Tufan Roy, Aparna Chakrabarti
    ICC-2015, Rajasthan University of Veterinary and Animal Sciences, Bikaner, October, 2015

11. $(Ni,Pt)_2CrGa$: Anti-ferromagnetic shape memory alloys?
    Tufan Roy, Aparna Chakrabarti
    International Conference on Ferromagnetic Shape Memory Alloys (ICFSMA16), Sendai, JAPAN, September, 2016

12. *Ab initio* study of effect of Co substitution on the magnetic properties of Ni_2MnGa
    Tufan Roy, Aparna Chakrabarti
    DAE-SSPS-2016, KIIT, Bhubaneswar, December, 2016

Not included in the thesis

In Journals

1. Magnetic properties and electronic structure of Mn-Ni-Ga magnetic shape memory alloys
   Sunil Wilfred D'Souza, **Tufan Roy**, Sudipta Roy Barman, Aparna Chakrabarti
   *Journal of Physics: Condensed Matter, **26**, 506001 (2014)*

2. Temperature dependent EXAFS study of chromium-doped GaFeO3 at gallium and iron Edges
   S. Basu, Ripandeep Singh, A. Das, **Tufan Roy**, A. Chakrabarti, A. K. Nigam, S. N. Jha, D. Bhattacharyya
   *Journal of Physical Chemistry (C), **119**, 2029 (2015)*

In Conferences

3. Study of structural, magnetic and electronic properties of Ni-Fe-Ga based ferromagnetic shape memory alloys
   Madhusmita Baral, **Tufan Roy**, Balaji Mondal, Aparna Chakrabarti, Tapas Ganguli
   DAE-SSPS-2016, KIIT, Bhubaneswar, December, 2016
   *AIP Conference Proceedings, **1832**, 090039 (2017)*

ACKNOWLEDGEMENT

First and foremost, I would like to thank my supervisor, Prof. Aparna Chakrabarti, for her constant help, encouragement and patience throughout all the stages of my PhD programme. During the course of my PhD work, her precious suggestions and constructive criticisms have helped me a lot to communicate the scientific results in an efficient manner. I would also like to take the opportunity to express my sincere gratitude to Prof. Chakrabarti for her very much caring attitude towards me and providing a homely environment here. I feel extremely lucky to have her as my thesis supervisor.

I would like to express my sincere thanks to Dr. C. Kamal for his continuous support and encouragement. He has helped me a lot in the improvement of my concept in basic physics. I discussed with him any problem, professional as well as personal, any time, without any hesitation.

I thank Prof. Arup Banerjee for fruitful discussions, which helped me a lot in the understanding of density functional theory. He gave some valuable suggestions about my work. I would like to extend my sincere thanks to Prof. S. R. Barman for his valuable suggestions and time given to read some of the manuscripts critically, which are included in this thesis.

I thank Prof. S. B. Roy for his valuable suggestions and critical comments. Prof. A. Arya is thanked his constructive suggestions on the structure of the thesis. Prof. S. K. Deb, Prof. G. S. Lodha and Prof. P. A. Naik are thanked for their constant support and encouragement. I thank Prof. Tapas Ganguli for his time for fruitful discussions. I am also thankful to Prof. S. R. Mishra, Prof. T. K. Sharma, Prof. Vinit Kumar, Prof. Anand Moorti, Prof. M. P. Singh, Prof. Satya Bulusu, Prof. Haranath Ghosh for their valuable suggestions. I thank Prof. Tapan K. Ghanty for his time for discussions. Mr. P. Thander is thanked for all the help during installation and running of the codes used in my PhD work and computer centre RRCAT, is thanked for providing computational facility. I thank all my collaborators during my PhD tenure. Director, RRCAT, all the members of ISUD, HRDS are thanked for their constant support and encouragement.

I thank Dr. Krishnakanta Mondal and Dr. Sunil Wifred D'Souza. They helped me to understand the nitty-gritty of the first principles calculation. Dr Sanjay Singh is thanked

for his fruitful suggestions.

I express my sincere gratitude to Prof. Abhijit Chakraborty, of Burdwan University for his motivating words.

I would like to mention some of the my friends who always stood beside me in the different stages of my academic life: Mr. Gangadhar Das, Ms. Riya Kesh, Mr. Satyajit Samanta, Mr. Arijit Chakraborty, Mr. Supriya Ghosh, Mr. Manas Garai, Mr. Satyajit Chowdhury, Mr. Chiranjit Ghosh, and Mr. Arun Baidya. During the last five years, I met Dhanshree, Sahadeb, Abyay, Madhusmita di, Smritijit, Paresh, Debashis, Srinivasarao, Sudheer, Aditya, Mangalika, Preeti, Priyabrata, Azam, Gopal Bhaiya, Paromita di. I enjoyed the friendship with them and thank all of them.

Finally, I express my deepest gratitude to my parents, Mrs. Ira Roy and Mr. Uday Sankar Roy, for their endless sacrifice, support and love. I also thank my maternal uncles, and cousins (Mr. Tarun Roy, Mr. Amiya Kesh, Ms. Riya Roy) for always being there for me.

Tufan Roy

Contents

SYNOPSIS

During the last few decades, study on full Heusler alloys (commonly with the stoichiometry A_2BC; where A and B are typically transition metal (TM) elements with d electrons, whereas in general, C is an element with s, p electrons) has drawn considerable attention of the researchers because of their very interesting properties, both from the application and the fundamental points of view. Some of the full Heusler alloys (FHAs) are well known as shape memory alloys (SMA). Upon cooling, SMAs tend to undergo a structural transition from a high temperature cubic phase to a low temperature phase with a lower symmetry, while the volume remains conserved.[1,2] This structural transition is named as martensite transition, and the temperature at which the transition takes place is known as the martensite transition temperature (T_M). The FHAs, which are known to undergo martensite transition, may find their application as various devices, such as, actuator, antenna etc. This group of FHAs are generally found to be metallic in nature, i.e. there is significant density of states (DOS) at the Fermi level (E_F) for both the spin channels. On the other hand, in 1983 de Groot et. al.[3], have mentioned about another class of Heusler alloys, which are half metallic in nature, with a much reduced DOS in case of one of the spin channels. These alloys may have potential application as a spin-injector material.

Among the SMAs, magnetic shape memory alloys (MSMAs) are of special interest because in this case the process of actuation, driven by magnetic field, becomes much faster than the conventional one (actuation driven by temperature). For room temperature application of magnetic FHAs as a device, it is necessary that both the ferromagnetic transition temperature (T_C) and T_M should be above the room temperature. As the shape of the materials used for devices has to change depending on the external perturbation in terms of heat or magnetic field, for a device application, it is also desired that the material is ductile enough such that it can regain its shape every time the perturbation is removed. It has been observed in the literature that we can tune T_C, T_M and the inherent crystalline brittleness (ICB) by changing

the composition of the alloy.[2,4–9] Hence, extensive studies are going on in searching for novel magnetic Heusler alloys with desirable mechanical, magnetic and electronic properties.

The elastic properties are among the most important physical properties related to the structure of materials. In crystalline materials, a high value of ratio of shear modulus (G) and bulk modulus (B) gives a fairly good phenomenological indication of the inherent crystalline brittleness of the material.[10] Further, the value of tetragonal shear constant of the cubic phase of a Heusler alloy can be correlated with the possibility of the martensite transition.[11] Depending on their chemical composition, the FHAs are shown to possess long-range ferromagnetic, ferrimagnetic and anti-ferromagnetic configuration, some of these are even found to carry no net magnetic moment. So, it is of immense interest to have an in-depth understanding of the magnetic interactions present in these systems. It is found that, in most of the FHAs, represented as A_2BC, primarily B is the moment carrying atom. There is the presence of a delocalized-like common d-band formed by the d-electrons of the A and B atoms, both of which are typically first-row transition metal atoms as well as carry magnetic moments.[12] Additionally, there is also an indirect RKKY-type exchange interaction[13] between the d-electrons of B atoms, which is typically mediated by the s, p electrons of the C atom. Hence, the C atom also plays an important role in defining the magnetic properties of these materials.[12,14] The electronic structure of FHAs has been seen to vary from semiconducting to half-metallic to metallic. The hybridization between different atoms plays an important role in deciding the electronic structure of the FHAs. Additionally, the value of T_M depends critically on the hybridization between the atoms and in turn, on, the electronic structure of the material. Ni_2MnGa and Mn_2NiGa are two prototype and most well known magnetic FHAs studied in the literature. In the ground state, Ni_2MnGa is known to possess the conventional Heusler alloy structure and it is ferromagnetic in nature. On the other hand, Mn_2NiGa possesses inverse Heusler alloy structure and its ground state magnetic configuration is ferrimagnetic. Despite the differences in their crystal structures and magnetic properties, both the alloys show the tendency to undergo martensite transition. In this thesis, in search of

novel magnetic Heusler alloys, we discuss the effects of substitution on mechanical, magnetic and electronic properties of Ni_2MnGa and Mn_2NiGa. We also study in detail, the magnetic and electronic aspects associated with the martensite transition of various Heusler alloy materials to probe when a FHA may show a tendency towards tetragonal distortion and when it does not.

In **Chapter 1**, we discuss the structure, properties and some possible applications of a few well-known full Heusler alloys. It is then followed by a brief introduction to the computational method employed in the electronic structure calculations based on density functional theory.

Ni_2MnGa is a prototype ferromagnetic Heusler alloy which undergoes martensite transition at 202 K[15] which is below the room temperature. We already discussed above about the dependence of physical parameters like T_M , T_C, inherent crystalline brittleness (ICB) and the magnetic properties on the chemical composition of a particular Heusler alloy. An increase of T_M have been observed as a result of Cu substitution at the Mn site and Pt substitution at Ni site of Ni_2MnGa.[5, 9,16] Both Cu and Pt are highly ductile material in their bulk form. Further, Pt and Pd are isoelectronic with Ni while Cu has one electron more compared to Ni. Hence, a comparative study is expected to yield interesting results if we substitute Ni with Pt, Pd and Cu in case of Ni_2MnGa. The existence of a modulated structure is known to be a prerequisite for a large MFIS on applying a small magnetic field. We note that a maximum magnetic field induced strain of 14% has been reported for $Ni_{1.75}Pt_{0.25}MnGa$ in the literature.[16] Further, based on a neutron diffraction study, Singh *et. al.*[17] have reported the existence of a modulated structure in Pt doped Ni_2MnGa. In the first part of **Chapter 2**, we discuss the effects of Cu substitution on the two prototype Heusler alloys namely, Ni_2MnGa and Mn_2NiGa. We study the changes in the structural, electronic as well as magnetic properties of these two systems with Cu substitution of 0%, 25%, 75% and 100% (in most cases) at the Mn, Ga as well as Ni sites of both the materials. We note that some of these compositions with Cu at Ga and Mn sites have been experimentally found to be stable.[5,9,18–21] It is observed that, except for one, all the compositions studied by us are stable in terms of the formation energy. A new material among these ones, namely, Ni_2MnCu shows a promise of exhibiting

magnetic shape memory effect. We find that partial and complete substitution of Mn by Cu lead to compounds, which are more stable than compounds in which Cu replaces Ni or Ga. Ga substitution by Cu is predicted to cause a large change in martensite transition temperature. Our study underlines that in spite of the different crystal and magnetic structure of Ni_2MnGa and Mn_2NiGa, the physics of martensite transformation as a result of Cu substitution at Ga, Mn, and Ni sites in these two materials is the same in these two systems.

In the second part of **Chapter 2**, we discuss the results of our calculated bulk mechanical as well as electronic and magnetic properties of Ni_2MnGa substituted by copper (Cu), platinum (Pt), palladium (Pd) and manganese (Mn) at the Ni site. It is observed that the tetragonal shear constant, C', has values close to zero or negative for all the compounds studied here, which indicates that, for all these materials, the cubic austenite phase might be prone to an elastic instability and hence, these materials are likely to undergo martensite transition. S. F. Pugh in 1954[10] conjectured that, the elastic property of a material is related to the ratio of the shear modulus (G) and bulk modulus (B) of that material. In his work, a high value of G/B has been associated with the inherent brittleness of a crystalline material. Based on the relative values of G/B and Cauchy pressure (C^p), we predict that Ni_2MnGa is expected to be inherently less brittle than Mn_2NiGa, however, Pt_2MnGa is the least brittle one among the three. From the analysis of our results of total and partial DOS of the materials, we observe that the hybridization between the *4p* orbitals of Ga and outermost *d* orbitals of the *A* atom plays a crucial role in the electronic stabilization of the material as observed in the literature.[22,23] We also study the Heisenberg exchange coupling parameters and calculate the Curie temperature using a mean field approximation, and we show the effects of substitution on the magnetic properties of these materials.

We mentioned above that, there is another group of FHAs which is found to be half metallic in nature.[3] Generally, many of the Co-based Heusler alloys exhibit this behavior [24,25]. On the contrary, Co_2NbSn and Co_2NiGa are found to exhibit SMA property and these are found to be metallic in nature.[26–28] Currently, Co_2NiGa and related alloys have gained

interest among the researchers, as they show SMA property and possess different crystal structure (inverse Heusler alloy structure), compared to the other Co-based materials, which are known to possess half metallicity and conventional Heusler alloy structure in their ground state.[27,28] In Chapter 2, we showed that, the substitution of Ni by Pt in case of Ni_2MnGa reduces the ICB as well as makes the tetragonal state more stable compared to the cubic phase. Furthermore, Siewert et. al. have observed an enhancement of T_C in case of Co doping in the Pt based systems.[16] Additionally, number of valence electrons has been shown to play an important role in determining the properties of these alloy systems.[8] So, studying the literature, we can expect that, the effect of replacement of Ni by Pt on various physical properties of Co_2NiGa may turn out to be interesting both from fundamental as well as application points of view. In **Chapter 3**, therefore, we discuss the changes in the magnetic, electronic as well as mechanical properties of A_2PtGa alloy, where *A* atom and consequently, the number of valence electrons are varied. Here, *A* atom has been taken to be a first row transition metal atom (*A* being Cr, Mn, Fe, Co). By comparing the energies of various types of magnetic configurations, we predict that Cr_2PtGa and Mn_2PtGa possess a ferrimagnetic configuration, whereas, Fe_2PtGa and Co_2PtGa possess a long-range ferromagnetic ordering in their respective ground states. By analysing the results of our calculated electronic, magnetic and mechanical properties of all these materials, Co_2PtGa, Cr_2PtGa and Fe_2PtGa are found to be three new FHA systems, which are likely to show the martensite transition. Among these material, Co_2PtGa is likely to possess the highest spin polarization at the E_F for both the cubic and tetragonal phases. It also exhibits the lowest inherent crystalline brittleness as well as the highest martensite transition temperature (T_M), melting temperature (Θ_m) and Curie temperature (T_C) - all the three values are found to be well above the room temperature, rendering Co_2PtGa interesting from application point of view.

Heusler alloy systems are well known to show different types of magnetism based on their chemical composition. In this regard, Fe and Cr substitution at the Mn site of Ni_2MnGa and Pt_2MnGa may lead to interesting magnetic properties as both Fe and Cr have high atomic

moments which are close to Mn. We note that, in bulk, Fe exhibits ferromagnetic (FM) configuration. On the other hand, both Cr and Mn atoms in their bulk form have anti-ferromagnetic in the ground state. Additionally, Cr possesses only one electron less than that of Mn. All these facts may have some interesting role to play in defining the magnetic as well as mechanical and electronic properties of the substituted materials. In **Chapter 4**, we therefore, discuss the effects of Fe and Cr substitution at the Mn site on magnetic, mechanical and electronic properties of Ni_2MnGa and Pt_2MnGa. We predict, on the basis of formation energy, that, all the substituted $A_2Mn_{1-x}B_xGa$ alloys (x = 0.00, 0.25, 0.75, 1.00; A = Ni, Pt; B = Fe, Cr) are stable materials. Further, all the substituted materials which we have studied here are likely to undergo martensite transition. We have probed how the stability of the austenite and martensite phase varies with the extent of substitution by Fe as well as Cr atoms at the Mn site. Further, we also study the bulk mechanical properties of the austenite and martensite phases of the systems. We predict that the Pt-based systems are inherently much less brittle in comparison to the Ni-based systems studied here. To predict the ground state magnetic configuration for all the systems studied here, we probe various possibilities of the magnetic configuration for these systems. Interestingly, contrary to the unsubstituted case as well as the case when Mn is substituted by Fe, the substitution of Mn by Cr leads to lowering of energy in case of an *intra-sublattice* anti-ferromagnetic configuration compared to the ferromagnetic configuration.

Both the existing literature and our work show that one group of the FHAs is likely to show SMA property and is generally metallic in nature whereas another group of FHAs possess high spin polarization at E_F and is not typically prone to a tetragonal transition on cooling. From both the points of view of fundamental understanding as well as technological application, it can be interesting to probe the similarities and differences in magnetic, bulk mechanical, and electronic properties of these two categories of materials. It will also be interesting to see if there is any FHA which has a tendency to undergo a tetragonal transition and at the same time possesses a high spin polarization at the E_F. Keeping these in mind, in **Chapter 5**, we probe

the bulk mechanical, magnetic and electronic properties of a series of Ni and Co-based FHAs, namely, Ni_2BC and Co_2BC (B = Sc, Ti, V, Cr and Mn as well as Y, Zr, Nb, Mo and Tc; C = Ga and Sn) materials. The choice of these two systems (Ni and Co-based FHAs) depended on the following facts. It has been observed that, typically, a large amount of work on the FHAs are on the Ni and Co-based compounds. It is also seen in the literature that, while quite a few of the Ni-based FHAs tend to undergo martensite transition, many of the Co-based FHAs exhibit a large spin-polarization at the E_F. So one of the interests here is to study if there is a possibility of coexistence of a tetragonal transition and a high spin polarization at the E_F.

Among the two categories of FHAs mentioned above, we find that the values of tetragonal shear constant show a consistent trend: a high positive value for materials which are not prone to a tetragonal transition and a low or negative value for the others. Further, we observe that the Ni-based materials are typically metallic in nature. However, all the Co-based alloys exhibit a significant spin polarization at the E_F (~66 to 100%). Most of the Ni-based materials have a *3d* band of the minority spin of the *A* atom close to and below the E_F . On the other hand, the peak position of the same band is above the E_F for the Co-based materials. We observe that, in both the cases of Ni and Co-based materials, these *3d* levels of electrons with minority spin play an important role in deciding the ground state. The relationship between the closeness of the peak corresponding to the e_g levels of the *3d* down spin electrons of the *A* atom to the E_F and the tendency of lowering of energy upon tetragonal distortion is found to be consistent across all the Ni and Co-based materials. Further, a rigid band model, along with the hybridization between different near-neighbor atoms, supports the results of partial and total magnetic moments of these systems. It is found that out of the four materials among the forty materials studied here, which exhibit a martensite phase as their ground state, three of these, namely, Ni_2MnGa, Ni_2MoGa and Co_2NbSn possess a truly metallic nature; on the contrary, Co_2MoGa exhibits a high spin polarization (~ 86%) at the Fermi level.

In **Chapter 6**, we present the results of detailed magnetic properties of a few series of materials, namely $A_{2-x}B_xXC$ (A = Ni or Pt; B = Co; X = Mn, Fe; C = Ga, Sn; x=0.00, 0.25, 0.50, 0.75, 1.25, 1.50, 1.75, 2.00), where the material, at one end (with x = 0.00) shows a SMA property, but at the other end (with x = 2.00) does not. In this chapter, we have carried out, in detail, the study on the evolution of the RKKY interaction for the materials, namely, $Ni_{2-x}Co_xMnGa$, $Ni_{2-x}Co_xFeGa$, $Pt_{2-x}Co_xMnGa$, $Pt_{2-x}Co_xMnSn$ as a function of x. Our results suggest that there is a decrease in strength of the RKKY interaction as we increase the Co substitution at the Ni or Pt site. It indicates that a dominant role is played by the A atom's d-electron in the formation of coupling between the localized-like moments of B atom in the A_2BC systems studied here. We also report the dependence of the strength of the RKKY interaction on the magnetic moment B atom. Our study signifies the implicit and important presence of RKKY interaction in the magnetic FHAs which show martensite transition.

Finally, all the above-mentioned work carried out in this thesis, has been summarized in **Chapter 7** and conclusions have been drawn. This is then followed by a brief discussion on the possible future work.

References

[1] Godlevsky, V. V.; Rabe, K. M. *Phys. Rev. B* **2001,** 63, 134407.

[2] Barman, S. R.; Chakrabarti, A.; Singh, S.; Banik, S.; Bhardwaj, S.; Paulose, P. L.; Chalke, B. A.; Panda, A. K.; Mitra, A.; Awasthi, A. M. *Phys. Rev. B* **2008,** 78, 134406.

[3] de Groot, R. A.; Mueller, F. M.; Engen, P. G. v.; Buschow, K. H. J. *Phys. Rev. Lett.* **1983,** 50, 2024.

[4] Chakrabarti, A.; Biswas, C.; Banik, S.; Dhaka, R. S.; Shukla, A. K.; Barman, S. R. *Phys. Rev. B* **2005,** 72, 073103.

[5] Kataoka, M.; Endo, K.; Kudo, N.; Kanomata, T.; Nishihara, H.; Shishido, T.; Umetsu, R. Y.; Nagasako, M.; Kainuma, R. *Phys. Rev. B* **2010,** 82, 214423.

[6] Khan, M.; Dubenko, I.; Stadler, S.; Ali, N. *J. Phys.: Condens. Matter* **2004**, 16, 5259.

[7] Khan, M.; Gautam, B.; Pathak, A.; Dubenko, I.; Stadler, S.; Ali, N. *J. Phys.: Condens. Matter* **2008,** 20, 505206.

[8] Li, C.-M.; Luo, H.-B.; Hu, Q.-M.; Yang, R.; Johansson, B.; Vitos, L. *Phys. Rev. B* **2011,** 84, 024206.

[9] Roy, S.; Blackburn, E.; Valvidares, S. M.; Fitzsimmons, M. R.; Vogel, S. C.; Khan, M.; Dubenko, I.; Stadler, S.; Ali, N.; Sinha, S. K.; Kortright, J. B. *Phys. Rev. B* **2009,** 79, 235127.

[10] Pugh, S. *Philos. Mag.* **1954,** 45, 823.

[11] Worgull, J.; Petti, E.; Trivisonno, J. *Phys. Rev. B* **1996,** 54, 15695.

[12]Kubler, J.; William, A. R.; Sommers, C. B. *Phys. Rev. B* **1983,** 28, 1745.

[13] Ruderman, M. A.; Kittel, C. *Phys. Rev.* **1954,** 96, 99.

[14] Sasioglu, E.; Sandratskii, L. M.; Bruno, P. *Phys. Rev. B* **2008,** 77, 064417.

[15] Ullakko, K.; Huang, J. K.; Kantner, C.; OHandley, R. C.; Kokorin, V. V. *Appl. Phys. Lett.* **1996,** 69, 1966.

[16] Siewert, M.; Gruner, M. E.; Dannenberg, A.; Chakrabarti, A.; Herper, H. C.; Wuttig, M.; Barman, S. R.; Singh, S.; Al-Zubi, A.; Hickel, T.; Neugebauer, J.; Gillessen, M.; Dronskowski, R.; Entel, P. *Appl. Phys. Lett.* **2011,** 99, 191904.

[17] Singh, S.; Ziebeck, K. R. A.; Suard, E.; Rajput, P.; Bhardwaj, S.; Awasthi, A. M.; Barman, S. R. *Appl. Phys. Lett.* **2012,** 101, 171904.

[18] Gautam, B. R.; Dubenko, I.; Mabon, J. C.; Stadler, S.; Ali, N. *J. Alloys Compd.* **2009,** 472, 35.

[19] Jiang, C.; Wang, J.; Li, P.; Jia, A.; Xu, H. *Appl. Phys. Lett.* **2009,** 95, 012501.

[20] Wang, J.; Bai, H.; Jiang, C.; Li, Y.; Xu, H. *Mater. Sci. Eng. A* **2010,** 527, 1975.

[21] Wang, J.; Jiang, C. *Scr. Mater.* **2010,** 62, 298.

[22] Li, C.-M.; Luo, H.-B.; Hu, Q.-M.; Yang, R.; Johansson, B.; Vitos, L. *Phys. Rev. B* **2010,** 82, 024201.

[23] Zayak, A. T.; Entel, P.; Rabe, K. M.; Adeagbo, W. A.; Acet, M. *Phys. Rev. B* **2005,** 72, 054113.

[24] Kandpal, H. C.; Fecher, G. H.; Felser, C. *J. Phys. D: Appl. Phys.* **2007,** 40, 1507.

[25] Kubler, J.; Fecher, G. H.; Felser, C. *Phys. Rev. B* **2007,** 76, 024414.

[26] Fujii, S.; Ishida, S.; Asano, S. *J. Phys. Soc. Jpn*. **1989,** 58, 3657.

[27] Siewert, M.; Gruner, M. E.; Dannenberg, A.; Hucht, A.; Shapiro, S. M.; Xu, G.; Schlagel, D. L.; Lograsso, T. A.; Entel, P. *Phys. Rev. B* **2010,** 82, 064420.

[28] Arryave, R.; Junkaew, A.; Chivukula, A.; Bajaj, S.; Yao, C.-Y.; Garay, A. *Acta Mater.* **2010,** 58, 5220.

List of Figures

Chapter 1

Introduction

1.1 Introduction

Heusler alloy was discovered more than 100 years back (in 1903) by a German scientist, Friedrich Heusler. The first discovered Heusler alloy is a Cu-Mn-Al system. The interesting fact about this Cu-Mn-Al system is that, although, none of its constituent atoms are ferromagnetic in bulk form, the resulting material exhibits ferromagnetic configuration.

Two types of Heusler alloy systems are discussed in the literature: (a) Full Heusler alloy, with a general formula A_2BC and (b) Half Heusler alloy, with a general formula ABC; where A and B are generally elements with d electrons and C is an element with s, p electrons. Some of the full Heusler alloys (FHAs) are known as shape memory alloys (SMA).[1, 2] Upon cooling, SMAs tend to undergo a structural transition from a high temperature cubic phase to a low temperature phase with a lower symmetry. This structural transition is named as martensite transition, and the temperature at which the transition takes place is known as the martensite transition temperature (T_M). The FHAs, which are known to undergo martensite transition, may find their application as various devices, such as, actuator, antenna etc. This group of FHAs are generally found to be metallic in nature, i.e. there is significant density of states (DOS) at the Fermi level (E_F) for both the spin channels. On the other hand, in 1983, de Groot et. al.[3] have predicted about another class of full Heusler alloys, which are shown to be half metallic in nature, with a much reduced DOS in case of one of the spin channels. These alloys may have a potential application as a spin-injector material.

1.1.1 Shape memory effect

Some systems are shown to recover their shape after a plastic deformation, this property of remembering their initial shape is termed as shape memory effect (SME). Alloys, exhibiting shape memory property, are termed as shape memory alloys. For showing SME, it is necessary that the material undergoes martensite transition, which is a displacive, diffusionless, volume conserving, first order structural transition. Because of the cooperative movement of the atoms relative to each other, martensite transition is often termed as a military transformation. Though, it involves very small displacement of the atoms but macroscopically the change in shape is quite large because of the transition. In conventional shape memory effect, upon cooling, there is a martensite transition from the high temperature phase to a low temperature, lower symmetry phase, below the martensite transition temperature. Now, in order to minimise the stress produced because of this structural transition, there will be a formation of twinning over the whole sample(Figure 1.1). These structural domains (variants) are separated by twin boundaries.

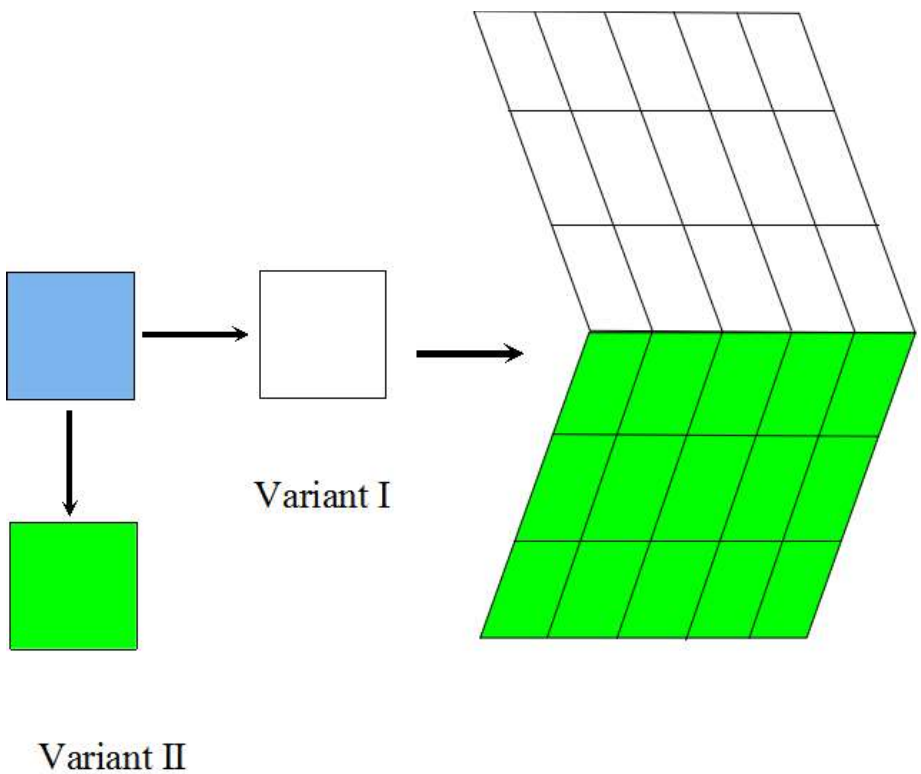

Figure 1.1: Schematic diagram of martensite transition and twin formation

The twin boundaries are mobile in nature. Due to the easy movement of the twin

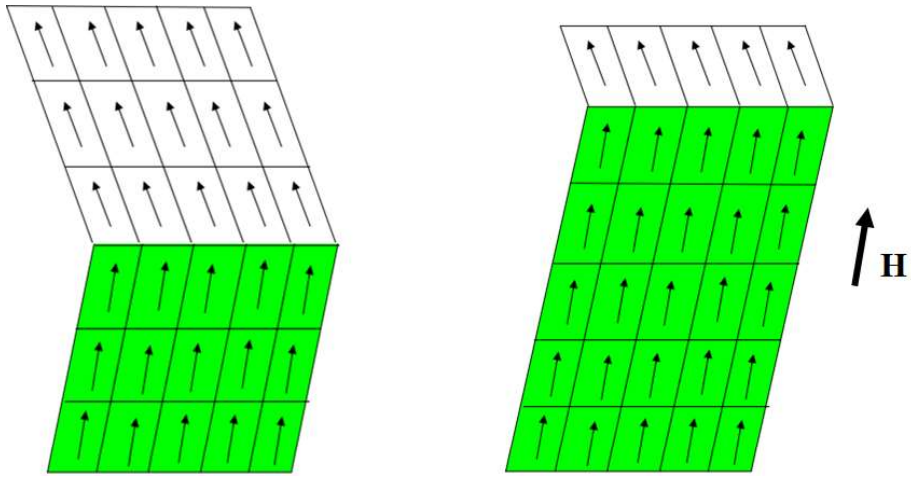

Figure 1.2: Orientation of magnetic moments (a) in absence of magnetic field, (b) in presence of magnetic field (H)

boundaries, the shape of the materials can be easily deformed by means of lowering down the temperature or applying mechanical stress on the system, if the material is in its martensite phase. Now, if we heat the sample, and the temperature reaches above the martensite transition temperature it will regain its initial high symmetry phase (austenite phase). This is the conventional shape memory effect. In case of conventional SME, the shape of the material is controlled by temperature, which makes the process of actuation slow, especially, when we need to cool the sample. This difficulty can be overcome by introduction of magnetic shape memory alloys (MSMA). In this case, shape of the SMA is deformed, *i.e.* a strain is developed by applying an external magnetic field and this strain is known as magnetic field induced strain (MFIS).

For a ferromagnet, below Curie temperature, there is a spontaneous magnetization in the absence of an external magnetic field, with the magnetic moments aligned along their easy axis. For a ferromagnetic SMA, at a temperature, below T_M and T_C ($T_C > T_M$), the twinning will be formed. In a twinned micro-structure the lattice variants will orient themselves in different directions. Consequently, the magnetic moments will also be aligned in different directions, depending on the direction of the easy axis of the respective variants. On the application of magnetic field, the moments will try to align themselves along the applied field. If the magnetic anistropy energy is high enough, such that the rotation of the magnetic moments away from the direction of the easy axis costs higher energy compared to the energy required to rotate the twin itself, then the size of

the variants, for which easy axis is along the direction of magnetic field will grow at the cost of the size of other variants. This will cause a change in the shape of the FSMA (Figure 1.2).

1.1.2 Crystal structure of Heusler alloys

FHAs in the cubic phase, crystallize in two types of crystal structures, namely, conventional and inverse Heusler alloy structures. In case of stoichiometric FHA (A_2BC), there are four face-centered-cubic (fcc) sublattices centered at (0.25, 0.25, 0.25), (0.75, 0.75, 0.75), (0.50, 0.50, 0.50), (0.00, 0.00, 0.00), which we label as P, Q, R and S sublattices, respectively. For conventional Heusler alloy structure (with a formula A_2BC), the A atoms occupy the P and Q sublattices, the B atom occupies the R sublattice and S sublattice contains the C atom. This structure shows a Fm$\bar{3}$m (number 225) space group. On the other hand, in case of inverse Heusler alloy structure (with a formula $ABAC$), A atom occupies the P and R sublattices and they are termed as $A2$ and $A1$, respectively, B and C atoms occupy the Q and S sublattices, respectively. This structure assumes a F$\bar{4}$3m (number 216) space group. For the martensite phase, we consider the tetragonal distortion of the cubic phase. Some Heusler alloys including Ni_2MnGa and Mn_2NiGa may show complicated modulated structures.[4–6] Due to the lack of knowledge about a suitable starting structure with a well-defined modulated orthorhombic distortion for the substituted systems studied in this thesis, we consider a tetragonal distortion of the cubic austenite phase as a first approximation of the structure of the martensite phase.

For both the types of Heusler alloy structure, conventional and inverse as well, the structure of the non modulated martensite phase are considered as body centred tetragonal. For conventional Heusler alloy structure the space group of the tetragonal phase is I4/mmm (number 139), whereas for inverse Heusler alloy structure the space group of the tetragonal phase is I$\bar{4}$m2 (number 119).

In this thesis, there are several cases, where we have carried out the calculations for substitution with different percentages (0%, 25%, 75% and 100%) at different sites of the studied FHA systems. To incorporate the substitution of percentages 25% and 75% we have carried out the calculation with sixteen atoms unit cell with P1 symmetry (no

symmetry at all) for both the cubic and tetragonal phases.

1.2 Objectives of the Present Thesis

In the family of the full Heusler alloys, Ni_2MnGa has first been reported in 1983 and was shown to undergo a martensite transition by Webster et. al.[1] They prepared the Ni_2MnGa sample which has a highly ordered $L2_1$ structure (space group $Fm\bar{3}m$). It was observed that Ni_2MnGa is a ferromagnetic material with a Curie temperature of 376 K. Later on, Ullakko et. al.[2, 7], observed a large magnetic field induced strain (MFIS) in Ni-Mn-Ga single crystal. They reported about 9.5% MFIS in an magnetic field of less than 1 Tesla at an ambient temperature. All these studies put together suggested that Ni_2MnGa is a promising ferromagnetic shape memory alloy. Apart from the shape memory application, there are significant studies on the occurrence of magnetocaloric effect in Ni-Mn-Ga systems.[8–10]

In 2005, Liu et. al.[11] prepared a single crystal of Mn_2NiGa. It has been reported that it undergoes a martensite transition at 270 K and its Curie temperature is 588 K.[11] A MFIS of around 4% has been observed in the single crystal of Mn_2NiGa.[11] Unlike Ni_2MnGa, Mn_2NiGa crystallizes in $F\bar{4}3m$ structure in the cubic austenite phase. From the magnetic properties point of view also, it is found to be different from Ni_2MnGa. Both from experimental and density functional theory based first principles study by Barman et. al.[12, 13] it has been shown that, Mn_2NiGa possesses a ferrimagnetic ground state. Based on experimental study by Singh et. al.[14], it has been observed that, there is a significant change in the magnetization as Mn_2NiGa undergoes martensite transition. This observation has been confirmed by theoretical study as well.[12, 13] In the martensite phase the magnetic moment is 1.01 μ_B/f.u. whereas in austenite phase the moment is around 1.12 μ_B/f.u. Because of this jump in magnetization in Mn_2NiGa, it shows inverse magnetocaloric effect[14], which can be utilized in the practical applications. However, both the systems Ni_2MnGa and Mn_2NiGa face the difficulties in terms of practical application because of their low martensite transition temperature.

For shape memory alloy systems, it is also important to ensure that the martensite transition temperature is above the room temperature. To this end, there are lot of

studies in the literature on Ni_2MnGa as discussed below. For a number of Ni-Mn-Ga samples, Lanska et. al.[15] have shown an empirical relationship between the T_M and the number of valence electrons per atom (e/a). For a range of compositions based on Ni-Mn-Ga, Jin et. al.[16] reported that, (a) increased Ni content increases T_M, whether it replaces Mn or Ga, (b) T_M increases as Mn replaces Ga but decreases if Ni is replaced by Mn, and (c) increased Ga percentage will always lower the T_M significantly whether it replaces Ni or Mn. A possible argument has been given for this kind of variation of T_M as in the last case e/a ratio decreases significantly compared to the average value for same for Ni-Mn-Ga. However, there are cases in which this correlation fails.[17] Hu et. al. mentioned about few parameters on which the T_M depends. Along with e/a ratio, these are conjectured to be (a) tetragonality of the martensite phase ($c/a - 1$), (b) the relative phase stability between austenite and martensite phase i.e. the energy difference between these two phases based on first principles calculation, and (c) the value of tetragonal shear constant (C') (lower the value of C', higher the T_M).[17] All these parameters can be tuned by changing the chemical composition of the materials such that the T_M attains a suitable value for the practical applications as has been observed both from experiments and first principles based studies.[10, 18–23]

Apart from searching for higher T_M, for practical application, mechanical properties are also important to probe. In literature, there are several experimental and first principles based studies on the mechanical properties of Ni_2MnGa.[24–27] Based on experimental studies, Worgull et. al.[24] measured the three independent elastic constants for the cubic crystal of Ni_2MnGa, these are C_L=0.5×(C_{11}+C_{12}+2C_{44}), C_{44}, and C'= 0.5×(C_{11}-C_{12}). Softening of the tetragonal shear constant C' has been observed during the martensite transformation.[24] Using density functional theory based first principles study, Kart et. al.[27] calculated all the elastic constants for both the austenite and martensite phases. Elastic instability of the cubic austenite phase of Ni_2MnGa has been indicated by the very small value (5.5 GPa) of C' in this phase. From the values of calculated elastic constants, bulk modulus (B) and shear modulus (G) have also been calculated by Kart et. al.[27] Further, S. F. Pugh in 1954, conjectured that, the elastic property of a material is related to the ratio of the shear modulus (G) and bulk mod-

ulus (B) of that material.[28] In his work, a value of G/B higher than ∼0.57 has been associated with the inherent brittleness of a crystalline material. The calculated G/B values for the different phases of Ni_2MnGa have been shown to be slightly lower than 0.57.[27] However, in the literature, Ni_2MnGa has been mentioned as a fragile material, which makes it unsuitable for technological application.[29, 30]

For the magnetic shape memory alloys (MSMA), it is also desired that, $T_C > T_M$, such that we can control the strain developed in the martensite phase by the application of magnetic field. Co-based systems are shown to exhibit high T_C, as is found in the literature.[31, 32] Further, Mario et. al. have observed an enhancement of T_C as a result of Co doping in the Pt-based systems.[4]

In this regard, we point out that one of the major and important goals of the present thesis is to search for novel magnetic shape memory alloys in a systematic way, with better electronic, magnetic and mechanical properties from the application point of view. Second aspect is to understand the differences and similarities between two classes of FHAs, which are prone to martensite transition and which are not prone to martensite transition in terms of electronic, mechanical and magnetic properties. These are described in detail below, with respect to each individual chapter. The thesis has been arranged in total of 7 chapters. In the later part of this first chapter, we provide a brief introduction to the computational method employed in the electronic structure calculations based on density functional theory.

Taking a cue from the existing literature, that the partial Cu doping at the Mn site of Ni_2MnGa, leads to increase of martensite transition temperature[10], in first part of **Chapter 2**, we discuss the effects of Cu substitution on the two prototype Heusler alloys namely, Ni_2MnGa and Mn_2NiGa. We study the changes in the structural, electronic as well as magnetic properties of these two systems with Cu substitution of 0%, 25%, 75% and 100% (in most cases) at the Mn, Ga as well as Ni sites of both the materials, which are different in terms of structural and magnetic properties.

We know that, both Cu and Pt are highly ductile material in their bulk form. Further, Pt and Pd are isoelectronic with Ni while Cu has one electron more compared to Ni. Hence, a comparative study is expected to yield interesting results if we substitute Ni

with Pt, Pd and Cu in case of Ni_2MnGa. The existence of a modulated structure is known to be a prerequisite for a large MFIS on applying a small magnetic field. We note that a maximum magnetic field induced strain of 14% has been reported for $Ni_{1.75}Pt_{0.25}MnGa$ in the literature.[4] Further, based on a neutron diffraction study, Singh et. al.[33] have reported the existence of a modulated structure in Pt doped Ni_2MnGa. These two studies suggest that probing of Pt substitution may be interesting from practical point of view. In the second part of the **Chapter 2**, therefore, we discuss the results of our calculated bulk mechanical as well as electronic and magnetic properties of Ni_2MnGa substituted by copper (Cu), platinum (Pt), palladium (Pd) and manganese (Mn) at the Ni site. We also study the Heisenberg exchange coupling parameters and calculate the Curie temperature using a mean field approximation, and we show the effects of substitution on the magnetic properties of these materials.

We mentioned above that, there is another group of FHAs which is found to be half metallic in nature.[3] Generally, many of the Co-based Heusler alloys exhibit this behavior.[31, 34] On the contrary, Co_2NbSn and Co_2NiGa are found to exhibit SMA property and these are found to be metallic in nature.[35–37] Currently, Co_2NiGa and related alloys have gained interest among the researchers, as they show SMA property and possess different crystal structure (inverse Heusler alloy structure), compared to the other Co-based materials, which are known to possess half metallicity and conventional Heusler alloy structure in their ground state.[36, 37] Our study showed that, the substitution of Ni by Pt in case of Ni_2MnGa reduces the inherent crystalline brittleness (ICB) as well as makes the tetragonal state more stable compared to the cubic phase. Furthermore, Siewert et. al. have observed an enhancement of T_C in case of Co doping in the Pt based systems.[4] Additionally, number of valence electrons has been shown to play an important role in determining the properties of these alloy systems.[23] So, studying the literature, we can expect that, the effect of replacement of Ni by Pt on various physical properties of Co_2NiGa may turn out to be interesting both from fundamental as well as application points of view. In **Chapter 3**, therefore, we discuss the changes in the magnetic, electronic as well as mechanical properties of A_2PtGa alloy, where A atom and consequently, the number of valence electrons are varied. Here, A atom has been taken to

be a first row transition metal atom (A being Cr, Mn, Fe, Co). An estimation based on DFT calculations has been given on inherent crystalline brittleness, martensite transition temperature (T_M), melting temperature (Θ_m) and Curie temperature (T_C) for each of the four materials..

Depending on their chemical composition, the FHAs are shown to possess long-range ferromagnetic, ferrimagnetic and anti-ferromagnetic configuration, some of these materials are even found to carry no net magnetic moment. So, it is of immense interest to have an in-depth understanding of the magnetic interactions present in these systems. It is found that, in most of the FHAs, represented as A_2BC, primarily B is the moment carrying atom. There is the presence of a delocalized-like common d-band formed by the d-electrons of the A and B atoms, both of which are typically first-row transition metal atoms as well as carry magnetic moments.[38] The C atom also plays an important role in defining the magnetic properties of these materials.[38, 39] Jin et. al.[16], have shown the existence of an empirical relationship between number of valence electrons present in the system and magnetic properties (T_C and saturation magnetization) of Ni-Mn-Ga systems.

Hence, it is expected that, Fe and Cr substitution at the Mn site of Ni_2MnGa and Pt_2MnGa may lead to interesting magnetic properties as both Fe and Cr have high atomic moments which are close to Mn. Further while Fe has ferromagnetic, Cr has anti ferromagnetic configuration in bulk like Mn Additionally, Cr possesses one electron less than that of Mn and Fe possesses one electron more. All these facts may have some interesting role to play in defining the magnetic and also the mechanical and electronic properties of the substituted materials. In **Chapter 4**, we therefore, discuss the effects of Fe and Cr substitution at the Mn site on magnetic, mechanical and electronic properties of Ni_2MnGa and Pt_2MnGa. Calculation of formation energy has been carried out to make a prediction on the stability of $A_2Mn_{1-x}B_xGa$ alloys (x = 0.00, 0.25, 0.75, 1.00; A = Ni, Pt; B = Fe and Cr). Further, we have probed how the stability of the austenite and martensite phase varies with the extent of substitution by Fe as well as Cr atoms at the Mn site. We also study the bulk mechanical properties of the austenite and martensite phases of the systems. To predict the ground state magnetic configuration for all the systems studied here, we probe various possibilities of the magnetic configuration for these systems.

Both the existing literature and our work show that one group of the FHAs is likely to show SMA property and is generally metallic in nature whereas another group of FHAs possess high spin polarization at E_F and is not typically prone to a tetragonal transition on cooling. From both the points of view of fundamental understanding as well as technological application, it can be interesting to probe the similarities and differences in magnetic, bulk mechanical, and electronic properties of these two categories of materials. Keeping these in mind, in **Chapter 5**, we probe the bulk mechanical, magnetic and electronic properties of a series of Ni and Co-based FHAs, namely, Ni_2BC and Co_2BC (B = Sc, Ti, V, Cr and Mn as well as Y, Zr, Nb, Mo and Tc; C = Ga and Sn) materials. The choice of these two systems (Ni and Co-based FHAs) depended on the following facts. It has been observed that, typically, a large amount of work on the FHAs are on the Ni and Co-based compounds. It is also seen in the literature that, while quite a few of the Ni-based FHAs tend to undergo martensite transition, many of the Co-based FHAs exhibit a large spin-polarization at the E_F. So one of the interests here is to study if there is a possibility of coexistence of a tetragonal transition and a high spin polarization at the E_F.

RKKY interaction[40] is known to be an important magnetic interaction present in the MSMA materials.[38] In **Chapter 6**, we present the results of detailed magnetic properties of a few series of materials, namely $A_{2-x}Co_xXC$ (A = Ni, Pt; X = Mn, Fe; C = Ga, Sn; x=0.00, 0.25, 0.50, 0.75, 1.25, 1.50, 1.75, 2.00), where the material, at one end (with x = 0.00) shows a SMA property, but at the other end (with x = 2.00) does not. In this chapter, we carry out, in detail, the study on the evolution of the RKKY interaction for the materials, namely, $Ni_{2-x}Co_xMnGa$, $Ni_{2-x}Co_xFeGa$, $Pt_{2-x}Co_xMnGa$, $Pt_{2-x}Co_xMnSn$ as a function of x. We discuss, the role played by the d-electron of the A atom in the coupling between the localized-like moments of B atom in the A_2BC systems studied here.

Finally, all the above-mentioned work carried out in this thesis, has been summarized in **Chapter 7** and conclusions have been drawn. This is then followed by a brief discussion on the possible future work.

1.3 Calculational methodology

In this section, we discuss about the theoretical methods, used here to study the structural, electronic and magnetic properties of the Heusler alloy systems. Here, we employ density functional theory (DFT) based first principles calculation, to carry out calculations on the all above mentioned properties.

1.3.1 Many-Body Problems

It is known to us that the physical and chemical behaviours of a material is governed by the electrons present in the system. Now to get the begaviour of any system, one must solve the Schrödinger equation,

$$\hat{H}\Psi = E\Psi \tag{1.1}$$

where Ψ denotes the stationary wave function of the system, E indicates the energy eigenvalue and the Hamiltonian of the system is denoted by $\hat{H}$, which contains the following terms,

$$\hat{H} = -\frac{\hbar^2}{2m_e}\sum_{i=1}^{N}\nabla_i^2 - \frac{\hbar^2}{2}\sum_{I=1}^{N_I}\frac{\nabla_I^2}{M_I} + \frac{1}{4\pi\epsilon_0}\sum_{i<j}^{N}\frac{e^2}{|\mathbf{r_i}-\mathbf{r_j}|} + \frac{1}{4\pi\epsilon_0}\sum_{I<J}^{N_I}\frac{Z_I Z_J e^2}{|\mathbf{R_I}-\mathbf{R_J}|} - \frac{1}{4\pi\epsilon_0}\sum_{i,I}^{N,N_I}\frac{Z_I e^2}{|\mathbf{r_i}-\mathbf{R_I}|} \tag{1.2}$$

On the R.H.S., the individual term represents

i) Kinetic energy of nuclei,

ii) Kinetic energy of electrons,

iii) Interaction between electrons themselves,

iv) Interaction between nuclei themselves,

v) Interaction between electrons and nuclei, respectively. In the Eq. 1.2, $\hbar$ and ϵ_0: Planck's constant and permittivity of vacuum, $\mathbf{r_i}$ and $\mathbf{R_I}$: positions of electrons and nuclei, m_e and M_I: masses of electrons and nuclei, e and $Z_I e$: charges of electrons and nuclei, N and N_I: numbers of electrons and nuclei in the system,

Now onwards, we use atomic unit, in which $\hbar$, e, m_e, and $\frac{1}{4\pi\epsilon_0}$ are taken as unity.

We know that the nuclei are much heavier and therefore, much slower than the electrons. We can hence 'freeze' the nuclei at fixed positions and assume the electrons to be in instantaneous equilibrium with them. In other words: only the electrons are kept as players in our many body problems. The nuclei are assumed to be at rest with respect to the electrons. They become 'external' to the electron cloud. This is an approximation, which is called the **Born-Oppenheimer** (BO) approximation.[41] Under BO approximation, we are left with only three terms in the Hamiltonian, which are

i) kinetic energy of electrons

ii) potential energy due to electron-electron interaction

iii) potential energy of electrons in the potential of nuclei

The Hamiltonian, only for the electrons can be rewritten as,

$$\hat{H} = -\frac{1}{2}\sum_{i=1}^{N}\nabla_i^2 + \sum_{i<j}^{N}\frac{1}{|\mathbf{r_i}-\mathbf{r_j}|} - \sum_{i,I}^{N,N_I}\frac{Z_I}{|\mathbf{r_i}-\mathbf{R_I}|} \tag{1.3}$$

Properties of matter primarily involve either the electronic ground state or the electronic excited states. Here, we will concentrate on the methods for ground state electronic structure calculations. The simplest electronic system to solve is the well-known hydrogen atom problem. It is known to us how to solve a one electron system like hydrogen atom. Now, if we consider a many electron system, then in the expression of the Hamiltonian, we have to introduce a term which is due to the mutual interaction between the two electrons (second term of the Eq. 1.3). This term, due to its interdependence, leads to complication in solving the many-particle problems. Nevertheless, several numerical and computational methods exist in the literature to tackle this problem.

In this present scope of the thesis, we have used density functional theory (DFT) to study many electrons systems. DFT allows one to find any observable, in terms of the ground state electron density of the particular system. In the following, we discuss in brief, the formalism of DFT.

1.3.2 Density functional theory

Density functional theory (DFT) has been regularly used in electronic structure calculations of many body systems. DFT is based on ideas that were around since the early 1920s which was given by Thomas-Fermi theory of electronic structure of atoms (1927). But Hohenberg and Kohn formulated DFT as an exact theory of a many body system in 1964.[42]

Hohenberg and Kohn Theorem

First theorem- There is a one to one correspondence between the ground state density ($n(\mathbf{r})$) and the external potential ($V_{ext}(\mathbf{r})$; the potential due to coulomb interaction between electron and nucleus ($V_{ne}(\mathbf{r})$)). It means that the Hamiltonian is a unique functional of $n(\mathbf{r})$, and solving time-independent Schrödinger equation, the obtained wavefunction will also be a unique functional of $n(\mathbf{r})$. So, we can write,

$$n(\mathbf{r}) \longleftrightarrow \Psi[n(\mathbf{r})] \tag{1.4}$$

An immediate consequence is that the expectation value of any observable $\hat{O}$ is a unique functional of the exact ground state electron density.

$$\langle \Psi[n] | \hat{O} | \Psi[n] \rangle = O[n] \tag{1.5}$$

The Eq. 1.3 may be expressed in a compact manner, such as,

$$\hat{H} = \hat{T} + \hat{V_{ne}} + \hat{V_{ee}} \tag{1.6}$$

where

$$\hat{T} = -\frac{1}{2} \sum_{i=1}^{N} \nabla_i^2 \tag{1.7}$$

is the kinetic energy operator, and

$$\hat{V_{ne}} = -\sum_{i,I}^{N,N_I} \frac{Z_I}{|\mathbf{r_i} - \mathbf{R_I}|} \tag{1.8}$$

represents the electron-nucleus interaction term and the electron-electron interaction is represented by

$$\hat{V_{ee}} = \sum_{i<j}^{N} \frac{1}{|\mathbf{r_i} - \mathbf{r_j}|} \tag{1.9}$$

The ground state energy, E_{gs}, can be written as

$$E_{gs}[n] = T[n] + V_{ne}[n] + V_{ee}[n] \tag{1.10}$$

where,

$$T[n] = \langle \Psi[n]|\hat{T}|\Psi[n]\rangle \tag{1.11}$$

$$V_{ee}[n] = \langle \Psi[n]|\hat{W}|\Psi[n]\rangle \tag{1.12}$$

$$V_{ne}[n] = \langle \Psi[n]|\hat{V_{ne}}|\Psi[n]\rangle \tag{1.13}$$

$$= \int n(\mathbf{r})V_{ne}(\mathbf{r})d\mathbf{r} \tag{1.14}$$

As discussed above, we consider, $V_{ne}(\mathbf{r}) = V_{ext}(\mathbf{r})$, so we can write,

$$V_{ne}[n] = \int n(\mathbf{r})V_{ext}(\mathbf{r})d\mathbf{r} \tag{1.15}$$

Now at this point it is convenient to separate the energy expression into two parts 'system specific part' and 'system independent part'. In this case the 'system specific part' is the potential energy term due interaction of electron and nucleus given by

$$V_{ne}[n] = \int n(\mathbf{r})V_{ext}(\mathbf{r})d\mathbf{r} \tag{1.16}$$

The 'system independent part' is the sum of kinetic energy of electrons and the po-

tential energy due to electron-electron interaction. This is given by

$F_{HK}[n] = T[n] + V_{ee}[n]$, called the Hohenberg Kohn functional and it is a universal functional, as its form is same for all the electronic systems.

So, now we can write

$$E_{gs}[n] = \int n(\mathbf{r})V_{ext}(\mathbf{r})d\mathbf{r} + F_{HK}[n] \tag{1.17}$$

Second theorem- It states for any positive definite trial density, $n'(\mathbf{r})$, such that $\int n'(\mathbf{r})d\mathbf{r} = N$

the exact ground state energy obeys the following relation

$$E_0 \leq E_{gs}[n'] \tag{1.18}$$

In other words, it can be stated as, the density which minimizes $F_{HK}[n]$, is the ground state density.

The ground energy, can be obtained by minimizing the energy functional of the Eq. 1.17 with respect to density, under the constraint, $\int n(\mathbf{r})d\mathbf{r} = N$ and satisfy the Euler-Lagrange equation

$$\frac{\delta F_{HK}[n]}{\delta n(\mathbf{r})} + V_{ext}(\mathbf{r}) = \mu \tag{1.19}$$

where μ is the Lagrange multiplier.

Applying, Hohenberg Kohn theorem, the ground state energy of the system can be solved, if the exact form of the universal functional is known. But unfortunately, the exact form of the $F_{HK}[n]$, is not known to us. To overcome this problem, Kohn and Sham in 1965 gave an idea. They replaced the actual interacting many-body problem with an auxiliary independent-particle model, under the assumption, that the ground state density of the original interacting system is equal to that of some chosen noninteracting system that is exactly solvable.[43]

1.3.3 Kohn-Sham approach

The idea of Kohn and Sham was to realize that it is not possible to determine the exact kinetic energy for an interacting system but we can determine the exact kinetic energy for a non-interacting system which contributes the major part of the total kinetic energy of the actual system. Then we can deal with the remainder part in an approximate manner. We obtain the exact kinetic energy of the non-interacting reference system with the same density as the real interacting one. The effect of the interaction has been put together by the inclusion of an effective potential, V_{KS}. Now, the universal functional can be rewritten as,

$$\begin{aligned} F_{HK}[n] &= T[n] + V_{ee}[n] \\ &= T_s[n] + (T[n] - T_s[n]) + E_H[n] + (V_{ee}[n] - E_H[n]) \\ &= T_s[n] + E_H[n] + E_{xc}[n] \end{aligned} \tag{1.20}$$

where, E_{xc}[n] is called the exchange correlation functional, and defined as E_{xc}[n]$= (T[n] - T_s[n]) + (V_{ee}[n] - E_H[n])$

$E_H[n]$, represents the classical coulomb energy of the system, between the electrons. The exchange correlation energy, E_{xc}[n] contains two parts, i) the kinetic energy difference between the actual (interacting) and the fictitious (noninteracting) system, ii) the difference between total electron-electron interaction energy and the classical coulomb energy between the electrons. But, unfortunately, the exact form of the E_{xc}[n], is not known to us.

But, we can calculate the kinetic energy of the noninteracting system, using the relationship,

$$T_s[n] = -\sum_i^N \int \phi_i(\mathbf{r})^* \left[\frac{\nabla^2}{2}\right] \phi_i(\mathbf{r}) d\mathbf{r} \tag{1.21}$$

The single particle orbital, $\phi_i(\mathbf{r})$ can be obtained by solving single particle equation,

$$\left(-\frac{\nabla^2}{2} + V_{ks}[n(\mathbf{r})]\right)\phi_i(\mathbf{r}) = \epsilon_i\phi_i(\mathbf{r}) \tag{1.22}$$

we define effective potential V_{ks} as,

$$V_{ks}[n(\mathbf{r})] = V_{ext}[n(\mathbf{r})] + V_H[n(\mathbf{r})] + V_{xc}[n(\mathbf{r})] \tag{1.23}$$

$$\text{with} \qquad V_H[n(\mathbf{r})] = \frac{1}{2}\int \frac{n(\mathbf{r}')}{|\mathbf{r}-\mathbf{r}'|}d\mathbf{r}' \qquad \text{and} \qquad V_{xc}[n(\mathbf{r})] = \frac{\delta E_{xc}[n(\mathbf{r})]}{\delta n(\mathbf{r})} \tag{1.24}$$

are the coulomb and the exchange correlation potentials respectively. From the single-particle orbitals, we can calculate the density of the real system, following the relationship-

$$n(\mathbf{r}) = \sum_i^N |\phi_i(\mathbf{r})|^2 \tag{1.25}$$

The Eq. 1.22, is called the Kohn Sham equation.

So we get the form of the non-interacting potential corresponding to the interacting potential of the real system. Now the challenge is to find out the exchange correlation term which essentially helps in mapping the interacting system to a pseudo-one-particle system. Up to now whatever we have done is exact. The various approximations will come into play to find out the exchange correlation term. Hence, we will discuss briefly some of them in the next section.

1.3.4 Exchange-Correlation functional

Their are various approximations, on the form exchange correlation functional. Among them, Local density approximation(LDA) is the simplest one. Within the local density approximation the exchange correlation energy can be written as

$$E_{xc}[n(\mathbf{r})] = \int n(\mathbf{r})\ \epsilon_{xc}[n]\ d\mathbf{r} \tag{1.26}$$

$\epsilon_{xc}[n]$, denotes the per electron exchange correlation energy of a uniform electron gas.

It can be further decomposed into two parts,

$$\epsilon_{xc}[n] = \epsilon_x[n] + \epsilon_c[n] \tag{1.27}$$

For uniform electron gas, Dirac calculated $\epsilon_x(n)$ exactly.[44] However the determination the other part of $\epsilon_{xc}(n)$, i.e. $\epsilon_c(n)$ is more difficult. However, based on Monte Carlo simulation Ceperly and Alder[45] calculated this part for finite number of electrons, which form uniform electron gas. Among the different forms of LDA, Vosko-Wilk-Nusair (VWN) is the most widely used one.[46]

Local density approximation is basically based on the uniform electron gas model, which can predict good result only when electron density varies slowly with space. But in most of the practical systems, we must take care of the significant spacial variation of electron density. So, we need to modify our approximated exchange correlation functional which is done within Generalized Gradient Approximation (GGA). Under GGA, the general form of the exchange correlation functional is given by

$$E_{xc}^{GGA}[n(\mathbf{r})] \quad = \quad \int \epsilon_{xc}^{GGA}\Big(n(\mathbf{r}), \nabla n(\mathbf{r})\Big)\, d\mathbf{r} \tag{1.28}$$

There are several forms available in the literature.[47, 48] For most of our calculations we used the GGA form given by Perdew-Burke-Ernzerhof (PBE). Now we give brief discussions on the different codes used in this thesis.

WIEN2k: For magnetic properties, the results from all-electron calculations are typically very reliable for systems containing first row transition metal atoms. Hence, we have carried out relativistic spin-polarized all-electron calculations on the optimized geometries of the studied systems using full potential linearized augmented planewave (FPLAPW) program.[49] We have also used this method for calculating the electronic density of states (DOS). For obtaining the electronic properties, the Brillouin zone (BZ) integration has been carried out using the tetrahedron method with Blöchl corrections.[50] Convergence tests have been carried out for all the different parameters for all the codes used in this thesis. An energy cut-off for the plane wave expansion of about 16 Ry is used

($R_{MT}K_{max}$=9.5). The cut-off for charge density is K_{max}=9.5. The number of k-points for the self-consistent field (SCF) cycles in the reducible (irreducible) BZ is about 8000 (256) for the cubic phase. The convergence criterion for SCF calculation of energy is about 0.1 mRy per atom. The charge convergence is set to 0.0001.

Vienna *Ab initio* Simulation Package (VASP): MedeA-VASP has been employed for the geometry optimization of the systems studied here. The implementation of projector augmented wave reduces the number of the plane waves in the basis set for carrying out electronic structure calculation.[51, 52] We have used an energy cut-off of minimum 500 eV for the planewaves and the convergence of the results has been tested. The final energies have been calculated with a k-mesh of 15×15×15 for the cubic case. The number of k-points for the self-consistent field (SCF) calculations has been tested. The energy and the force tolerance for our calculations were 10 μeV and 10 meV/Å, respectively.

CASTEP: Elastic constants of some of the materials have been calculated from the second derivative of the energy with respect to the strain tensor. For the calculation of elastic constants, we have used the software package CASTEP (Materials Studio 6.1).[53] We use ultrasoft pseudopotential and PW91 GGA over the LDA for the exchange-correlation functional.[54] For fine calculations, required for response properties, the number of k-points and the energy cut-off have been increased from the values used in SCF calculations till the convergence of the mechanical properties of each individual material has been achieved. Maximum mesh of k-points has been taken as 17×17×17 and energy cut-off has been increased up to 1500 eV according to the requirement.

SPRKKR: To gain detailed insight into the magnetic properties of the systems, we calculate the Heisenberg exchange coupling parameters. We use the Spin-polarized-relativistic Korringa-Kohn-Rostoker method (SPR-KKR) to calculate these exchange coupling parameters, J_{ij}, within a real-space approach, which is proposed by Liechtenstein et al[55] and implemented in SPR-KKR programme package.[56] Full-potential method has been used for the SCF calculations and the results of the same have been used further for calculating the exchange parameters. The number of k points for the SCF cycles has been taken as 500 in the irreducible BZ. The angular momentum expansion up to lmax=3

has been taken for each atom. Curie temperature (T_C) is derived from the Heisenberg exchange coupling parameters using a mean field approximation (MFA).[57] Convergence of the T_C has been tested with respect to the cluster radius, where the cluster radius (R_{ij}) is the radius of a cluster of atoms (j) surrounding a central atom, i.

Chapter 2

Effect of Cu, Pt, Pd Substitution on the Electronic, Magnetic and Mechanical Properties of Ni_2MnGa and Mn_2NiGa

2.1 Introduction

The tunability of important physical properties of magnetic shape memory alloys such as martensite transition temperature (T_M), Curie temperature (T_C) and inherent crystalline brittleness (ICB) with changing composition has been observed in the literature and discussed in the previous chapter.[10, 20, 22, 58–63] Ni-Mn-Ga, a well-known such alloy, shows upto 9.5% magnetic field induced strain (MFIS).[2, 7, 64] With the help of partial or complete replacement by various elements or altering relative concentrations of manganese (Mn), gallium (Ga) and nickel (Ni) in Ni_2MnGa, different properties, including those related to the martensite phase transition, can be probed in search of betterment of these properties.

Similar to Ni_2MnGa, the recently discovered material Mn_2NiGa also holds the promise of practical application as a MSMA with 4% magnetic field induced strain and high magnetic transition temperature.[11, 12, 67–69] Contrary to the ferromagnetic behavior, which is observed in Ni_2MnGa, Mn_2NiGa is ferrimagnetic in nature.[13] Furthermore, Mn_2NiGa shows promise of existence of an inverse magnetocaloric effect unlike Ni_2MnGa.[70] Hence, it may be interesting from a fundamental point of view to understand how the Cu substitution at Ni, Mn and Ga sites affects the properties of Mn_2NiGa *vis-a-vis* those of Ni_2MnGa. This may eventually have a technological implication also, specifically in the screening of new MSMA materials with desirable properties.

In the first part of this chapter (Part A), we discuss the results of our calculations on the effect of Cu substitution in Ni_2MnGa and Mn_2NiGa. We study the changes in the structural, electronic as well as magnetic properties of these two systems for Cu substitution of 0%, 25%, 75% and 100% (in most cases) at the Mn, Ga as well as Ni sites. As discussed earlier, some compositions with Cu at Ga and Mn sites of Ni_2MnGa have been experimentally found to be stable.[10, 20, 22, 58–63] In this part of the chapter, we are particularly interested in the stability and changes in various properties as a result of small to large Cu substitution in Ni_2MnGa as well as Mn_2NiGa. The lattice constant, the bulk modulus and the probability of martensite transition of the alloys with Cu substitution are compared with the corresponding properties of the parent compounds. We study the effect of Cu substitution at Ni, Mn, and Ga sites of Ni_2MnGa and Mn_2NiGa by using a sixteen atom unit cell as mentioned in the first chapter.

The disadvantage related to the mechanical properties of Ni_2MnGa in terms of its technological suitability has been already addressed in the literature and studies aiming to improve the ductility of SMA alloys have been carried out in the literature.[71–77] The elastic constants are amongst the most important physical properties related to the structure and the mechanical stability of a material. In the second part of this chapter (Part B), we carry out in depth study of the bulk mechanical stability in terms of the elastic stability criteria[78] and elastic constants of Mn_2NiGa and Ni_2MnGa as well as substituted at the Ni site by Cu and isoelectronic elements Pt as well as Pd. Since both Cu and Pt are highly ductile materials, we choose these two elements for substitution with the hope of improvement of relevant elastic properties of the substituted materials. Further, because Pt and also Pd are isoelectronic with Ni while Cu has only one electron more than Ni, a comparative study is expected to be interesting, when we substitute Ni with Pt, Pd and Cu. The choice of Pt is further driven by some recent interesting experimental and theoretical observations found in the literature. A maximum MFIS of 14% has recently been predicted for Pt doped Ni_2MnGa (composition $Ni_{1.75}Pt_{0.25}MnGa$)[4] on the basis of first-principles calculations. Neutron diffraction study establishes the existence of a modulated structure in $Ni_{1.8}Pt_{0.2}MnGa$, which is a prerequisite for a large MFIS in small magnetic fields.[33] It is also shown very recently[79] that $Ni_{1.8}Pt_{0.2}MnGa$ exhibits sizable

magnetocaloric effect (MCE) near room temperature. A large increase in martensite transition temperature has also been reported earlier for Pt-doped Ni-Mn-Ga.[80] Hence, by studying the literature it appears that, Pt-doped Ni_2MnGa is expected to have similar or better properties in comparison to Ni_2MnGa in terms of technological applications.

Therefore, we study in detail the elastic properties of Ni_2MnGa,Mn_2NiGa and its substituted alloyss. We also carry out calculations of the electronic structures in terms of the density of states (DOS). In addition, we evaluate the magnetic properties of these alloy materials in terms of the Heisenberg exchange coupling parameters from which we derive the Curie temperature (T_C) within a mean field approximation.[81] We also compare the results of our calculations of mechanical properties where Cu is substituted at Mn or Ga site of the Ni_2MnGa and some of the substituted alloys.

2.2 Part A: Results and Discussions

In this section, the results of the Cu substitution on the electronic, mechanical and magnetic properties of the Ni_2MnGa and Mn_2NiGa systems have been presented. These data are compared with the results obtained in the literature, wherever results are available, and it is observed that our results match well with the earlier data. For Ni_2MnGa and Mn_2NiGa compounds, we take an ordered A_2BC and $ABAC$ type of structure (A, B, typically elements with d-electrons and C typically elements with s, p electrons), respectively. We make use of the commonly used structures for both the materials, conventional Heusler and inverse Heusler structures for Ni_2MnGa and Mn_2NiGa, respectively, as these are found to be the lowest energy structures. In the austenite phase, Ni_2MnGa has a cubic $L2_1$ structure.[1] For Mn_2NiGa, we have considered the inverse Heusler alloy structure.[11, 12] To simulate Cu substitution in Ni_2MnGa and Mn_2NiGa, we have replaced the Ni, Mn or the Ga atoms at their respective sites by Cu atoms, either partially or fully. For example, in a 16 atom cell, 75 % Cu substitution at the Ni site amounts to replacing three of the four Ni atoms by Cu atoms in Mn_2NiGa. To study the stability of the substituted materials, we have calculated the mixing energy for each system. The mixing energy can be obtained by subtracting the total sum of the bulk energy of all the material components, E_i, weighted by its concentration c_i from the ground state energy

Table 2.1: Calculated values of bulk properties of the cubic structures and the mixing energy, in electron volts (eV) per formula unit (f.u.), for all the Cu doped Ni_2MnGa compounds are presented here. Experimental values, wherever available, are given in bold and within parentheses. For comparison, present calculations yield values of bulk modulii of Cu and Ni to be 135 and 191 GPa, respectively, which are about 140 and 180 GPa, respectively, from experiments. The negative value of the mixing energy ensures that the compound is more stable compared to its individual bulk components. More negativity indicates more stability.

Material	Nature of substitution (sub-lattice)	Lattice constant (Å)	Bulk Modulus (GPa)	Mixing Energy (eV/f.u.)
Ni_2MnGa	None	5.810 (**5.82**)	161 (**150**)	-1.2390
$Ni_{1.75}Cu_{0.25}MnGa$	Ni by Cu (P)	5.827	149	-1.0999
NiCuMnGa	Ni by Cu (P)	5.874	132	-0.7162
Cu_2MnGa	Ni by Cu (P,Q)	5.961	118	-0.2107
$Ni_2Mn_{0.75}Cu_{0.25}Ga$	Mn by Cu (R)	5.794 (**5.799**)	155	-1.1671
$Ni_2Mn_{0.25}Cu_{0.75}Ga$	Mn by Cu (R)	5.757	160	-1.0952
Ni_2CuGa	Mn by Cu (R)	5.744	162	-1.0117
$Ni_2MnGa_{0.75}Cu_{0.25}$	Ga by Cu (S)	5.791	154	-0.9608
$Ni_2MnGa_{0.25}Cu_{0.75}$	Ga by Cu (S)	5.756	155	-0.4335
Ni_2MnCu	Ga by Cu (S)	5.733	146	-0.1281

of the total alloy system, E_{tot} (total energy of the unit cell),

$$E_{mix} = E_{tot} - \Sigma_i c_i E_i \tag{2.1}$$

where i denotes different types of atoms present in the unit cell of the material system. A more negative mixing energy of a system indicates that it is more stable. The equilibrium lattice constants are obtained by geometry optimization using VASP code.[51, 52] The reference bulk states considered here for the mixing energies are: fcc for bulk Cu, Ni, α-Mn and orthorhombic for bulk Ga. The bulk modulus has been calculated from the double derivative of the total energy, by using the Murnaghan's equation.[82]

2.2.1 Cu substitution at different sites in Ni_2MnGa

i) Stability and bulk Properties - First, we focus on the effects on the electronic stability and bulk property because of Cu substitution at different sites in Ni_2MnGa. In Table 2.1, we compare the lattice constant, bulk modulus and the mixing energy of the austenite (cubic) phases of all the Cu-substituted Ni_2MnGa (Ni-Cu-Mn-Ga) materials studied in

this work. We observe that the mixing energy is negative in all the compounds, which indicates that Cu substitution leads to stable materials even up to 100% replacement at different sites. The parent compound Ni_2MnGa is found to be the most stable, and any amount of Cu in the alloy invariably leads to a mixing energy whose absolute value is lower than that of Ni_2MnGa. The substitutions at the Ni and Ga sites (P, Q or S sub-lattices) are energetically less favorable compared to the substitution at Mn site (R sub-lattice). As is clear from Figure 2.1(a), when Cu substitutes Ga or Ni, the absolute value of mixing energy decreases linearly with increase of Cu content. In contrast, we observe that the mixing energy decreases only marginally for Cu substitution at the Mn site (R sub-lattice). Interestingly, 25% substitution of Cu at Mn yields a reasonably favorable mixing energy. It is -1.167 eV per formula unit (f.u.). This is rather close to the mixing energy of Ni_2MnGa (-1.239 eV/f.u.). We note that this material has already been experimentally prepared and it shows promise for practical applications.[10, 20] Cu substitutions at the Ga and Mn sites seem to cause a slight compression of the unit cell. This trend has already been observed in experimental results.[20, 60] On the contrary, replacement of Ni by Cu leads to a systematic expansion of the unit cell. The substantial difference in the covalent radii of Cu (1.32 Å) and Ni (1.24 Å) may play a role in the increase of the lattice parameter a. The slight contraction, observed when Cu replaces Mn, may also be partly due to the fact that the covalent radius of Mn (1.39 Å) is slightly larger than that of Cu. However, the lattice contraction with the replacement of Ga by Cu (S sub-lattice) can not be understood in terms of the difference in the covalent radii alone. In this regard, we note that in these compounds, metallic bonding is also prevalent and it too is expected to play a crucial role.

ii) Prediction of the martensite transition - Here, we try to predict whether a system is likely to show martensite transition or not based on its energetics. For a thorough calculation of structural phase transitions from first-principles, apart from total energy, also the various contributions to the free energy, as vibrational, electronic and, if applicable, also magnetic entropy must be determined.[83, 84] This is computationally demanding in particular for off-stoichiometric compositions hindering the identification of simple heuristic trends from electronic structure theory. In the literature, it was thus attempted to

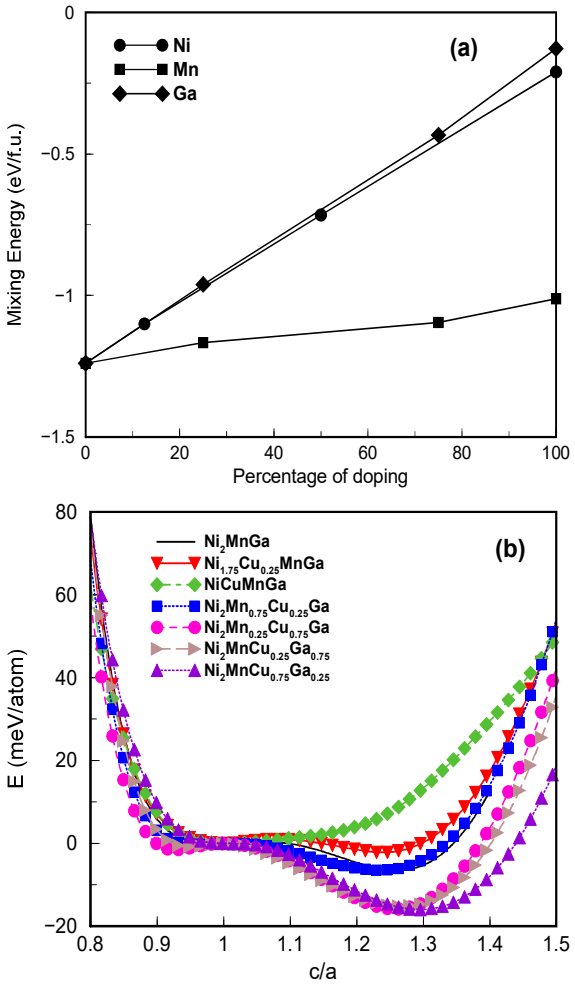

Figure 2.1: (a) Mixing energy in eV per formula unit as a function of Cu substitution at different sites in Ni_2MnGa. The line is only guide to the eyes. (b) Energy in meV/atom as a function of c/a for different Cu-doped Ni_2MnGa systems. The energy (E) of the martensite phase is normalized with respect to the austenite phase. $c/a = 1$ corresponds to the austenite phase. The lines are guide to the eyes only.

Table 2.2: Total energy differences (ΔE in meV/atom) between the austenite and the martensite for all the Cu substituted Ni_2MnGa materials obtained from VASP calculations are given in second column, which give a relative estimation of theoretical transition temperatures of different compounds. Whenever there is no sign of a tetragonal phase or magnetism, the ΔE values are not given and a dash is put instead. Third column gives the e/a, the number of valence electrons per atom. The last column gives the information about the possibility of a martensite transition - Y stands for possible transition and N stands for no transition; an estimate of T_M in Kelvin based on ΔE. Note: The ΔE and T_M values presented in this table are only for the predicted MSM alloys

Material	ΔE (meV/atom)	e/a	volume Å^3	austenite to martensite
Ni_2MnGa	6.5	7.5	196.12	Y
$Ni_{1.75}Cu_{0.25}MnGa$	2.17	7.5625	197.82	Y (25K)
NiCuMnGa	-	7.75	202.71	N
Cu_2MnGa	-	8	211.81	N
$Ni_2Mn_{0.75}Cu_{0.25}Ga$	6.45	7.75	194.52	Y (65K)
$Ni_2Mn_{0.25}Cu_{0.75}Ga$	15.83	8.25	190.78	Y (165K)
Ni_2CuGa	-	8.5	189.51	Y
$Ni_2MnGa_{0.75}Cu_{0.25}$	16.11	8	194.25	Y (165K)
$Ni_2MnGa_{0.25}Cu_{0.75}$	15.95	9	190.68	Y (165K)
Ni_2MnCu	20.5	9.5	188.43	Y (210K)

correlate other physical observables to the martensitic transition temperature in order to obtain heuristic rules for compositional trends. These quantities were in particular number of valence electrons per atom, elastic constants, energy difference between austenite and the martensite phases (ΔE), etc.[4, 18, 85–88] e/a, *i.e.* the number of valence electron per atom has been identified to be closely related to T_M in a large variety of Heusler alloys. The larger the e/a, the larger is the T_M. Such a correlation often holds good within one alloy system, but it is frequently seen to break down when the C-components or the type of order are changed, *e.g.*, for Ni_2MnGa and Mn_2NiGa, where the former has larger e/a but smaller T_M. Chen *et. al.* argued that a better agreement may be obtained when the effect of volume is incorporated.[85] But such a description pays only restricted attention to the specific details of the electronic structure of the system, which are important for the martensitic instability.[23] The band Jahn-Teller anomaly has significant effect on the elastic constants, as it leads, in particular, to a softening of C', which in turn can be used to improve the prediction of T_M, if the composition and temperature dependence are taken into account.[86, 87] For a given system, a simple comparison of the theoretical energy difference ΔE between the austenite and martensite state as a func-

tion of composition can also provide an estimate of T_M within a reasonable confidence interval, as shown, *e.g.* by Barman *et. al.*[18] This requires a comparison of ΔE with the experimental transition temperature of a reference composition. The entropic contributions are neglected, which are assumed to vary only slowly with composition. In the following, thus, we analyze the values of ΔE and make a heuristic prediction of T_M of Ni_2MnGa and also Mn_2NiGa based materials as a function of increasing Cu substitution at different sites. However, to make a final statement, finite temperature calculations, taking into account the entropic contribution or detailed experimental measurements are required which are beyond the scope of the present work.

The martensite phase, that is the low temperature phase, is more stable when the total energy difference between the austenite and the martensite phases (ΔE) is positive subject to the condition that the calculations of energy for both the phases are performed at the respective optimized lattice constants within the same set of calculational parameters. We note that as a first approximation, ΔE can be considered to be proportional to $k_B\mathrm{T}_M$, where T_M is the martensite transition temperature and k_B is the Boltzmann constant and hence, ΔE can provide an estimate of T_M.[18, 88] We have estimated T_M by using an empirical linear plot (taking cue from Ref.[18]), where the experimental T_M values for known Ni-Mn-Ga compounds as well as some other compounds were plotted against the calculated ΔE values. The T_M values thus obtained are compiled in Table 2.2. Here we mention that when we introduce the linear fit, the transition temperatures of some of the compounds (e.g. Ni_2MnGa) do not quite fall within the confidence interval.[18] The possible reasons behind this observation may be due to the presence of modulation in the martensite phase or due to some disorders, including anti-site disorder. We also note here that the effect of phonons is neglected in the present study. So these empirical values of the predicted transition temperatures may not necessarily be close to the real values of the transition temperatures. However, these estimates are expected to give a reliable trend of martensite transition temperatures of alloys,[18] as the percentage of Cu substitution is increased, however, this needs to be verified experimentally. The experimental trend of increase in T_M with Cu substitution at Mn (R sub-lattice)[10, 20] can be observed from Table 2.2. We probe the trend of T_M for Cu substitution at Ga (S sub-lattice) as

well. We find that ΔE and hence T_M is large for Cu substitution at Ga (S sub-lattice). We observe that alloys with as high as 100% Cu substitution at Mn (R sub-lattice) and Ga (S sub-lattice) are also likely to undergo an austenite to martensite transition. However, unlike the case of Cu substitution at Mn or Ga sites, which exhibits an increase in ΔE value, substantial substitution of Ni by Cu (P or Q sub-lattice) tends to stabilize the austenite phase over the martensite phase (Figure 2.1(b)). We summarize that in Ni_2MnGa, by analyzing both ΔE and T_M values as well as the other bulk properties that Cu substitution at the Ni site has an opposite effect compared to the substitution at the Mn and Ga sites.

iii) Electronic Properties - We now discuss about the effect of the Cu substitution on the electronic structure with respect to the parent material (Ni_2MnGa). In Figure 2.2, we plot the density of states (DOS) as a function of percentage of Cu substitution for the austenite phase of the Cu-substituted compounds along with the unsubstituted compounds. Figure 2.2(a), (b) and (c) depict the results of Cu substitution at Ni, Mn and Ga positions (P and/or Q, R and S sub-lattices), respectively. Figure 2.2(c) shows that

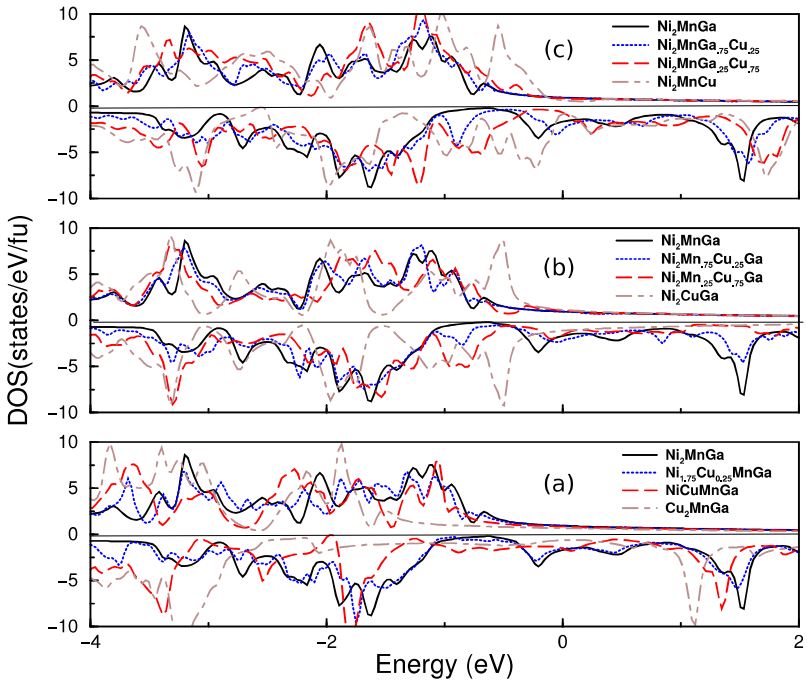

Figure 2.2: Total spin-polarized density of states as a function of energy for different amounts of Cu substitution (a) at the Ni site, (b) at the Mn site, and (c) at the Ga site in Ni_2MnGa. The zero on the X-axis corresponds to the Fermi level.

Ni_2MnCu, where Ga is fully replaced by Cu, has a large DOS near the Fermi level (at

Table 2.3: Bulk properties of the cubic structures and the mixing energy in eV per f.u. for all the Cu-substituted Mn_2NiGa cases. Experimental values, wherever available, are given in parentheses and in bold. The negative value of mixing energy ensures that the compound is more stable than its individual bulk components.

Material	Nature of substitution (sub-lattice)	Lattice constant (Å)	Bulk Modulus (GPa)	Mixing Energy (eV/f.u.)
Mn_2NiGa	None	5.843 (**5.907**)	114	-0.7394
$Mn_{1.75}Cu_{0.25}NiGa$	Mn by Cu (Q)	5.858	100	-0.6897
MnNiCuGa	Mn by Cu (Q)	5.851	182	-0.5454
Cu_2NiGa	Mn by Cu (Q,R)	5.812	144	-0.6483
$Mn_2Ni_{0.75}Cu_{0.25}Ga$	Ni by Cu (P)	5.869	116	-0.6111
$Mn_2Ni_{0.25}Cu_{0.75}Ga$	Ni by Cu (P)	5.910	110	-0.3572
Mn_2CuGa	Ni by Cu (P)	5.940	105	-0.2470
$Mn_2NiGa_{0.75}Cu_{0.25}$	Ga by Cu (S)	5.831	101	-0.4988
$Mn_2NiGa_{0.25}Cu_{0.75}$	Ga by Cu (S)	5.803	117	-0.0678
Mn_2NiCu	Ga by Cu (S)	5.805	...	+0.1276

about -0.5 eV), while these peaks are shifted to lower energy by about 0.5 eV in case of the parent Ni_2MnGa. As discussed for the bulk properties including the lattice constant, Cu substitution at Ni site in Ni_2MnGa yields quite different energetic properties when compared to the substitution at Mn and Ga sites. We have already discussed that the possibility of a transition from the austenite to the martensite phase keeps decreasing as ΔE keeps decreasing with increase in Cu substitution at the Ni site (Figure 2.1(b)). Subsequently, it is clear from our results that while Ni_2MnGa shows a martensite transition, Cu_2MnGa does not. It is expected that cubic phase of Cu_2MnGa is more stable since the majority of the DOS of the austenite phase of Cu_2MnGa shifts away from the Fermi level towards higher binding energy compared to the case of Ni_2MnGa. It is possible that this gives stability to the austenite phase which might render a martensite transition unlikely in case of Cu_2MnGa.

2.2.2 Cu substitution at different sites in Mn_2NiGa

i) Stability and Bulk Properties - The overall interesting results as well as the possibility of a large Cu substitution at different sites in Ni_2MnGa have motivated us to explore Cu substitution in Mn_2NiGa. Now, we discuss about the effects of Cu substitution at various sites of Mn_2NiGa, on electrnic stability and bulk mechanical properties. We observe that

the substitution of Cu at different sites is energetically possible in all the compositions studied, except for Mn_2NiCu (Table 2.3). While the replacement of Mn by Cu seems to perturb the system energetically the least (Figure 2.3(a)), replacing Ga by Cu turns out to be energetically the least favorable.

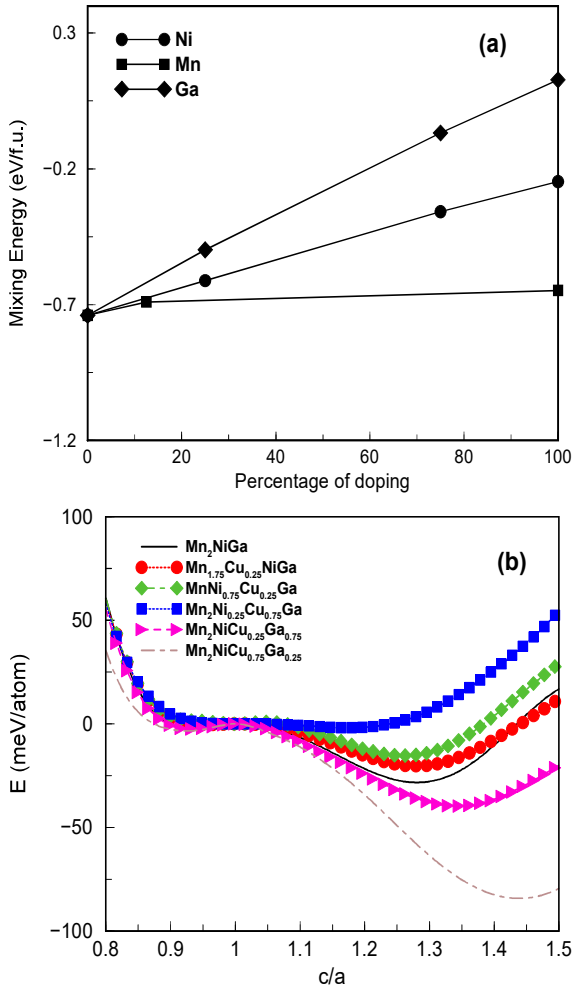

Figure 2.3: (a) Mixing energy in eV/f.u. as a function of Cu substitution at different sites in Mn_2NiGa. The line is only guide to the eyes. (b) Energy in meV/atom as a function of c/a for different Cu-doped Mn_2NiGa systems. The energy (E) of the martensite phase is normalized with respect to the austenite phase. $c/a = 1$ corresponds to the austenite phase. The lines are guide to the eyes only.

We discuss here the probable reasons of the difference in stability of both the materials Ni_2MnGa and Mn_2NiGa when Cu substitutes the Ni, Mn or Ga atoms. In this context, we note here that the stabilizing effect of an s, p element at the C position in Heusler alloys with stable martensite phase is well established in the literature. As shown by Zayak et. al.[89], the stability of the Ni_2MnGa type Heusler alloys is known to be closely related to the minority (spin down) DOS at the Fermi level.[23] A double peak structure is observed

at the Fermi level indicating a covalent interaction between the Ga $4p$ and Ni $3d$ states, which is caused by the $4p$ and $3d$ hybridization. This covalent interaction between the Ga $4p$ and Ni $3d$ spin down states is known to play a crucial role in the stability. Our analysis of the partial DOS shows the signature of this strong hybridization at the Fermi level for the systems which are stable. The Cu substitution at the Ga site lacks this strong $4p$ and $3d$ hybridization. Similarly, when Cu replaces Ni, higher binding energy of the Cu atom in comparison to Ni leads to a much reduced DOS at the Fermi level. This is not the case in case of Mn replacements by Cu, such as in non-magnetic Ni_2CuGa and Mn_2CuGa which agrees with the results in the literature.[89] So the covalent interaction in the system is significantly reduced when Cu substitutes either Ni or Ga. We find from the partial DOS that in the stabler materials, the $3d$-$3d$ interaction between the atoms at the A and B position is also more predominant.

Overall, the results of energetics are qualitatively quite similar to those of Ni_2MnGa.

Further, we concentrate on the bulk properties including the lattice constant. As is observed in case of Ni_2MnGa, the lattice constant expands whenever Ni is replaced by Cu (P sub-lattice). On the contrary, for Mn_2NiGa the lattice constants are close or slightly lower compared to the parent compound for Cu substitution at Ga (S) or Mn (R or Q) sites. It is to be noted that there are two possible systems where each of Ni, Mn, Cu and Ga components are present in equal proportion. In MnNiCuGa, (in Mn_2NiGa, out of two Mn atoms, Mn_{Mn} is fully replaced by Cu which occupies the R sub-lattice), Mn and Ni occupy symmetry equivalent positions (P and Q sub-lattices), and Cu (R sub-lattice) and Ga (S sub-lattice) occupy another set of symmetry equivalent positions. On the contrary, in NiCuMnGa, (arrived at by replacing one Ni fully by Cu out of the two Ni atoms in Ni_2MnGa) Ni and Cu occupy symmetry equivalent positions (P and Q sub-lattices), and Mn and Ga occupy another set of symmetry equivalent positions (R and S sub-lattices). We observe that MnNiCuGa is higher in energy compared to the NiCuMnGa case by about 0.45 eV. On the basis of this, we have disregarded the energetically higher configuration of the two (i.e. MnNiCuGa) and will concentrate only on NiCuMnGa. We have also carried out a calculation of Cu_2NiGa where both Mn are replaced by Cu. We observe that in this case, like Mn_2NiGa an inverse Heusler alloy structure is energetically

Table 2.4: Total energy difference (ΔE in meV/atom) between the austenite and the martensite (tetragonal structure) for all the Cu substituted Mn_2NiGa materials obtained from VASP calculations are given in second column, which give a relative estimation of theoretical transition temperatures of different compounds. Whenever there is no sign of a tetragonal phase or magnetism, the ΔE values are not given and a dash is put instead. Third column gives the e/a, the number of valence electrons per atom. The last column gives the information about the possibility of a martensite transition - Y stands for possible transition and N stands for no transition; an estimate of T_M in Kelvin based on ΔE. Note: The ΔE and T_M values presented in this table are only for the predicted MSM alloy.

Material	ΔE (meV/atom)	e/a	volume (Å^3)	austenite to martensite
Mn_2NiGa	28	6.75	199.48	Y
$Mn_{1.75}Cu_{0.25}NiGa$	20	7	200.99	Y (210K)
Cu_2NiGa	-	8.75	196.33	Y
$Mn_2Ni_{0.75}Cu_{0.25}Ga$	15	6.8125	202.13	Y (155K)
$Mn_2Ni_{0.25}Cu_{0.75}Ga$	1.8	6.9375	206.44	Y (17K)
Mn_2CuGa	-	7	209.58	N
$Mn_2NiGa_{0.75}Cu_{0.25}$	39.63	7.25	198.28	Y (410K)
$Mn_2NiGa_{0.25}Cu_{0.75}$	84.20	8.25	195.45	Y (880K)

more stable compared to the conventional Heusler alloy structure. From results of Table 2.1 and 2.2, it is clear that for both the parent compounds, Ni_2MnGa and Mn_2NiGa, the overall effect of Cu substitution is rather similar. In both the alloys substitution at Mn and Ga sites shows similar trend, while substitution at the Ni site displays an opposite trend. This is observed from the martensite phase transition behavior as well, which is discussed below.

ii) Prediction of the martensite transition - We predict the possibility of the martensite transition for all the systems originated from the parent material, Mn_2NiGa. Figure 2.3(b) summarizes the results for ΔE versus c/a for all the substituted Mn_2NiGa compounds. It is interesting to note that the trends of ΔE and hence T_M as a function of Cu substitution are also similar in both Mn_2NiGa and Ni_2MnGa. Large substitution of Cu at Ni (P sub-lattice) in Mn_2NiGa is not likely to favor the martensite transition (Table 2.4). Rather, it tends to stabilize the austenite phase of the system. But the Cu substitution at Mn (R sub-lattice) and Ga (S sub-lattice) helps in stabilizing the martensite phase, and the effect is more pronounced in the case of substitution at Ga site. However, we note that the mixing energies for large amount of substitution of Cu at the Ga site are increasingly unfavorable in this system of materials (Table 2.4).

iii) Electronic Properties - We plot the DOS as a function of percentage of Cu substi-

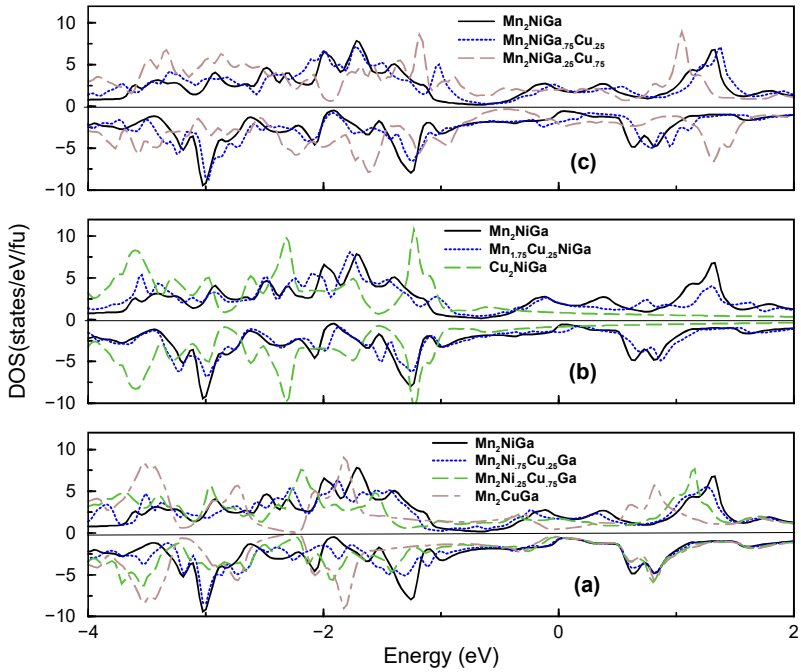

Figure 2.4: Total spin-polarized density of states as a function of energy for different amounts of Cu substitution (a) at the Ni site, (b) at the Mn site, and (c) at the Ga site in Mn_2NiGa. The Fermi level is at 0 eV.

tution for the austenite phase (Figure 2.4). Figure 2.4(a), (b) and (c) depict the results of Cu substitution at Ni (P sub-lattice), Mn (Q, R sub-lattices) and Ga (S sub-lattice), respectively. The DOS as a function of Cu substitution at the Ga and the Mn site show similar nature (Figure 2.4(c) and(b), respectively) as in Ni_2MnGa. The substitution of Cu at the Ni site (P sub-lattice) in both Mn_2NiGa and Ni_2MnGa alloys also has similar effect and also yields properties of the substituted materials which are different compared to when Mn and Ga sites are substituted. It is seen that Mn_2NiGa exhibits a considerable number of states at E_F which can support a martensitic transition while in Mn_2CuGa number of states at E_F becomes low in both spin channels. Overall DOS in Mn_2CuGa shifts to higher binding energy compared to the unsubstituted compound Mn_2NiGa. Further, in Mn_2CuGa, like in Cu_2MnGa, the hybridization between Cu and Mn $3d$ states is rather weak and both Cu and Mn partial DOS shift towards higher binding energies in comparison to Ni and Mn partial DOS in Ni_2MnGa and Mn_2NiGa. All these observations and trends are rather similar to Ni_2MnGa.

Table 2.5: Total magnetic moments per formula unit for the austenite and the martensite phases of Cu substituted Ni_2MnGa. The average moment of Mn atoms is given in the parenthesis in each case. First value in the parentheses corresponds to the average moment of Mn atom, second to the Ni atom, whenever present. It is to be noted that Cu carries almost zero partial magnetic moment.

Material	austenite (μ_B/f.u.)	martensite (μ_B/f.u.)
Ni_2MnGa	4.096 (3.413,0.361)	4.115 (3.348,0.418)
$Ni_{1.75}Cu_{0.25}MnGa$	4.039 (3.444,0.354)	4.090 (3.389,0.426)
NiCuMnGa	3.762 (3.436,0.271)	-
Cu_2MnGa	3.626 (3.578)	-
$Ni_2Mn_{0.75}Cu_{0.25}Ga$	3.184 (3.405,0.326)	3.218 (3.365,0.367)
$Ni_2Mn_{0.25}Cu_{0.75}Ga$	1.157 (3.377,0.159)	1.081 (3.340,0.129)
Ni_2CuGa	0	0
$Ni_2MnGa_{0.75}Cu_{0.25}$	4.240 (3.406,0.433)	4.087 (3.338,0.401)
$Ni_2MnGa_{0.25}Cu_{0.75}$	4.495 (3.387,0.565)	4.105 (3.311,0.402)
Ni_2MnCu	4.292 (3.321,0.506)	4.095 (3.3,0.383)

Table 2.6: Total magnetic moments per formula unit for the austenite and the martensite phases of Cu substituted Mn_2NiGa. The average moments on two inequivalent Mn atoms, Mn_{Ni}, Mn_{Mn}, and Ni atom are given in the parentheses in each case separately. First value in the parenthesis corresponds to the Mn_{Ni} atom, second to the Mn_{Mn} atom and third to the Ni atom, whenever present. It is to be noted that Cu carries almost zero partial magnetic moment.

Material	austenite (μ_B/f.u.)	martensite (μ_B/f.u.)
Mn_2NiGa	1.188 (-2.371,3.172,0.343)	1.005 (-2.365,3.067,0.274)
$Mn_{1.75}Cu_{0.25}NiGa$	0.108 (-2.738,3.228,0.184)	0.180 (-2.676,3.109,0.150)
Cu_2NiGa	0	0
$Mn_2Ni_{0.75}Cu_{0.25}Ga$	0.947 (-2.535,3.193,0.317)	0.926 (-2.439,3.097,0.307)
$Mn_2Ni_{0.25}Cu_{0.75}Ga$	0.549 (-2.733,3.162,0.298)	0.541 (-2.695,3.126,0.294)
Mn_2CuGa	0.333 (-2.825,3.126,-)	-
$Mn_2NiGa_{0.75}Cu_{0.25}$	1.065 (-2.533,3.21,0.357)	0.579 (-2.694,3.092,0.171)
$Mn_2NiGa_{0.25}Cu_{0.75}$	0.817 (-2.798,3.187,0.455)	0.115 (-3.075,3.172,0.026)

2.2.3 Influence of Cu substitution on the magnetic moments

Now we discuss the effects of the Cu substitution on the magnetic moments in case of both Ni_2MnGa and Mn_2NiGa systems. In order to determine the magnetic ground state, we have calculated the total energies of the Cu substituted systems with different starting magnetic configurations.[13, 66] We have probed the phase with net zero magnetic moment (NM) and ferromagnetic (FM) phases in all the cases. We have found that the FM configuration is energetically the most favorable for Cu substituted Ni_2MnGa as in case of the parent compound. The NM phase lies at much higher energy as is observed from the energy versus lattice constant results. In Mn-rich cases, antiferromagnetic (AFM) or ferrimagnetgic (FIM) configurations of two symmetrically inequivalent Mn atoms in the unit cell are also possible. We have probed the AFM configurations as well. As is the case of the parent compound Mn_2NiGa,[11, 12] the resultant magnetic solution is FIM in nature for different Cu substituted Mn_2NiGa alloys. However, the energy difference of this phase with respect to the FM phase is relatively small. The NM phase has much higher energy compared to the FM and AFM phases. In Table 2.5 and 2.6, we list the total magnetic moments as well as the magnetic moments of the Mn (also Ni) atoms for the Cu-substituted alloys of Ni_2MnGa and Mn_2NiGa, respectively. The total magnetic moments of Ni_2MnGa in the austenite and martensite phases are 4.096 and 4.115 μ_B, while for Mn_2NiGa these are 1.188 and 1.005 μ_B, respectively. In case of Ni_2MnGa the moment of the austenite phase is smaller than that of the martensite phase, while in case of Mn_2NiGa the trend is the opposite. For Ni_2MnGa the lowest energy solution is ferromagnetic in nature, while Mn_2NiGa has a ferrimagnetic solution. These trends and the absolute values of the magnetic moments of these materials are in very good agreement with the results of existing literature.[12, 90] As is the trend in case of parent compounds, the overall moments of Cu substituted Ni_2MnGa system have much larger values compared to the total moments of Cu substituted Mn_2NiGa, as the latter has basically ferrimagnetic character.

Mn-based alloys are generally systems where the moment is primarily due to the Mn atom.[38] This is clear from Tables 2.5 and 2.6 which display the moments of the Mn atoms along with the total moments for Cu-substituted alloys of Ni_2MnGa and Mn_2NiGa,

respectively. As is discussed in the literature[91], the moments of Mn atoms in substituted Ni_2MnGa systems are found to have large value, the maximum being about 3.6 and minimum about 3.2 μ_B. For substituted Mn_2NiGa systems Mn_{Mn} atom has moments between about 3 to 3.3 μ_B. Mn_{Ni} atom has smaller moments and has a ferrimagnetic orientation with respect to Mn_{Mn} atom. The values of moments of Mn_{Ni} atom are in the range of about 2.3 to 3 μ_B. Since the moment of the Mn atom is most crucial for the magnetism in these two alloy systems, the total moment goes down when Cu substitution is increased at the Mn site itself. Consequently, for 100 % substitution at the Mn site, the systems turn out to zero net magnetic moment. As expected, the same trend is observed for the austenite as well as the martensite phases for both Ni_2MnGa and Mn_2NiGa.

Interestingly, in the austenite phase of Ni_2MnGa, the replacements of Ga by Cu (at S sub-lattice) induce larger moments in the system leading to a slightly stronger ferromagnetic system. This is possibly due to the stronger Ni-Mn interaction which prevails due to the reduction in the lattice constant as a result of Cu substitution at the Ga site. This reduction leads to an increased moment in Ni due to stronger coupling between Ni and Mn, as has already been observed in the literature for other Mn based compounds.[91] To understand the exchange coupling between Ni and Mn further, we calculate the exchange coupling constant as a function of the normalized distance between Mn and Ni in case of Ni_2MnGa and Ni_2MnCu using the SPR-KKR programme package.[56] The results of these calculations are plotted in Figure 2.5. It is clearly seen from this figure that the exchange coupling parameters between Ni and Mn in Ni_2MnCu are larger, vindicating our argument about the increase in interaction between these two atoms in this material. However, in the martensite phase of Ni_2MnGa where Cu substitutes Ga, the total and the partial moments remain very close to those of the parent compound. It is observed that in the austenite phase, the difference between the nearest-neighbor (NN) distances (d_{Ni-Mn},$d_{Ni-Ga/Cu}$,d_{Mn-Ni}) of Ni_2MnGa and Ni_2MnCu is 0.032 Å. On the other hand, in the martensite case, the same differs by 0.013 Å. It is possible that due to the smaller compression in the martensite phase as a result of substitution of Cu at the Ga site, the moments are affected less. Therefore, in the martensite phase the substituted system retains values of the total and partial magnetic moments close to those of the parent com-

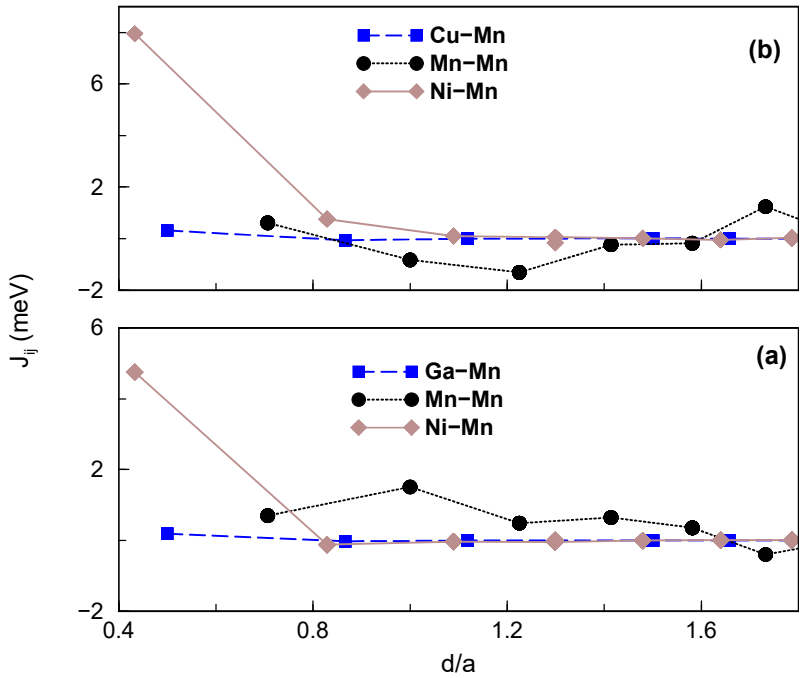

Figure 2.5: Heisenberg exchange parameters J_{ij} of Mn atom with its neighbors as a function of normalized distance, d/a, where a is the respective lattice constants of the austenite phases for cubic (a) Ni_2MnGa and (b) Ni_2MnCu. The lines are guide to the eyes only.

pound. Similar to Ni_2MnGa, in case of Mn_2NiGa as well, the lattice constant decreases with Cu substitution at Ga site. There are two types of Mn atoms: (a) Mn_{Mn} (at R sub-lattice), (b) Mn_{Ni} (at Q sub-lattice). We observe that the effective moments of Ni change in both the austenite and martensite phases. The moment of the Ni atom, which has only Mn and Ga atoms as NN, increases as the distance between Ni and its NN atom decreases. In case of Mn, something interesting happens. The Mn_{Mn} atom (at R sub-lattice) has similar moments (absolute value about 3.2 μ_B) throughout the substitution. However, Mn_{Ni} (at Q sub-lattice) with Cu and/or Ga as one of the NN, has increasingly larger absolute value of moment (absolute value about 2.4, 2.5 and 2.8 μ_B for 0 %, 25 % and 75 % substitution, respectively). This in turn brings the moments of the two Mn atoms close to each other which is about 3 μ_B. Since Mn_{Ni} and Mn_{Mn} have anti parallel alignment of moments, this results in an increasingly better ferrimagnetic arrangement. Consequently, this leads to a situation where the total moment of the system primarily comprises of the moment of Ni atom only. The overall trend for the total moment of the system is similar in both austenite as well as martensite phases.

In case of Ni_2MnGa, when Ni is replaced by Cu (at P and/or Q sub-lattice), the total moment shows a trend of slow decrease with increase in Cu concentration. This is because, though Mn is providing marginally higher moments as the substitution increases, the average moment at the Ni site decreases as Cu has no significant moment. The same trend is observed in the martensite case as well. Similar to Ni_2MnGa, when Cu replaces Ni (P sub-lattice) in Mn_2NiGa, the average moment at the Ni site goes down as Cu has a much smaller moment than Ni. Consequently, the Mn atoms have closer but opposite moments. Hence, the FIM interaction between the two nearest neighbour Mn atoms gets stronger.

2.3 Part B: Results and Discussions

Now, we present our results of Cu, Pt and Pd substitution at Ni site in Ni_2MnGa on elastic, electronic and magnetic properties. To simulate the substitution at Ni site in Ni_2MnGa, we have replaced the Ni atom at its respective site by these substituent atoms. Commonly used structures, the conventional Heusler and inverse Heusler alloy structures have been tested for all these materials and conventional structures are found to possess lower energy. On the other hand, for calculations on Mn_2NiGa, the inverse Heusler structure has been used as it has been found to be lower in energy.[92]

2.3.1 Electronic Stability of substituted Ni_2MnGa

We discuss now the electronic stability of Ni_2MnGa, and the derivatives of this alloy with substitution at Ni site. To analyze the electronic stability, we plot the total DOS of Ni_2MnGa, Pt_2MnGa, Pd_2MnGa and Cu_2MnGa in Figure 2.6 at the respective optimized lattice constants. A double peak structure, as well as a clear pseudogap close to the Fermi level for one of the spin channels are observed in all the materials except in Cu_2MnGa. These features arise due to hybridization between the Ga $4p$ and the outermost d-electrons of the transition metal atoms (Ni, Pt and Pd) and this is known to play a crucial role in the stability of these types of materials.[89, 93] On the other hand, the peak occuring just below the Fermi level (at about -0.2 to -0.4 eV) is expected to give rise to a band Jahn-Teller instability giving a lower symmetry lowest energy structure in Ni_2MnGa, Pt_2MnGa

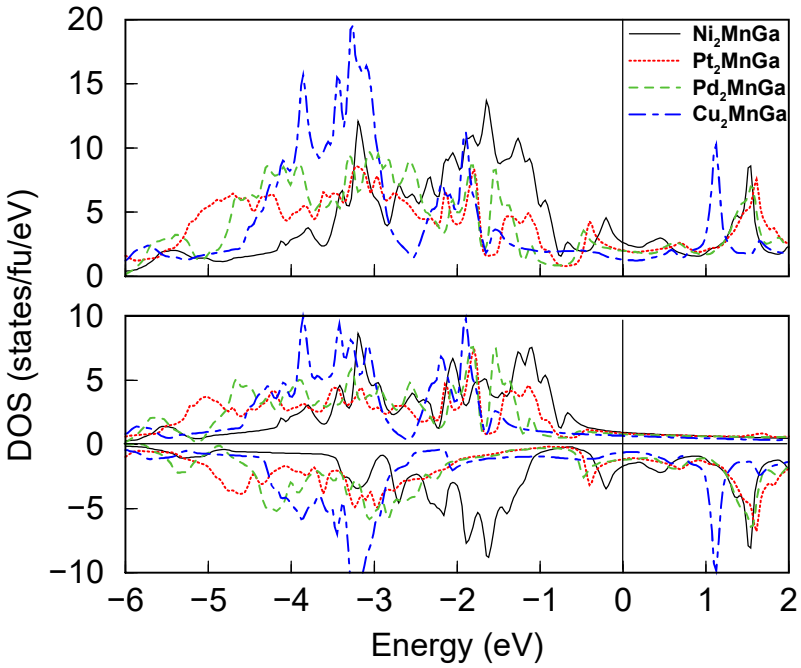

Figure 2.6: Total DOS of Ni_2MnGa, Pt_2MnGa, Pd_2MnGa and Cu_2MnGa at the respective optimized lattice constants. For Ni_2MnGa there is a double peak structure around the Fermi level, with one peak at -0.199 eV and the other at 0.482 eV. There is a dip or pseudo-gap at -0.453 eV. For Pt_2MnGa, the peaks are at -0.418 and 0.643 eV, while for Pd_2MnGa these peaks are at -0.465 and 0.6 eV. The respective pseudo-gaps are at -0.661 and -0.799 eV for Pt_2MnGa and Pd_2MnGa, respectively. The lower panel gives the spin-polarized DOS of the same materials. For further details, see text.

and Pd_2MnGa, but not in Cu_2MnGa.

To gain further insight, we present here the partial DOS (PDOS) of some of the materials. Figure 2.7 shows the PDOS of Ga atom and its nearest neighbor Pt atom in Pt_2MnGa. For comparison, in Figure 2.8, we show the PDOS of Ga atom and its nearest neighbor (NN) Ni atom in Ni_2MnGa. From analyzing Figures 2.7 and 2.8, we observe a double peak structure at the Fermi level for down spin channel in the PDOS of both Ga and its NN atom, Pt and Ni, for Pt_2MnGa and Ni_2MnGa respectively. This indicates hybridization of Ga $4p$ and Ni (or Pt) $3d$ (or $5d$) electrons in down spin channel leading to stability of the material as discussed in the literature.[89] Similar features appear when the PDOS of Ga and its nearest neighbors in Mn_2NiGa (NN of Ga: Ni and Mn_{Ni}) as well as Pd_2MnGa (NN of Ga: Pd) are analyzed. From the PDOS of Ga as well as its NN atoms, we observe the double peak structure at and a pseudogap close to the Fermi level. This is a signature of hybridization between Ga and its NN atoms. On the contrary, the total DOS as well as PDOS of Cu and its nearest neighbor Ni, in Cu_2MnGa, shows no

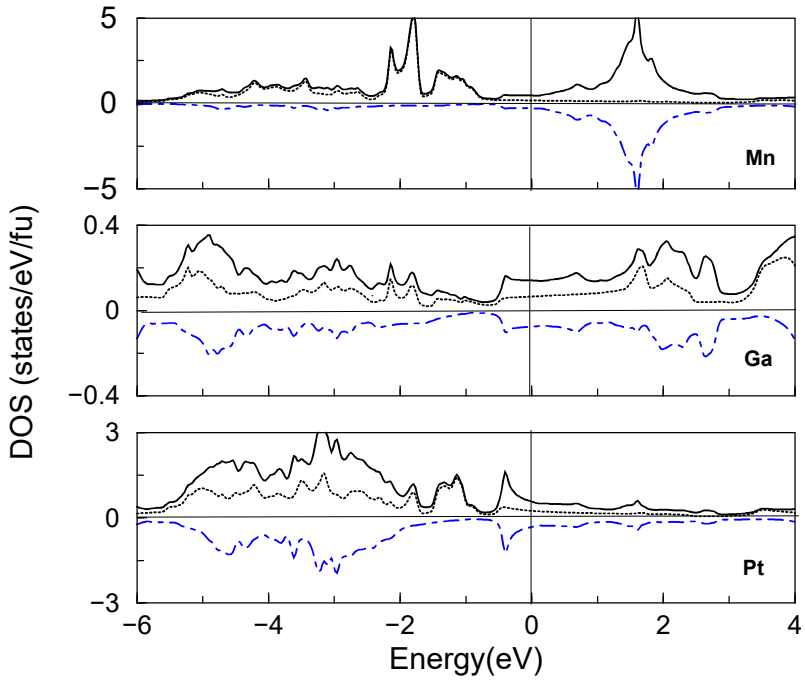

Figure 2.7: PDOS of Ga atom and its nearest neighbor Pt atom in Pt_2MnGa. The solid, dotted and dot-dashed lines represent total, up and down spins, respectively. The extent of hybridization between the Ga and its nearest neighbor atom is shown (see text). The PDOS of Mn atom is also provided for showing the exchange-splitting.

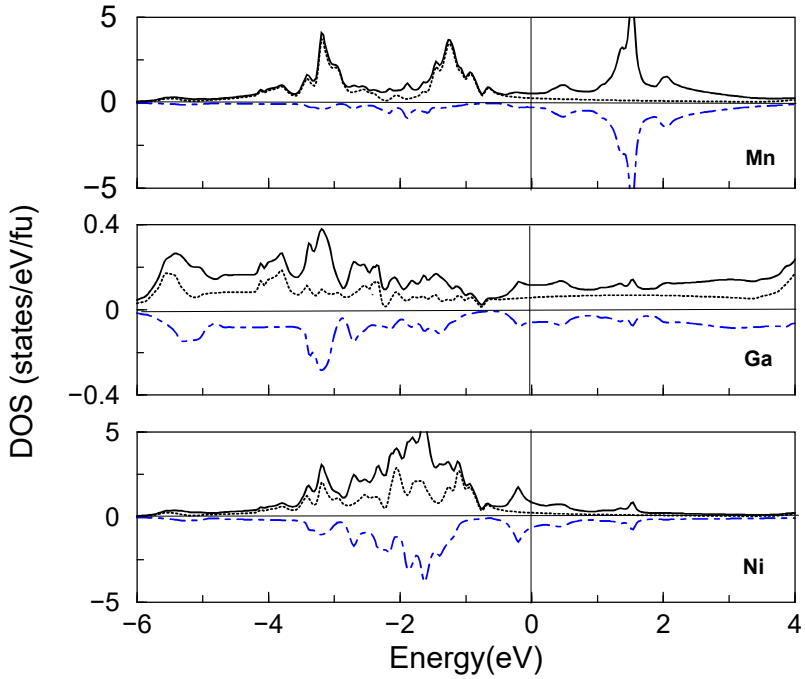

Figure 2.8: PDOS of Ga atom and its nearest neighbor Ni atom in Ni_2MnGa. The solid, dotted and dot-dashed lines represent total, up and down spins, respectively. The extent of hybridization between the Ga and its nearest neighbor atom is shown (see text). The PDOS of Mn atom is also provided for showing the exchange-splitting.

Table 2.7: Total magnetic moments per formula unit for the austenite phases of Cu, Pt, Pd and Mn substituted Ni_2MnGa as well as T_C values are listed here. The average partial moments are given in the parentheses. In the first four rows, first value in the parentheses corresponds to the average moment of Mn atom, second value to the Ni, Pt, Pd and Cu atom, whichever present. For Mn_2NiGa, first value in the parenthesis corresponds to the Mn_{Ni} atom, second to the Mn_{Mn} atom and third to the Ni atom.

Material	Moments (μ_B/f.u.)	T_C (K)
Ni_2MnGa	4.096 (3.413,0.361)	414
Pd_2MnGa	4.151 (3.928,0.121)	206
Pt_2MnGa	4.155 (3.845,0.139)	176
Cu_2MnGa	3.626 (3.578, 0.04)	800
Mn_2NiGa	1.188 (-2.371,3.172,0.343)	775

such double peak structure at the Fermi level as well as there is no clear pseudo-gap close to the Fermi level for either up or down spin channels. Further, due to the (nearly) full d-band of Cu, the d-orbitals are centered at different energies compared to Ni. These lead to a lack of strong hybridization for A_2BC systems, between the atoms in the A and the C positions in the Cu-based material and consequently a weaker covalent character. The filling up of the pseudo-gap and decrease in the intensity of the peak close to Fermi level indicate a weaker Jahn-Teller instability. The overall electronic stability of the cubic phase is a resultant of these effects. Notably the mixing energy calculations in the first part of this chapter have shown that the Cu-derived material is much less stable compared to the parent Ni_2MnGa compound. We concentrate in this part of the chapter (Part B) mainly on Pt and Pd substitution at the Ni site of Ni_2MnGa.

2.3.2 Magnetic Properties of substituted Ni_2MnGa

In this subsection, we discuss about the magnetic properties of substituted Ni_2MnGa systems. In Table 2.7 we give the magnetic moments calculated using all-electron WIEN2k package.[49] Here also, we focus on the effects Pt and Pd substitution at the Ni site of Ni_2MnGa, as in the Part A of this chapter, we discussed the effects of Cu substitution at different sites of Ni_2MnGa.The total moments increase as Ni is replaced by Pd and Pt at the Ni site in Ni_2MnGa. This increase is due to the larger moment at the Mn site. As the Ni atom is replaced by Pd or Pt, the lattice constant increases, leading to larger a Mn-Mn distance. This probably gives rise to a stronger atomic-like moment in Mn. On

the contrary, the moment of the A atom (Pt or Pd) is smaller than the one found in case of Ni_2MnGa. We have further calculated the Heisenberg exchange coupling constants using SPR-KKR package.[56] We use local density approximation for the exchange correlation functional.[46] It is observed that for all the materials, in comparison to the other magnetic coupling terms, the nearest inter-site exchange interaction term is the most important one. Typically the dominant exchange interactions in most cases are confined to a cluster of radius (R_{ij}) less than or equal to the lattice constant (a), which we have observed in the cases of Ni_2MnGa and Ni_2MnCu in the first part of this chapter. In Table 2.7, we also present T_C calculated from the Heisenberg exchange coupling constants within a mean field approximation as has been done earlier in the literature.[81] It is to be noted that the experimental T_C of Ni_2MnGa and Mn_2NiGa are 376K and 588K, respectively. Keeping in mind that T_C calculated from a mean field-approximation always gives an overestimation of T_C, we find that while the agreement between the experimental and our theoretical result is good in the former material, the mismatch in case of the latter is quite evident. We find that Pt_2MnGa has a much lower T_C value compared to that of Ni_2MnGa. This is in agreement with the experimental (as well as theoretical) trend of lowering of T_C values as a function of Pt-doping in Ni_2MnGa.[4] We now probe the reason behind this observation. From Table 2.7, it is noted that the A atom in Pt_2MnGa has a lower moment (0.139 μ_B) compared to the moment on Ni atom (0.361 μ_B) in Ni_2MnGa. Subsequently, the A-Mn exchange interaction is found to be weaker in the former compound.[94] Since the A-Mn exchange interaction is the dominant exchange coupling in these materials, T_C is much smaller in case of Pt_2MnGa. Further, in Heusler alloys, it has been shown that T_C increases upon hydrostatic pressure, *i.e.* dT_C/dp is greater than 0.[81] In other words, a positive pressure coefficient of T_C is likely to exist in these materials due to an increased overlap. In the present case the larger lattice constant in the case of Pt-material may have led to a reduction of overlap, in turn, leading to a smaller T_C. Furthermore, we observe that the T_C shows an anomalous dependence on the total magnetic moment[81] when Ni is replaced by Pt or Pd in the material Ni_2MnGa, namely, the T_C value decreases when the total magnetic moment increases as a result of Pt or Pd substitution at the Ni site. Though for the isoelectronic elements, Ni, Pd and Pt, where the number of valence

electrons are the same, the total moments increase from Ni_2MnGa to Pt_2MnGa (Table 2.7), the individual moment on the Ni atom is more than that on Pt/Pd. This causes a reduction of the strength of direct interaction in the Pt/Pd-based materials and the J_{ij} values, hence the value of T_C. This trend is in agreement with the literature.[95] On the other hand, for Mn_2NiGa, since Mn atom (Mn_{Mn}) is the next nearest neighbour of another Mn atom (Mn_{Ni}) with a ferrimagnetic configuration between the two, this leads to a low value of total magnetic moment, but individual moments on each type of Mn (Mn_{Mn} and Mn_{Ni}) are high as seen in Table 2.7. In this material, therefore, the exchange interaction (J_{ij}) between two types of Mn atoms (Mn_{Mn}, Mn_{Ni}) is much stronger[96] which may have given rise to a high Curie temperature as reported in the literature.[11] Hence, to summarize, we observe here that, there seems to exist no consistently linear relationship between the value of the total moment and the T_C of a material as is also observed in case of experimental results of Ni_2MnGa[5, 6] versus Mn_2NiGa[11] as well as observed in other Heusler alloys.[97] Furthermore, the influence of choice of the XC potential on T_C has also been probed. The listed T_C values have been obtained using LDA XC potential.[46] It has been observed that in most of the cases, the values of T_C obtained using GGA are close to but slightly higher compared to the values obtained using LDA, with a maximum deviation of 100 K. However the trends remain consistent.

2.3.3 Elastic Stability of substituted Ni_2MnGa

In this section, we discuss the mechanical stability of the cubic austenite phase of Ni_2MnGa and its substituted alloys. For cubic lattices, there are only three independent elastic constants, C_{11}, C_{12} and C_{44}, and from symmetry, we have the following conditions: $C_{11} = C_{22} = C_{33}$; $C_{12} = C_{23} = C_{13}$ and $C_{44} = C_{55} = C_{66}$. Table 2.8 lists all the relevant elastic constants along with the lattice parameters calculated for all the materials studied here using the CASTEP programme package.[53] The optimized geometries are found to be very similar to the geometries obtained using the VASP programme package.[51, 52] It is well-known that the elastic constants C_{44}, $C' = 0.5*(C_{11} - C_{12})$ and $C_L = 0.5*(C_{11} + C_{12} + 2C_{44})$ can be directly measured from experiments and are related to the TA_1, TA_2 and LA accoustic phonon modes.[24] Here we compare our calculated data with the

experimental results wherever available in the literature. For Ni_2MnGa, we observe that the values of C_{11}, C_{12} and C_{44} agree quite well with the available experimental values of Worgull et. al.[24] and Stenger et. al.[25] However, these results are different from the data obtained from an earlier experiment of Vasilev et. al.[98] and the issue of this mismatch has already been addressed in detail by Worgull et. al.[24] For Mn_2NiGa also, we observe that the values of C_{11}, C_{12} and C_{44} agree well with the available experimental values of Jian-Tao et. al.[99]

For cubic crystal it is well known that the *elastic stability criteria* are as follows[78]: $C_{11} > 0$; $C_{44} > 0$; (C_{11} - C_{12}) > 0 ; (C_{11} + $2C_{12}$) > 0. From Table 2.7, it is observed that while most of the criteria are satisfied for all the materials, for some of them, the 3rd one is not, which then leads to a negative C' value for those (Cu_2MnGa, Mn_2NiGa and Pt_2MnGa). For the remaining materials, the computed value of C', the tetragonal shear constant, is positive but quite close to zero, indicating that, for *all* the materials studied here, the cubic austenite phase tends to become unstable with respect to a tetragonal distortion. To this end, calculation of elastic constants for the tetragonal martensite phase along with the cubic austenite phase for these materials can be interesting to compare. These calculations have been carried out in the next chapter, for some of these materials.

Now we discuss the two isotropic mechanical parameters, which are also important modulii for applications, namely, *bulk modulus* and *shear modulus*. The bulk modulus, B, which is a ratio of volume stress and volume strain and represents the resistance to fracture. It is connected to the elastic constants as follows: $B = (1/3)*(C_{11} + 2\ C_{12})$. The calculated values of B have been listed in Table 2.7. The isotropic shear modulus, G, which is the ratio of shearing stress and shearing strain, is related to the resistance of the material to the plastic deformation. Typically, G is calculated as an average value of the shear modulii given by formalisms of Voigt (G_V)[100] and Reuss (G_R)[101], which means $G = (G_V + G_R)/2$. Here it is worth-noting that, in calculating the G, Voigt made an assumption that homogeneous strain is maintained throughout the stressed sample while calculating the modulii. On the contrary, Reuss's calculation of the modulii was based on the assumption that homogeneous stress is maintained throughout the stressed sample in all directions. However, Hill[102] later concluded that the true

Table 2.8: Calculated bulk mechanical properties of Ni_2MnGa and its substituted materials

Elastic properties	Ni_2MnGa	Cu_2MnGa	Mn_2NiGa	Pt_2MnGa	Pd_2MnGa
Lattice parameter(Å)	5.82 5.81[92] 5.82[1]	5.96 5.96[92]	5.87 5.84[92] 5.90[11]	6.23	6.21
Bulk modulus (B)(GPa)	158.78 161[92],146[24] 170[103],156[104]	117.56 118[92]	114.76 114[92] 115.51[99]	177.40	146.75
Shear modulus (G_V)(GPa)	66.26 63.6[24],61.4[25], 57.96 [105],80.4[98]	53.65	64.57 67.16[99]	30.31	50.13
Shear modulus (G_R)(GPa)	6.19 10.56[24],14.78[25] 18.44[105],77.69[98]	-0.13	-17.39 -60.46[99]	-128.04	9.07
G_V/B	0.42	0.46	0.56	0.17	0.34
C_{11} (GPa)	162.20 152.0[24], 156[25], 139.4[105],213[98]	117.49	106.28 90.55[99]	145.75	151.94
C_{44} (GPa)	108.72 103[24], 103[106], 98[25], 91[105]	89.45	111.87 124.42[99]	66.34	80.95
C_{12} (GPa)	157.07 143[24], 143[25], 122.6[105], 87[98]	117.60	119.00 128[99]	193.22	144.16
C^p (GPa)	48.35 40[24], 45[25], 31.6[105], -5[98]	28.15	7.13 3.58[99]	126.88	63.21
C'(GPa)	2.57 4.5[24], 14[99] 8.4[105], 63[98],	-0.05	-6.36 -18.72[99]	-23.73	3.89
Poisson's ratio	0.31	0.30	0.26	0.42	0.36

values of the shear modulii would lie in between the two values given by Voigt[100] and Reuss[101] and can be considered as an average of the two. The argument given by him is that the samples can not be in equilibrium under the assumption of constant strain or constant stress. In many cases the difference between the values given by these two methods is within the experimental accuracy. Hence, although there is no particular justification given in the literature for using the Hill's averaging method, it is generally used and, by and large, it seems to work well. Analytical expressions of G_V and G_R in terms of elastic constants are given as: $G_V = (1/5)*(C_{11} - C_{12} + 3*C_{44})$ and $G_R = (5*C_{44}*(C_{11} - C_{12}))/(4*C_{44} + 3*(C_{11} - C_{12}))$. Table 2.7 lists all the G_V and G_R values for all the materials. We observe that the G_V values agree well with the experimental values (which are derived from the experimental elastic constants C_{11}, C_{12} and C_{44} for both Ni_2MnGa and Mn_2NiGa) wherever the results are available. The G_R values are found to

differ considerably from the G_V values. In all cases studied here, including the parent compounds, G_V is found to have reasonable value, but the value of G_R is very different which is contrary to the general trend where the two values are very close and while G_V gives the higher limit, G_R sets the lower limit. We note that G_V and G_R being close to each other is a general trend which is observed in the literature for predominantly half-metallic or semiconducting full and half-Heusler alloys.[107–110] Therefore, we probe now the reason behind the *large underestimation* of G_R values for all the compounds studied here. A well-known observation is : for stable cubic crystals, typically the value of C_{11} is 2 to 2.2 times greater than each of the remaining constants. But from Table 2.7, it can be noted that the values of C_{11} are only slightly different from those of C_{12} and this small difference is either positive or negative for all the alloys. Further, as a result of this small difference between C_{11} and C_{12}, the constant C' is seen to possess either a negative value or a value close to zero when positive. From the expressions of the shear modulii, it is seen that the difference between C_{11} and C_{12} (= 2*C') comes as a multiplicative factor in the numerator in the expression of G_R, unlike G_V. Hence, a small value of C' manifests itself in bringing down the value of G_R. On the contrary, 2*C' comes only as an additive factor in the numerator of the expression of G_V, so a large dominance of the C_{44} term in the expression yields reasonable values of G_V for all the compounds. It is worth-noting here that in the literature it has been shown that shear modulii obtained from Voigt formalism (G_V) and Reuss formalism (G_R) for many materials, including few Heusler alloys, are very close as discussed above. Further, we wish to point out here that since the experimental G_V values (derived from the experimental elastic constants) agree with the calculated data on the materials studied here, we consider only the G_V value as the shear modulus (G) for further consideration, though it is to be noted that G_V is typically expected to be the higher limit of G. Since in our further discussion, we are only interested in the relative values or in the trend of different mechanical properties, the slightly higher value of the shear modulus is not expected to affect the following analysis of the results.

We now focus on the value of *Cauchy Pressure*, C^p, which is defined as C^p = C_{12} - C_{44}. According to Pettifor[111], *a simple relationship exists between the sign of* C^p *and*

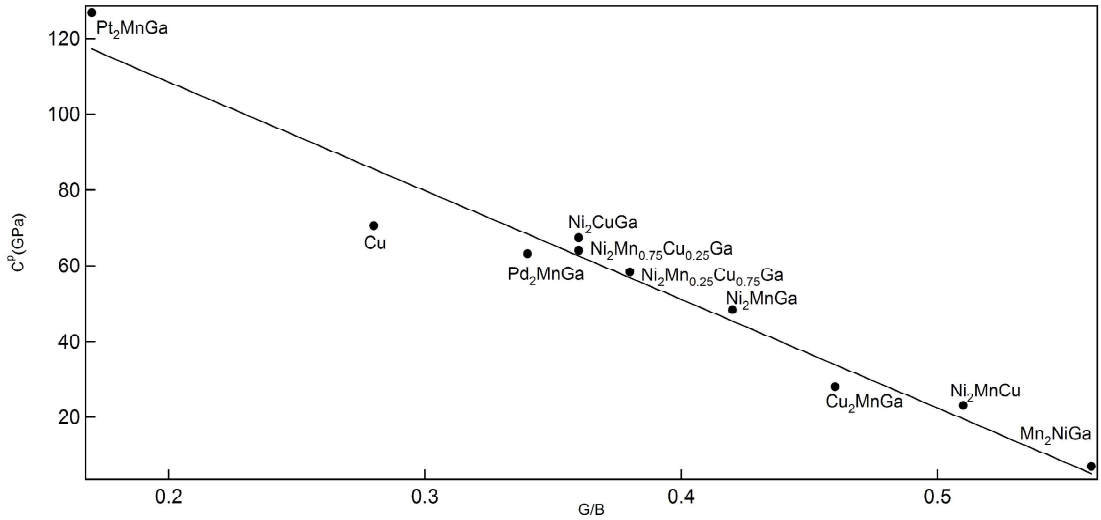

Figure 2.9: Cauchy pressure, C^p, versus G_V/B; a linear fitting of the data is carried out and shown here. An inverse linear-type relation is seen to exist between the two parameters (see text). The line is just the guide to the eyes.

the metallicity of the materials. A large negative value of C^p indicates a strong covalent bonding in the material, or in other words, represents a more directional character of the bonds. On the other hand, increasing positivity of this term means increasing extent of non-directional bonding as in metals. It is found that all these materials have positive C^p values. Further, along this line, there is another simple and empirical relationship, proposed by Pugh[28] which says that *the plastic property of a material is related in the following way to the ratio of the shear and bulk modulus of the material.* A high value (greater than $\sim$ 0.57) of ratio of shear and bulk modulus, namely, G/B, is connected with the inherent brittleness of a crystalline material. By analyzing the G_V/B values from Table 2.8, we find that Pt_2MnGa is expected to be inherently less brittle than Ni_2MnGa. The G_V/B ratio of the former turns out to be 0.17, which is much lower than all the substituted alloys, including the parent compound Ni_2MnGa. It is indeed interesting to note that the G_V/B value of Pt_2MnGa is comparable or lower than the G_V/B value of metal Cu and Pt, and slightly higher than that of Au as is found from the standard literature. The *Poisson's ratio* is calculated from the expression, $\nu = 0.5 * (3*B/G - 2)/(3*B/G + 1)$. A value smaller than 0.33 is considered to be associated with an inherently more brittle material. As per the G_V/B as well as the ν values (calculated using B/G_V values), Mn_2NiGa seems to be inherently more brittle compared to the other

materials. Since recent studies indicate the importance of Pt_2MnGa from studies related to MFIS and MCE, we probe its elastic properties in detail while comparing the same with the parent compound Ni_2MnGa. From Table 2.8, it is evident that Pt_2MnGa has a very high Poisson's ratio and Cauchy pressure as well as a very low G_V/B value when compared to Ni_2MnGa. Further, the calculated value of Young's modulus for Pt_2MnGa is found to be 85.15 GPa, while Ni_2MnGa has a value of 181.01 GPa. This is consistent with the trend of the comparative values of C^p and Poisson's ratio as well as G_V/B values of the two compounds (See Table 2.8). Furthermore, we compare the Debye temperature (Θ_D) values calculated from the elastic constants for Ni_2MnGa and Pt_2MnGa. For the former, the Θ_D value has been obtained to be 411K (which is close to the value 419K obtained from the phonon density of states calculated using CASTEP programme[53]). This value, however, is somewhat higher from the reported experimental value of 261K[112] and earlier theoretical result of 323K.[27] Our calculated Θ_D value for Pt_2MnGa is observed to be lower than the value of Ni_2MnGa and it is found to be 200K obtained from the averaged sound velocity.[27] It is worth noting that from our study, we only predict the trend and note that Pt-doping in Ni_2MnGa is likely to give rise to lowering of Debye temperature.

2.3.4 Comparative study of Elastic Stability of substituted (Ni, Pt, Pd)$_2$MnGa and Mn$_2$NiGa

In this subsection, we discuss about the mechanical stability of Ni_2MnGa, Pt_2MnGa, Pd_2MnGa, Mn_2MnGa, based on the calculated values of the elastic constants of these materials. It is observed from Figure 2.9, that the inherent brittleness decreases with Mn replacement by Cu in Ni_2MnGa. Taking a cue from this finding, we probe the effect of replacement of Mn by Cu in Pt_2MnGa and also Pd_2MnGa on the ICB of these materials. We mention here that though there are studies in the literature on substitution of various elements in different sites in Ni-Pt-Mn-Ga compounds[4, 113], Cu doping at the Mn site in Pt_2MnGa (or Pd_2MnGa) was not considered earlier. Here first we study the stability of all the Pt-derived materials. Figure 2.10(a) shows the percentage of Cu-substitution at Mn site versus mixing energy for Pt_2MnGa. It is found that this substitution leads to stable compounds with negative mixing energies. Further, we find that the material

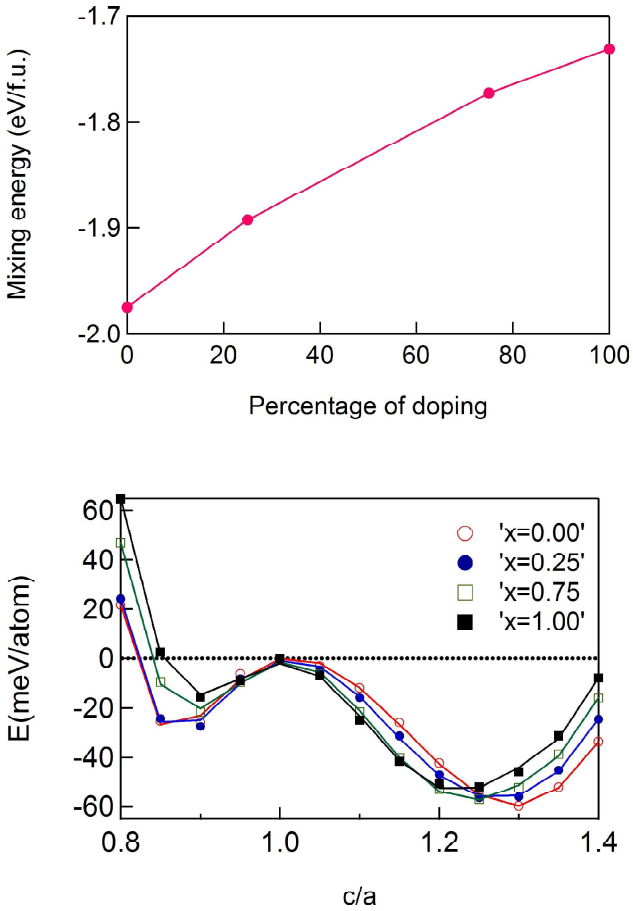

Figure 2.10: (Top panel) Mixing energy in eV/f.u. as a function of Cu substitution at Mn sites in Pt_2MnGa. The line is only guide to the eyes. (Bottom panel) Energy in meV/atom as a function of c/a for $Pt_2Mn_{1-x}Cu_xGa$ system with x=0.00, 0.25, 0.75, 1.00. The energy (E) of the martensite phase is normalized with respect to the austenite phase. c/a = 1 corresponds to the austenite phase. The lines are guide to the eyes only.

Table 2.9: Calculated bulk mechanical properties of Pt_2MnCu, Pd_2MnCu, Ni_2MnCu, and Mn_2NiCu

Elastic properties	Pt_2MnCu	Pd_2MnCu	Ni_2MnCu	Mn_2NiCu
Lattice parameter(Å)	6.07	6.01	5.75	5.83
Bulk modulus(B)(GPa)	204.48	192.32	146.61	124.54
Shear modulus(G_V)(GPa)	38.67	76.23	74.08	53.04
Shear modulus(G_R)(GPa)	–	29.87	11.96	-116.70
G_V/B	0.19	0.40	0.51	0.43
C_{11}(GPa)	122.43	211.11	153.41	86.66
C_{44}(GPa)	105.47	117.65	120.07	107.18
C_{12} (GPa)	245.50	182.93	143.21	143.26
C^p (GPa)	140.03	65.27	23.14	36.08
C'(GPa)	-61.53	14.09	5.10	-28.3
Poisson's ratio	0.41	0.32	0.28	0.31

Pt_2CuGa possesses a low G_V/B ratio of 0.12 and a high Poisson's ratio of 0.44. Pd_2CuGa has a G_V/B value of 0.26 and Poisson's ratio is 0.39. We have also tried to assess the effect of replacement of Ga by Cu on the properties of Pt_2MnGa, Pd_2MnGa, Ni_2MnGa, and Mn_2NiGa (Table 2.9). From Table 2.9 we observe that, the C^p values are high positive for all four materials Pt_2MnCu, Pd_2MnCu, Ni_2MnCu and Mn_2NiCu, suggesting the dominant metallic nature of bonding in these materials. Further, in Figure 2.9, we plot all the available data for C^p versus G_V/B calculated in case of Ni_2MnGa and the partially and fully substituted compounds. We find that overall, there is a clear trend of inverse (linear) relationship between G_V/B and C^p. In the literature also, it is observed that, the higher the C^p, the lower the ratio G/B; in particular, a nearly-linear inverse correlation between the Cauchy pressure and the G/B ratio is well established for various related compounds.[114] Along with the alloys studied, we have also plotted the C^p and G_V/B values for Cu bulk calculated by us in Figure 2.9, for comparison.

Further C' values are found to be negative for Pt_2MnCu and Mn_2NiCu, which stands for probable mechanical instability of the cubic phase of these two materials. However, we note that, in the Part A of this chapter, we observed that Mn_2NiCu is also electronically unstable, as it is having positive formation energy. By summarizing all the data, we find that interestingly Pt_2CuGa is expected to possess the least G_V/B value and highest Poisson's ratio among all the compounds studied here. Furthermore, in context of MSMA properties of these materials, we have probed the probability of martensite transition for the compounds with Cu-substitution at Mn site in both Pt_2MnGa and Pd_2MnGa. In

Figure 2.10(b) we plot the energy versus the tetragonality (lattice constant ratio c/a) for the compounds with Cu-substitution at the Mn site in Pt_2MnGa. It is interesting to find that all the substituted compounds are likely to be prone to martensite transformation as is seen in case of the parent compound.[4] It is to be noted that for all the Pt and Pd-derived compounds, the conventional Heusler alloy structure has been found to have a lower energy compared to the inverse structure and hence we have taken the former structure for all these compounds.

2.4 Conclusion

In the first part of this chapter, we investigate in depth the effect of Cu substitution in Ni_2MnGa and Mn_2NiGa alloy systems. We study the stability and properties of these substituted compounds and in the process explore the possibility of finding new magnetic Heusler alloys. We study the changes in the structural, bulk mechanical, electronic and magnetic properties of these two systems as a result of Cu substitution at the Ni, Mn as well as Ga sites. It is observed that, except for one, all the stoichiometric compositions studied by us are stable in terms of the mixing energy: Complete replacement of Ga by Cu in Mn_2NiGa leads to an unstable compound. Ni_2MnCu shows a promise of martensite transition, though it has much smaller mixing energy compared to the parent compound, Ni_2MnGa. From the results of mixing energy values it is clear that partial and even complete substitution of Mn by Cu lead to compounds, which are more stable than the compounds in which Cu replaces Ni or Ga atoms. It is further to be noted that partial and also complete replacement of Mn by Cu yield mixing energies close to the parent compounds, Ni_2MnGa and Mn_2NiGa. As discussed in literature, the probable reason of this stability seems to originate from the strong hybridization of the $4p$ electrons of Ga and the $3d$ electrons of Ni atom (in case of Ni_2MnGa) or Mn atom at the Ni site (in case of Mn_2NiGa).

Both the Ni_2MnGa and Mn_2NiGa alloy systems are least destabilized, structurally and electronically, when Mn is substituted by Cu. Keeping this in mind, we note that Cu substitution, specifically at the Mn site, in both Ni_2MnGa and Mn_2NiGa, can lead to interesting possibilities in terms of tuning the stability of the martensite phase, the

transition temperature as well as the magnetocaloric effect. Furthermore, substitution of Ga atom by Cu is predicted to cause a large change in martensite transition temperature, though larger substitutions are increasingly energetically less favorable. On the other hand, interestingly, substitution at the Ni site by Cu leads to stabler cubic austenite phase over the tetragonal phase. Our detailed investigations on substitution of Cu at Ni, Mn and Ga sites in both Ni_2MnGa and Mn_2NiGa provide a clear picture as to how the magnetic and electronic properties change as a result of substitution. Consequent to these results, our present study underlines that the physics of martensite transformation including the possible magnetic shape memory effect as a result of Cu substitution at Ga, Mn and Ni sites is the same in these two different alloy systems.

In the second part of this chapter, we investigate the effect of Pt, Pd and Mn substitution at the Ni site in Ni_2MnGa alloy system on the mechanical properties of these substituted compounds. We also include the Cu substitution at the Ni site of Ni_2MnGa for the sake of comparison. The elastic constants agree well with the literature wherever the data are available. It is observed that for all the Heusler compounds studied here the shear modulus obtained using Reuss formalism is much lower compared to the one given by Voigt formalism. Hence we consider the G_V as the shear modulus. We have explained this difference numerically in terms of the values of the tetragonal shear constant C' of the materials. However, it remains a conceptually open question as to why the G_R values, for Ni_2MnGa and the substituted alloys, are so much underestimated compared to the G_V values. Detailed analysis is warranted for the same, which is beyond the scope of the present work. Further, when the Cauchy pressure (C^p) of different materials is compared it is observed that, a trend of a nearly linear inverse correlation exists between the C^p and the G_V/B ratio among all the materials studied. This trend is already phenomenologically established in the literature for various other compounds. Based on the relative values of G_V/B and C^p, we predict that Ni_2MnGa is expected to be inherently less brittle than Mn_2NiGa, while Pt_2MnGa is the least brittle one among the three. Further, a Cu-substitution at the Mn site for Pt_2MnGa seems to have led to an increase of the C^p value and Poisson's ratio and, there is a substantial reduction in the G_V/B value, rendering Pt_2CuGa a material with the least inherent crystalline brittle, among all the materials

studied here.

From analyzing our results of total and partial DOS of the materials, existence of a double peak structure at the Fermi level and a pseudo-gap close to the Fermi level is found for the stable materials. This indicates hybridization and interaction of p states of the C atom and d electrons of the A atom leading to electronic stability of the material as observed in the literature. Further, our result of the magnetic properties is in agreement with the observed trend of lowering of T_C values as a function of Pt-doping in Ni_2MnGa. Furthermore, we observe that the T_C shows an anomalous dependence on the total magnetic moment when Ni is replaced by Pt (or Pd) in the material Ni_2MnGa[81], namely, the T_C value decreases while the total magnetic moment increases as a result of Pt (or Pd) substitution at the Ni site as has been observed in the literature for similar Heusler alloys.[95]

Finally, the present study along with the studies in the literature indicates that, Pt substitution at the Ni site, along with the substitution of Cu at the Mn site, may lead to a higher martensite transition temperature as well as reduction of the G_V/B and Young modulii values and increase of the C^p value and the Poisson's ratio indicating a lowering of the inherent crystalline brittleness in these substituted materials, which may be promising from technological application point of view.

Chapter 3

Electronic, Magnetic and Mechanical Properties of A_2PtGa (A = Cr, Mn, Fe, Co) Heusler Alloys

3.1 Introduction

In the last chapter, we have discussed about the effects of substitution on electronic, magnetic and mechanical properties of two prototype Ni and Mn based Heusler alloys, namely, Ni_2MnGa and Mn_2NiGa. We have observed that most of those substituted systems are likely to undergo martensite transition, which is one of the most important aspects of the Heusler alloys from the point of view of practical application. We have also discussed about the tunability of the martensite transition temperature (T_M), Curie temperature (T_C) and mechanical property as well, with the change of chemical composition of the Heusler alloy. As discussed earlier, for high temperature application of a magnetic shape memory alloy, it is desirable to have T_M and T_C above the room temperature as well as better mechanical properties in terms of ductility.

Unlike the above-mentioned two prototype magnetic Heusler alloys, which are metallic in nature, a class of full Heusler alloys has been shown, by de Groot et. al., to exhibit half metallicity.[3] The density of states in one of the spin channels vanishes at the Fermi level and consequently, these materials may have a potential application as spin-injector materials. Generally, many of the Co-based Heusler alloys exhibit this behavior, for example: Co_2CrGa, Co_2MnGa, Co_2MnSn.[34, 31] Further these materials are not prone to tetragonal distortion. However, Co_2NbSn and Co_2NiGa are found to be prone to martensite transition and these are found to be metallic in nature.[35–37, 115–117] Hence,

it may turn out to be interesting to probe if there are some Co-based Heusler alloys which show both the features i.e. martensite transition as well as high spin polarization at the Fermi level.

Recently, Co_2NiGa and related alloys have gained interest among the researchers. Some of these have been studied in detail theoretically[36, 37] as well as have already been prepared experimentally.[115, 116] Interestingly, Co_2NiGa is prone to martensite transition as well as it possesses a different (inverse Heusler alloy) structure unlike many of the other Co-based systems, which are known to exhibit half-metallicity, no martensite transition and are found to possess the conventional Heusler alloy structure in their lowest energy state. These findings in the literature have motivated us to probe Co_2NiGa-derived Heusler alloy systems in detail.

In the previous chapter, we have shown that, substitution of Ni atom by Pt in case of Ni_2MnGa leads to reduction of the inherent crystalline brittleness (ICB) of the material and it makes the tetragonal state more stable compared to the cubic phase. Besides that, Co-based systems are shown to exhibit high T_C, as is found in the literature.[31, 32] Further, Mario et. al. have observed an enhancement of T_C as a result of Co doping in the Pt-based systems.[4] So, taking the results from the literature into account[4, 118, 119], we expect that, the effect of replacement of Ni by Pt in Co_2NiGa may lead to modification in various physical properties which may be interesting both from application as well as fundamental points of view. Furthermore, number of valence electrons has been shown to play an important role in determining the properties of the Heusler alloy systems.[15, 16] In this chapter, therefore, we discuss the changes in the magnetic, electronic as well as mechanical properties of A_2PtGa system as A is varied. The number of valence electrons of the A element, which is a first row transition metal atom (TM), is changed systematically (A being Cr, Mn, Fe and Co). Among these materials Mn_2PtGa is already experimentally prepared and theoretically studied.[39, 120–122] It shows an inverse Heusler alloy structure and possesses a ferrimagnetic configuration as is the case for Mn_2NiGa.[96] A point to note is thatMn_2PtGa, in its ideal stoichiometric configuration, is shown to exhibit martensite transition from theoretical calculations[39], however, experimentally it is not the case.[121]

3.2 Results and Discussion

3.2.1 Geometry Optimization, Electronic Stability and Possibility of Martensite Transition

Geometry Optimization - Geometry optimization has been carried out for both the possibilities of structures, i.e. conventional and inverse Heusler alloy structures, for all the materials, using VASP code.[51, 52] We have carried out full geometry optimization which include, relaxing atom positions, unit cell volume and shape, for each of these structures. **Electronic Stability and Ground State Magnetic Configuration -** Here we discuss about the electronic stability and ground state magnetic configuration of the systems studied here. For A_2PtGa (A being Cr, Mn, Fe and Co), the formation energies in the cubic structure have been calculated and compared (Table 3.1) for both the inverse and conventional Heusler alloy structures with different starting magnetic configurations to probe the lowest energy state, both in terms of crystal structure and the magnetic configuration. We have considered three different kinds of magnetic configurations: long-range ferromagnetic (FM), ferrimagnetic (FIM) ordering and a configuration having net zero magnetic moment (NM) having all partial moments ideally zero. For FM configuration, all the moments of the A and Pt atoms are parallel to each other. Only one magnetic arrangement is possible under the FIM configuration in case of the conventional Heusler alloy structure, with A and Pt atoms being anti-parrallel to each other. In this case the FIM type of magnetic configuration is almost similar to the FM configuration of the respective structure because the magnetic moment associated to the Pt atom is always almost negligible. It is observed that this configuration, after optimization of structure, converges to the FM configuration. Consequently, we have not included any results corresponding to this magnetic structure (FIM) in Table 3.1.

In case of inverse Heusler structure, under FIM configuration, there are actually three types of magnetic configurations possible. This is because there are two structurally inequivalent A atoms, noted as $A1$ and $A2$ atoms which are occupying the crystallographically inequivalent sites, (0.25, 0.25, 0.25 and the fcc equivalent sites) and (0.50, 0.50,

Table 3.1: Comparison of formation energies between inverse and conventional Heusler alloy structure of the cubic phase of different materials with different magnetic configurations. Optimized lattice parameters (a_{opt}) are also reported. Values from the literature are given along with the references which are shown in square brackets.

Material	Crystal structure	Magnetic Configuration	Formation Energy (kJ/mol)	a_{init}(Å)	a_{opt} (Å)
	Inverse	FM	-62.63 (converged to FIM)	6.10	6.10
	Inverse	FIM	**-62.63**	6.10	6.10
Cr_2PtGa	Inverse	NM	+2.88	6.10	5.99
	Conventional	FM	+6.36	6.10	6.22
	Conventional	NM	+68.92	6.10	6.03
	Inverse	FM	-72.75	6.13	6.15
	Inverse	FIM	**-117.67**	6.13	6.13
					6.13[39]
Mn_2PtGa	Inverse	NM	+25.45	6.13	5.93
	Conventional	FM	-71.29	6.10	6.21
	Conventional	NM	+45.98	6.10	5.94
	Inverse	FM	**-99.58**	6.00	6.00
	Inverse	FIM	-36.98	6.00	6.02
Fe_2PtGa	Inverse	NM	+47.89	6.00	5.91
	Conventional	FM	-29.46	6.00	6.02
	Conventional	NM	+37.67	6.00	5.91
	Inverse	FM	**-58.83**	5.95	5.95
	Inverse	FIM	-23.22	5.95	5.89
Co_2PtGa	Inverse	NM	-12.72	5.95	5.90
	Conventional	FM	-46.57	5.95	5.93
	Conventional	NM	-14.35	5.95	5.90

0.50 and the corresponding fcc equivalent sites), respectively. In the first case (FIM-1), the moment of Pt atom is taken to be anti-parallel to the A atoms (both $A1$ and $A2$ atoms are parallel to each other). Another ferrimagnetic configuration (FIM-2) is that where moments of $A1$ and $A2$ are anti-parallel to each other and the moment of Pt is now parallel to $A2$. The third ferrimagnetic configuration (FIM-3) is that where moments of $A1$ and $A2$ are anti-parallel to each other again and the moment of Pt is parallel to $A1$. However, after optimization, the FIM-1 configuration converges to the corresponding FM structure. FIM-2 and FIM-3 turn out to be energetically same for all the systems. As a consequence, for the inverse structure, we are only reporting the results of FIM-3 (which is same as FIM-2) configuration (expressed as FIM hereafter) in the table and for the latter part of the discussion.

In Table 3.1, we report the initial guess value of the lattice parameter (a_{init}) which has been chosen from the literature in case of Mn_2PtGa. For Cr_2PtGa, Fe_2PtGa and Co_2PtGa, a_{init} has been chosen intuitively. In the same table, the optimized lattice parameter (a_{opt}) after full geometry optimization has also been reported along with the formation energies. More negative values of formation energy in case of inverse Heusler alloy structure (Table 3.1) suggest that all the systems studied here possess the inverse structure, which is consistent with the valence electron rule.[123] For Cr_2PtGa and Mn_2PtGa, inverse Heusler alloy structure with FIM configuration and for Fe_2PtGa and Co_2PtGa the inverse structure with FM configuration possess the lowest formation energy. Further calculations of properties of these materials are carried out for these respective lowest energy structures only.

Possibility of Martensite Transition - As we discussed in the previous chapter also, Heusler alloys may have the potential to be used as shape memory alloy device if they undergo a structural phase transition, namely, martensite transition. As is well-known this is a transition from a (low temperature) non-cubic phase to a (high temperature) cubic phase above a certain transition temperature, known as martensite transition temperature, T_M. This transition requires that the non-cubic phase must have lower energy compared to the cubic phase. Therefore, we applied tetragonal distortion on the cubic system to probe whether there is a lowering of energy with respect to the cubic phase in their respective ground state magnetic configuration. A global minimum has been observed for all the materials at a $c/a > 1$ (c is the lattice parameter along the z axis and a is the same along x or y direction) as shown in Figure 3.1. The relative volume change between the cubic and tetragonal phases is nominal (Table 3.2). It is to be noted here that the starting magnetic configuration for both the cubic and tetragonal phase has been taken to be the same in our calculations.

Here first we discuss in detail about how we arrive at the volume change between the high temperature cubic and the low temperature tetragonal phases as reported in Table 3.2. We first consider the fully optimized lattice parameter for each case (Table 3.1) and assume that both the cubic and tetragonal phases have the same volume. Then we vary the ratio of c and a keeping the volume same as that of the optimized cubic

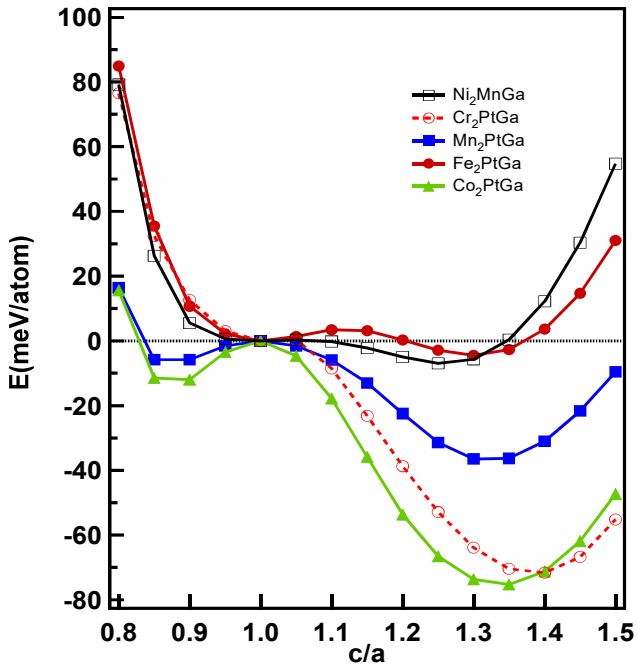

Figure 3.1: Variation of the total energy of A_2PtGa (A = Cr, Mn, Fe, Co) systems in their respective ground state magnetic configurations as a function of c/a. Equilibrium c/a values are expected to be around 1.3 to 1.4 for all the systems. The energy of the tetragonal phase has been normalized with respect to that of the cubic phase of the respective system. Hence, energy E in the Y-axis signifies the energy difference between the cubic and tetragonal phase. Ni_2MnGa is presented as a reference material. The lines are guide to the eyes only.

phase (Table 3.1). If a system shows a lowering of energy for $c/a > 1$, then we obtain the value of that particular c/a for which the energy of the system is the lowest. Next, we vary the volume of the tetragonal phase keeping that same c/a. From there we get a variation of energy as a function of total volume of the tetragonal phase. The volume for which the energy of the tetragonal phase is minimum we consider that as the equilibrium volume of the tetragonal phase. Then we calculate the relative change in volume between the optimized cubic and tetragonal phase, which we report in Table 3.2. The maximum variation of volume is about 2.6% which is for Mn_2PtGa. This conservation of the volume and lowering of energy as a result of tetragonal distortion indicate that these materials are likely to be prone to martensite transition.[18, 103]

To obtain the approximate values of T_M, we have used the following equation[18, 88]:

$$k_B T_M = \Delta E \tag{3.1}$$

Table 3.2: Calculated lattice parameter $(c/a)_{eq}$, martensite transition temperature (T_M) relative change in volume between the optimized cubic and tetragonal phase ($|\Delta V|$/V) and difference of energy between the two phases (ΔE) as well. Values from the literature are given along with the references which are shown in square brackets.

Material	$(c/a)_{eq}$	ΔE(meV/atom)	T_M(K)	$\|\Delta V\|$/V(%)
Cr_2PtGa	1.41	71.94	834.5	1.00
Mn_2PtGa	1.33 1.32[39]	41.06	476.3	2.60 3.13[39]
Fe_2PtGa	1.29	4.40	51.0	0.11
Co_2PtGa	1.37	76.43	886.6	1.50

where k_B is the Boltzman constant and we have used the following conversion factor, 1 meV = 11.6 K. The calculated T_M values are also listed in Table 3.2. It is found that except Fe_2PtGa, all the alloys are expected to possess a martensite transition temperature which may be well above the room temperature and Co_2PtGa yields the maximum value.

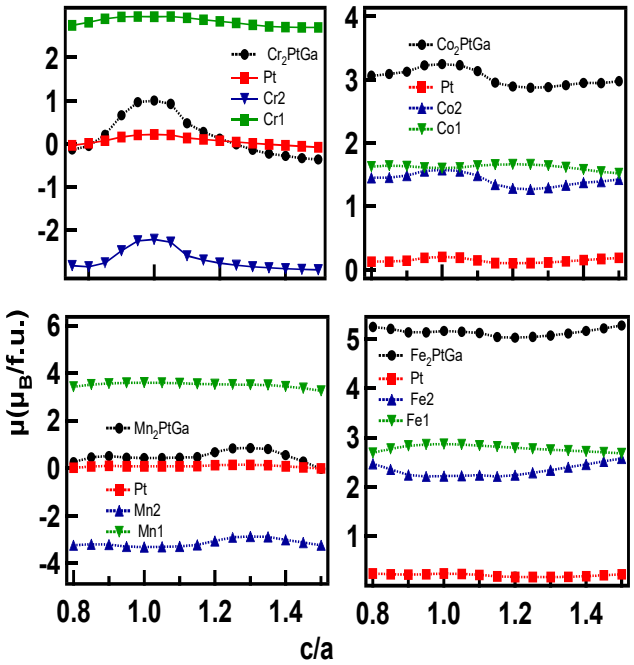

Figure 3.2: Variation of the total magnetic moment and partial moments of A_2PtGa (A = Cr, Mn, Fe, Co) systems as a function of c/a. The lines are just guide to the eyes.

3.2.2 Magnetic, Electronic and Mechanical Property

Analysis of Magnetic State - Now, we discuss about the magnetic and electronic properties of all the systems studied here. In Figure 3.2, we present the variation of total

Table 3.3: Calculated magnetic moments and Curie temperatures for both austenite (μ_c, $T_{C,c}$) and martensite phases (μ_t, $T_{C,t}$). In the parentheses of the second and fifth columns, first two values are corresponding to the inequivalent $A2$ and $A1$ atoms (A = Cr, Mn, Fe, Co) and the third value corresponds to the Pt atom. P_c and P_t are the percentage of spin polarization at Fermi level for cubic and tetragonal phase, respectively. The values from the literature are given in the table in case of Mn_2PtGa, along with the relevant reference in square bracket.

Material	$\mu_c(\mu_B)$	$P_c(\%)$	$T_{C,c}$(K)	$\mu_t(\mu_B)$	$P_t(\%)$	$T_{C,t}$(K)
Co_2PtGa	3.25 (1.57, 1.60, 0.21)	80.14	584	2.89 (1.33, 1.58, 0.14)	71.59	724
Fe_2PtGa	5.16 (2.21, 2.86, 0.23)	1.96	972	5.06 (2.32, 2.75, 0.16)	42.34	909
Mn_2PtGa	0.44, 0.44[39] (-3.31,3.60, 0.08)	24.18 23[39]	583, 799[39]	0.86, 0.75[39] (-2.76, 3.42, 0.14)	20.75 26[39]	490, 326[39]
Cr_2PtGa	1.00 (-2.21, 2.95, 0.22)	74.39	1500	0.28 (-2.74, 2.92, 0.04)	5.26	1540

magnetic moment and partial moments as a function of c/a for all the systems. Table 3.3 presents the magnetic moments, percentage spin polarizations (P_c and P_t for cubic and tetragonal phases, respectively) and Curie temperatures (calculated from the Heisenberg exchange coupling parameters as discussed earlier) in their respective cubic and tetragonal phases. From the Tables 3.1 and 3.3 it is clear that Cr_2PtGa and Mn_2PtGa are likely to be ferrimagnetic; on the other hand, Co_2PtGa and Fe_2PtGa may possess long-range ferromagnetic ordering, in their respective ground states. The results from the literature, wherever available, have been presented in the same table and it is found that the matching between the data from literature and our calculations is reasonably good. For Cr_2PtGa, the alignment of spin for Cr2 atom is found to be opposite to that of Cr1 atom. Same is observed in case of Mn_2PtGa also, resulting in a ferrimagnetic ground state as in the case of Mn_2NiGa.[96] It is worth mentioning that both Cr and Mn atoms possess anti-ferromagnetic ground state in their bulk forms. So for this type of (inverse Heusler alloy structure) crystal structure, where two A atoms are the nearest neighbor of each other, the resulting magnetic configuration seems to get influenced by the magnetic configuration of the bulk A atom. This is also the case for the other two materials, namely, Co_2PtGa and Fe_2PtGa. Both these materials have a long-range ferromagnetic ordering and notably both Co and Fe atoms are having ferromagnetic ground state in their respective bulk forms.

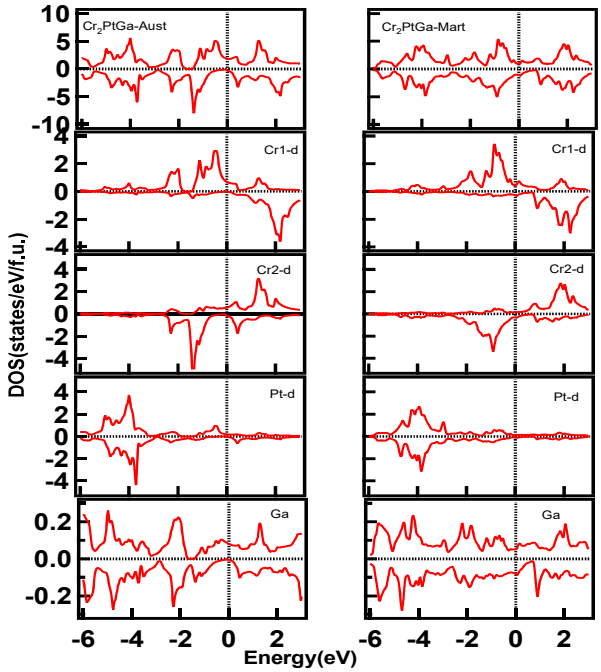

Figure 3.3: Spin polarized DOS of Cr_2PtGa (Left Panel). Cubic phase (Austenite), (Right Panel). Tetragonal phase (Martensite).

Electronic Density of States - The origin of ferrimagnetism in both cubic as well as tetragonal phases for Cr_2PtGa can be understood from the electronic density of states presented in Figure 3.3. The moments of Cr1 and Cr2 atoms are opposite to each other (Table 3.3) because of the anti-parallel nature of the spins of Cr1 and Cr2 atoms below the Fermi level, which is evident from the partial DOS (Figure 3.3). Further, the density of states of Cr1 and Cr2 atoms gives rise to unequal anti-parallel moments in Cr1 and Cr2 atoms, resulting in a ferrimagnetic ground state for Cr_2PtGa. Similar is the case for Mn_2PtGa. Figure 3.4 gives the total and partial DOS for Co_2PtGa in cubic as well as tetragonal phase. While in case of Cr_2PtGa, from the partial DOS of the two Cr atoms, the presence of exchange splitting is clearly evident, the exchange splitting is not clear in case of both the Co atoms of Co_2PtGa. In both the materials Cr_2PtGa and Co_2PtGa partial DOS of Pt atoms show: (1) the up and down spin DOS are almost compensated, (2) there is no significant contribution of DOS near the Fermi level.

Variation of Magnetic Moments as a Function of c/a - To understand the underlying reason behind the variation of magnetic moments as a function of c/a (Figure 3.2) as well as stability of the tetragonal phase over cubic phases, we calculate and analyse

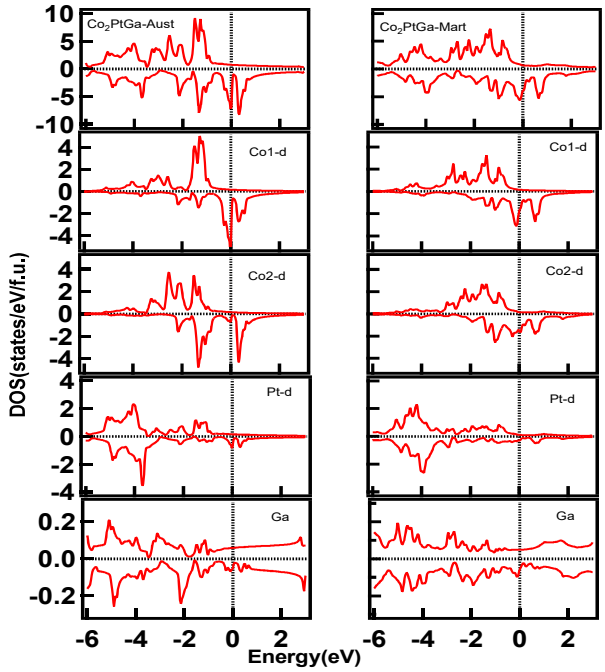

Figure 3.4: Spin polarized DOS of Co_2PtGa (Left Panel). Cubic phase (Austenite), (Right Panel). Tetragonal phase (Martensite)

the spin polarized total and partial density of states for both cubic and tetragonal phases (Figure 3.3 and 3.4). We also show the DOS of the e_g states of the minority d electrons ($5d$ for Pt and $3d$ for other TM atoms) near the Fermi level for $A1$, $A2$ and Pt atoms as a function of c/a (Figure 3.5 and 3.6) for two typical materials, namely, Cr_2PtGa and Co_2PtGa. The first material is ferrimagnetic and the other one is ferromagnetic in their respective lowest energy states.

We observe from Figure 3.2 that there is very little change in the total magnetic moment of Fe_2PtGa as a function of c/a which is observed for both the cubic and tetragonal phases as is evident from the values given in Table 3.3. For Co_2PtGa, we find that, there is a maximum at c/a=1 but in the tetragonal phase, the total moment decreases, which can be correlated with the increased distance between Co1 and Co2 atoms resulting in a weaker long-range ferromagnetic interaction between them. On the contrary, for Mn_2PtGa the total moment increases in the tetragonal phase. Being the nearest neighbors, Mn1 and Mn2 atoms are anti-ferromagnetically coupled to each other. Hence, in this case the increased separation between Mn1 and Mn2 makes the anti-ferromagnetic interaction weaker in the tetragonal phase compared to its cubic phase which results in a larger total

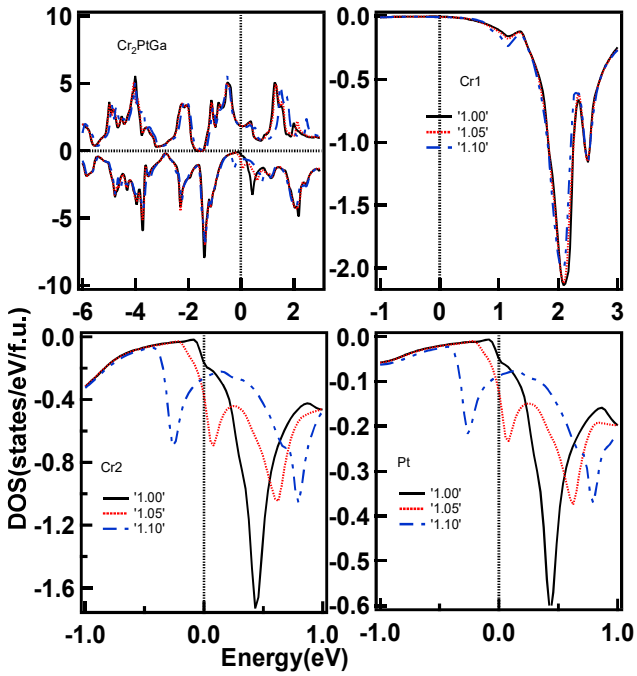

Figure 3.5: Spin-polarized DOS of Cr_2PtGa and corresponding minority $3d$ e_g level electrons of Cr1 (top panel), as well as Cr2, and e_g states of the minority $5d$ electrons of Pt atom (bottom panel) as a function of c/a, maximum value taken to be 1.1 for showing the splitting of levels.

moment in the tetragonal phase. For Cr_2PtGa the maximum of total magnetic moment at c/a=1 can be correlated with the high spin polarization (75%) at the Fermi level in cubic phase. However, in the tetragonal phase the spin polarization has decreased significantly (5%) as is also seen from the corresponding partial moments on Cr1 and Cr2 atoms. This decrease in spin polarization in the tetragonal phase leads to the reduction in the total moment in the tetragonal phase with respect to the cubic phase of Cr_2PtGa. We observe that in all the cases, the magnetic moment is found to be primarily due to the A atoms as is observed from Table 3.3. The change in the total magnetic moment between cubic and tetragonal phase is observed to be maximum for Cr_2PtGa. Because the total moment is substantially lower in the low temperature phase, both Cr_2PtGa and Co_2PtGa are likely to show an inverse magnetocaloric effect.[124]

T_C from Heisenberg Exchange Coupling Constants - Now we discuss the Heisenberg exchange coupling paramaters in the cubic phase. In Heusler alloys, there is a direct exchange interaction and an indirect RKKY-type of interaction.[40] In the prototype

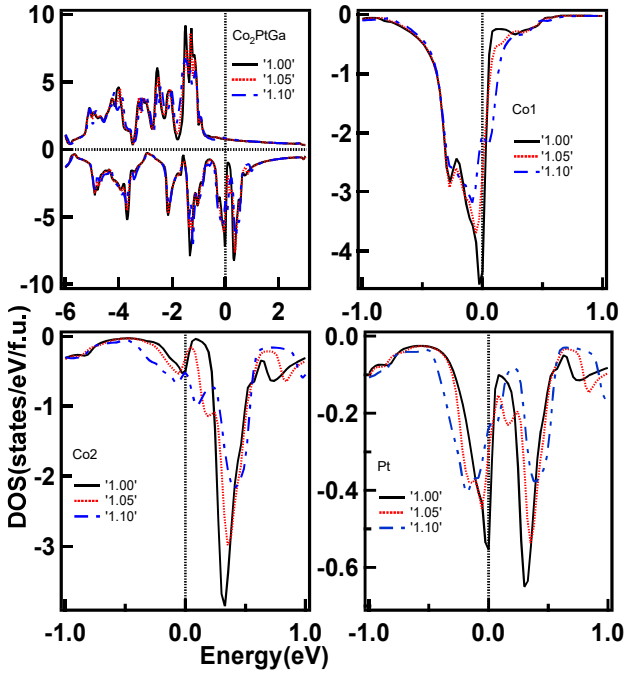

Figure 3.6: Spin-polarized DOS of Co_2PtGa and corresponding minority $3d$ e_g level electrons of Co1 (top panel), as well as Co2, and e_g states of the minority $5d$ electrons of Pt atom (bottom panel) as a function of c/a, maximum value taken to be 1.1 for showing the splitting of levels.

shape memory alloy, Ni_2MnGa, which possesses a conventional Heusler alloy structure, a strong ferromagnetic direct interaction exists between the Ni and Mn atoms, whereas the interaction between the two Mn atoms is of indirect nature.[38, 92] In case of Mn_2NiGa, with an inverse Heusler alloy structure, there is a direct anti-ferromagnetic interaction between the two inequivalent neighboring Mn atoms.[96] This interaction is observed to be much stronger compared to the direct exchange interaction observed between the Ni and Mn atoms as is observed in case of Ni_2MnGa. In Figure 3.7, we present the Heisenberg exchange coupling parameters (J_{ij}) between ith and jth atoms for A_2PtGa materials (A = Cr, Mn, Fe, Co), as a function of normalized inter-atomic spacing between them in their cubic phase. The J_{ij}'s for intra sublattice ($A1$-A1, $A2$-$A2$) and inter sublattice ($A1$-$A2$, $A1$-Pt, $A2$-Pt) are depicted here. It is quite clear from the plots that in all cases the $A1$-$A2$ interaction is the most dominant one and plays a crucial role in determining the T_C value of the corresponding material. A weak oscillatory type of indirect exchange interaction is observed for intra sublattice exchange interactions ($A1$-$A1$ and $A2$-$A2$),

which is an indication of presence of RKKY type of interaction in these systems.

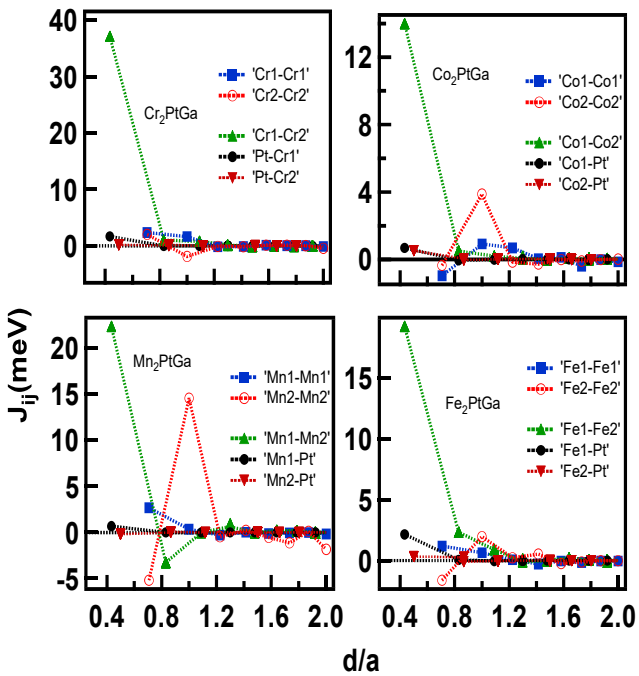

Figure 3.7: J_{ij} parameters between different atoms of A_2PtGa as a function of distance between the atoms i and j (normalized with respect to the respective lattice constant). The lines are guide to the eyes only.

The Curie temperatures for both the austensite and martensite phases have been calculated from the Heisenberg exchange coupling parameters following the approach of Liechtenstein et. al.[125] In the literature, it has been mentioned that, in the mean field approximation, there is an overestimation of Curie temperature.[126–128] It has been argued that, in the mean field approximation, spin fluctuations are neglected and the magnetic moments are taken to be more rigid, which causes an overestimation of Curie temperature. Further, it is known that a change in T_C is observed during a structural transition.[39] This has been experimentally observed by Khovailo et. al.[129] for Ni-Mn-Ga alloy system. This change is because of the differences in the partial moment and interatomic spacing between the two phases. The strength of hybridization between the atoms depends on their separation. The hybridization and the magnetic moment of the interacting atoms control the strength of exchange interaction between the atoms[130], and consequently, the T_C of the corresponding system, as has been observed from our results (Table 3.3). The Curie temperatures for all the systems are expected to be higher

compared to the room temperature for the both cubic and tetragonal phases.

Spin Polarization - Table 3.3 suggests that the spin polarization (P) at the Fermi level for Co_2PtGa is the highest in both the cubic and tetragonal phases compared to all the other materials. This is much higher than the spin polarization of the prototype shape memory Heusler alloy, Ni_2MnGa. This can be understood from Figure 3.4, which presents the spin projected DOS of cubic as well as tetragonal phase of this material. We can see that in both the cases, the minority spin has a significantly larger contribution to the DOS at the Fermi level compared to the majority spin. Mn_2PtGa and Fe_2PtGa exhibit lower spin polarization compared to Co_2PtGa. We have already discussed that Cr_2PtGa possesses high spin polarization in the cubic phase but in the tetragonal phase spin polarization is considerably low.

Stabilization of Tetragonal Phase versus the Density of States - The stabilization of the tetragonal phase over the cubic phase of the shape memory Heusler alloys has been argued in the literarure using the band Jahn-Teller mechanism.[35, 90] In a latter chapter, for a series of Ni and Co-based FHAs with a conventional structure, i.e. the A_2BC type, we show[117] that the closeness of DOS peak of the minority spin $3d$ electrons of A atom, with e_g symmetry is closely related to the possibility of martensite transition. Here, in this work, all the materials possess inverse heusler alloy structure (ABAC). A detailed analysis of density of states shows that for these systems the stability of the tetragonal phase over its cubic phase can be correlated with the presence of minority DOS peak corresponding to the e_g levels of d electrons close to the Fermi level for $A2$ and Pt atom in their respective austenite phase. Here we show in detail DOS of two representative cases, one of Cr_2PtGa and another Co_2PtGa. Figure 3.5 and 3.6 show partial and spin polarized DOS of Cr_2PtGa and Co_2PtGa, respectively. From Figure 3.5 we observe that, at $c/a = 1$, DOS peak of $3d$ electrons with down spin (of e_g symmetry) of Cr2 atom is located just above the Fermi level (about +0.43 eV). Under tetragonal distortion, this peak is split into two. For $c/a = 1.1$, one part of the peak enters below Fermi level and other part moves above the Fermi level. The same kind of changes is also observed with the minority DOS of the e_g levels of $5d$ electrons of Pt atom which is located at the same energy as in case of Cr2 atom, in the cubic phase. The redistribution

of density of states for these two atoms as a function of tetragonal distortion leads to the reduction of free energy and to stabilization of the tetragonal phase over the cubic phase. However, for Cr1 atom, not much change is observed in the peak of minority DOS peak for the e_g levels of $3d$ electrons under tetragonal distortion.

In case of Co_2PtGa also, we find the same kind of redistribution in the DOS of e_g states of minority spin $3d$ electrons of Co2 and $5d$ electrons of Pt atom under the tetragonal deformation (Figure 3.6). The single DOS peak of e_g states of $3d$ electrons with minority spin for Co2 atom is observed at +0.33 eV. Under tetragonal deformation this single peak splits into two parts, one part of the peak moves to the higher energy side (+0.35 eV for $c/a = 1.05$) and another part of the peak moves toward the Fermi level (+0.19 eV for $c/a = 1.05$). Here also we find that there is small change in the DOS of e_g states of $3d$ electrons of Co1 atom, causing not much of a change in the moment of Co1 atom as a function of c/a. For both the materials Cr_2PtGa and Co_2PtGa, we find that the tetragonal distortion leads to the change of peak position of DOS of e_g levels of d electrons, primarily of the $A2$ and Pt atoms. Consequently, the moment of $A2$ atom contributes significantly toward the total moment. This is the reason the variation of total moment as a function of c/a follows primarily the variation of the moment of $A2$ atom (Figure 3.2). For all the materials studied here, we find minimum change in the moment of $A1$ atom as a function of c/a. We note here that Luo et. al.[131] have observed for Mn_2NiGe which is also an inverse Heusler alloy, the variation of magnetic moment of the two inequivalent Mn atoms follows different trend because of their different chemical surroundings leading to different hybridization effects.

Tetragonal Ground State versus Tetragonal Shear Constant- We have discussed above from the electronic properties, the possibility of the studied materials to be prone to tetragonal distortion, we now focus on the mechanical properties, specifically the tetragonal shear constant (C'). The elastic constants of all the materials have been calculated in their cubic phase. There are three independent elastic constants for a cubic structure. These are C_{11}, C_{12} and C_{44}. These three elastic constants can be found by calculating energies for three different types of strain on the From these three linearly independent energy versus strain data, we can find out C_{11}, C_{12} and C_{44}. The applied

Table 3.4: Mechanical properties of the austenite phase of materials

Material	C_{11} (GPa)	C_{12} (GPa)	C_{44} (GPa)	C' (GPa)	B (GPa)	G_V (GPa)	G_R (GPa)	G_V/B	C^P (GPa)	Θ_m(K) (± 300K)
Cr_2PtGa	151.08	135.96	99.86	7.56	141.00	62.94	16.97	0.45	36.90	1445
Mn_2PtGa	120.11	140.67	100.32	-10.28	133.82	56.08	-30.36	0.42	40.35	1262
Fe_2PtGa	190.53	166.93	109.87	11.80	174.80	70.64	25.40	0.40	57.06	1679
Co_2PtGa	140.18	199.71	110.22	-29.77	179.87	54.22	-125.11	0.30	84.49	1381

strains have the form as (δ, δ, δ, 0, 0, 0), (0, 0, $\delta^2/(1\text{-}\delta^2)$, 0, 0, δ) and (δ, δ, $(1+\delta)^{-2}$-1, 0, 0, 0). δ has been taken in the range of -0.02 to +0.02 in steps of 0.005. To start with, we calculate the equilibrium lattice parameter (a_0) as well as equilibrium volume (V_0), and the corresponding energy is considered as the equilibrium energy (E_0). Then strain is applied to the system. Under this strained condition, the energy (E) is calculated and subsequent to that, the elastic constants are obtained from our calculations as discussed below. The energies $\frac{E-E_0}{V_0}$ are plotted as a function of applied strain and fitted with a fourth order polynomial. The second order coefficient of the fit gives the elastic constants. For the cubic crystal the elastic stability criteria are- $C_{11} > 0$; $C_{44} > 0$; C_{11}-$C_{12} > 0$; C_{11} + $2C_{12} > 0$.[78] It is observed that all the alloys satisfy these conditions but the 3rd condition is not satisfied by some of the materials. This leads to a negative value of C' for those materials. Rest of the materials show small positive values of C'. This softening of C' indicates the instability of the cubic phase. For the prototype shape memory alloy, Ni_2MnGa, the softening of C' is already observed from experiment.[132] For Cr_2PtGa and Fe_2PtGa, C' is a small positive quantity, with values 7.56 GPa and 11.80 GPa, respectively. On the other hand, Co_2PtGa and Mn_2PtGa exhibit negative values for the same.

We know that Cauchy pressure (C^P) is defined in terms of the difference between the values of C_{12} and C_{44}. Taking cue from the literature[28], we predict from our calculations that, Co_2PtGa is likely to possess the lowest inherent crystalline brittleness. The upper panel of Figure 3.8 shows an inverse linear relationship between C^P and G/B ($= G_V/B$). This inverse linear relationship between these two parameters is already reported in literature for a large number of systems.[114, 118] Figure 3.8(a) suggests that the ICB of Co_2PtGa is quite low with respect to that of Ni_2MnGa. The bottom panel of Figure 3.8 shows the variation of G/B as a function of atomic number (Z) of the A atom of A_2PtGa

(A = Cr, Mn, Fe, Co). It is to be noted that the value of G/B is lowest for Z = 27, i.e. for Co_2PtGa. In the literature[133], it has been mentioned that the materials with lower value of G are likely to undergo shear deformation and become more prone to ductility instead of brittle fracture when strain is applied which indicates about a lower inherent crystalline brittleness.

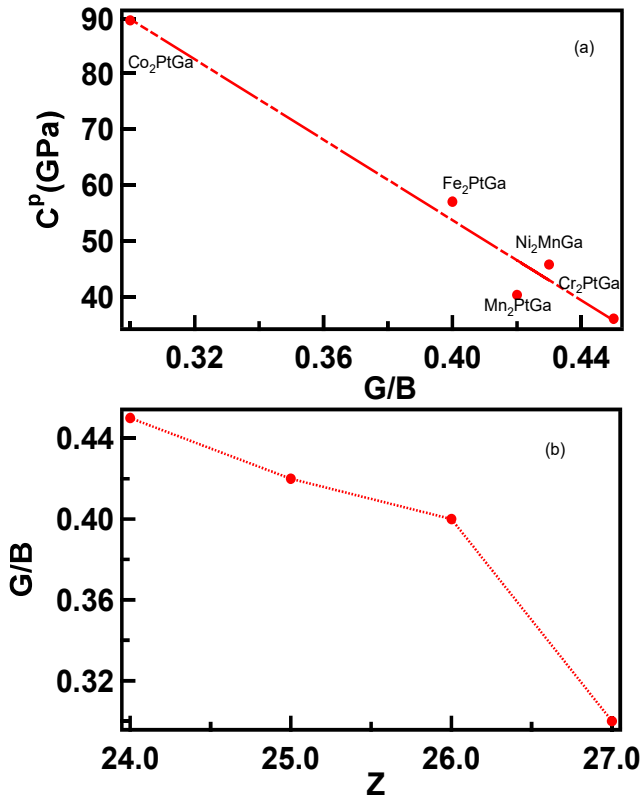

Figure 3.8: (a) C^P versus G/B plot: A linear fitting has been done, which shows an inverse linear relationship between them. Ni_2MnGa is used as a reference material. (b) G/B versus Z plot. Z is the atomic number of the A atom. The lines are just the guide to the eyes.

High Melting Temperature of the Studied Systems - For high temperature application of a material, it is mandatory to have a high melting temperature as well. Fine et. al.[134] have correlated the elastic constant C_{11} of the cubic metallic as well as inter-ametallic systems with the melting temperature by the following empirical relationship with an uncertainty of $\pm 300K$:

$$\Theta_m(K) = 553K + 5.91 \times C_{11}(GPa) \tag{3.2}$$

Using the above equation, we calculate the Θ_m values for all the systems, studied here. From our calculations (Table 3.4) it is predicted that the melting temperature of these systems are sufficiently high leading to a possibility of application of these materials as SMA even at high temperature. This is particularly true for Co_2PtGa, which is predicted to possess a high Θ_m (1381 $\pm$ 300K)as well as a high T_M (around 886 K),, which are well above the room temperature.

3.3 Conclusion

From first-principles calculations, we study the electronic and magnetic properties of A_2PtGa (A being Cr, Mn, Fe and Co) Heusler alloys. We predict a few new materials with Pt being an essential ingredient. By comparing the energies of various types of magnetic configurations, we predict that Cr_2PtGa and Mn_2PtGa are likely to possess a ferrimagnetic configuration, whereas, Fe_2PtGa and Co_2PtGa may exhibit a long-range ferromagneic ordering in their respective ground states. Analyzing the electronic, magnetic and mechanical properties of all these materials, Co_2PtGa, Cr_2PtGa and Fe_2PtGa are predicted to be three new full Heusler alloy systems, which are likely to show the martensite transition. Among these, Co_2PtGa is likely to possess the highest spin polarization at the Fermi level for both the cubic and tetragonal phases. It also exhibits the lowest inherent crystalline brittleness as well as the highest martensite transition temperature (T_M), high melting temperature (Θ_m) and high Curie temperature (T_C); all of these well above the room temperature. All these observations render Co_2PtGa interesting from both application as well as fundamental points of view.

Chapter 4

Effects of Cr and Fe Substitution at Mn site of Ni_2MnGa and Pt_2MnGa

4.1 Introduction

Interesting magnetocaloric properties as well as an increase of T_M have been experimentally observed as a result of Cu substitution at the Mn site of prototype Heusler alloy Ni_2MnGa.[10, 20] Motivated by these studies, we have studied in detail the effects of medium to large Cu substitution at Mn site of Ni_2MnGa and Mn_2NiGa and the results of the same have been presented in the second chapter of this thesis. We show that a systematic increase of martensitic transition temperature (T_M) is likely as the amount of substitution of Cu at Mn site increases. Further, a difficulty in case of technological application of Ni_2MnGa is that its brittleness is somewhat large.[29, 30] Therefore, we have studied in detail the elastic properties of the austenite phases of Ni_2MnGa, and some of its substituted alloys and presented the results in the same chapter. We observe that Cu substitution at the Mn site leads to a decrease in the inherent crystalline brittleness (ICB) of the material (see Figure 2.9 of this thesis). In chapter 3, we have predicted a new material Co_2PtGa which has higher T_M and lower ICB compared to Ni_2MnGa. Tunability of T_M, T_C and ICB has been a subject of active research for last couple of decades.

Recently, in the literature there have been studies where Mn has been replaced by Fe in Ni_2MnGa and existence of a modulated phase is observed in this substituted material.[135] Furthermore, substitution of Fe at the Mn site has gained importance due to a report of decrease in the brittleness of the material.[136, 137] Moreover, it is interesting to note that some composition of Fe substituted alloy yields T_M which is close to room temperature

as well as higher than that of Ni_2MnGa.[136, 138] These studies on Fe substituting the Mn atom are important from the point of view of application. It is also interesting that Fe has only one electron more than Mn and has high atomic moment close to Mn. On the other hand, in bulk, while Fe bulk has ferromagnetic (FM) configuration, Mn in bulk form exhibits an anti-ferromagnetic (AFM) configuration. Hence, analysis of a systematic substitution of Mn by Fe may provide interesting microscopic insight into the elastic, magnetic and electronic properties of the substituted alloys.

In this work, in addition to Fe, we choose Cr atom as well, for replacing Mn. The motivation behind substituting Cr at the Mn site is that both the elements in bulk form are anti-ferromagnetic in their ground state. Additionally, Cr possesses only one electron less than that of Mn and possesses high atomic moment similar to Mn. These facts may have some interesting role to play in defining the magnetic properties of the substituted materials. Though there exist a few relevant studies in the literature[136–138], the stability of different phases (austenite and martensite) of the materials and the trend of changes in the properties, as a result of increasing substitution of Fe and Cr at the Mn site of Ni_2MnGa , has not been systematically studied so far. We are, thus, particularly interested in the comparative study of stability and magnetic properties of alloys derived from Ni_2MnGa, resulting from substitution of Mn by Cr and Fe atoms. Probing the possibility of martensite transition in materials with Mn substituted by Fe and Cr at different percentages of substitution may also lead to results, important from both application and fundamental points of view.

Recently, as has been discussed in the first chapter of this thesis, for Pt doped Ni_2MnGa (composition $Ni_{1.75}Pt_{0.25}MnGa$)[4], a maximum MFIS of 14% has been predicted on the basis of first-principles calculations. The existence of a modulated structure, which is a prerequisite for a large MFIS[33], has also been shown for $Ni_{1.8}Pt_{0.2}MnGa$, by Neutron diffraction study. Significant magnetocaloric effect (MCE) near room temperature has also been found in $Ni_{1.8}Pt_{0.2}MnGa$.[79] Further, a large increase in martensite transition temperature has already been reported for Pt-doped Ni-Mn-Ga in the literature[80] as well as a decrease in the ICB compared to Ni_2MnGa has been predicted by us (in the earlier chapter) in case of Pt_2MnGa and some of its substituted alloys, for example,

Pt_2CuGa.[118] Hence, it is clear that, Ni_2MnGa, with substitution by Pt at Ni site is expected to have better properties compared to the parent compound (Ni_2MnGa) which may be suitable for technological applications. This has motivated us to probe further the effect of Ni substitution by Pt in Ni_2CrGa and Ni_2FeGa.

Therefore, in the present chapter, we carry out calculations on the stability and of various properties of $A_2Mn_{1-x}B_xGa$ (x = 0.00, 0.25, 0.75, 1.00; A = Ni and Pt; B = Fe and Cr) and present the results. All these alloys have been found to possess a conventional Heusler alloy structure in their ground state configuration. To study the in-between compositions, it has been assumed that the substitution is possible without any kind of phase segregation and consequently, the trend of the energetic stability following the substitution has been obtained from the formation energy calculations of the materials as a function of substitution. We have shown the changes in the formation energy and the martensitic stability as a function of x. For the austenite phase, we consider the cubic symmetry ($L2_1$ structure) and for the martensite phase, we consider the tetragonal distortion of the cubic phase. As is known, some Heusler alloys including Ni_2MnGa show complicated modulated structures. In what follows,, we present and analyze the bulk mechanical and magnetic properties of the materials, Ni_2CrGa, Ni_2MnGa, Ni_2FeGa as well as Pt_2CrGa, Pt_2MnGa and Pt_2FeGa.

4.2 Results and Discussion

4.2.1 Electronic Stability of the bulk austenite and martensite phases

We now, we discuss and compare the electronic stability of the bulk austenite and martensite phases of the Heusler alloys, studied here. From the energy calculations, we find that the conventional Heusler structure of all the materials $A_2Mn_{1-x}B_xGa$ (x = 0.00, 0.25, 0.75, 1.00; A = Pt, Ni; B = Fe, Cr) is lower in energy in comparison to the corresponding inverse structure in the cubic phase. We perform the calculations of the formation energies of all the materials in ferromagnetic configuration using VASP code[51, 52] since the parent compounds Pt_2MnGa and Ni_2MnGa show FM configuration of the Mn atoms.[4, 92]

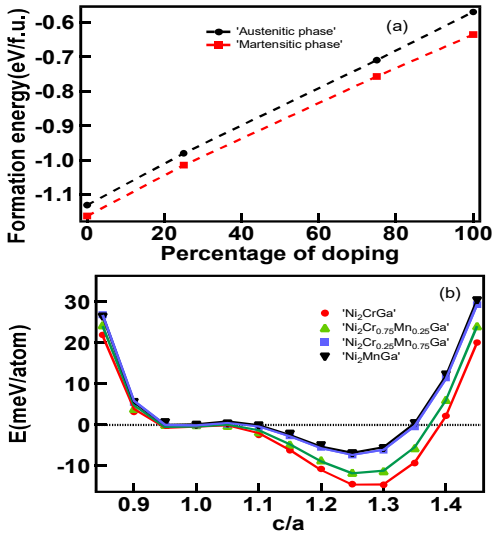

Figure 4.1: (a) Formation energy plotted for $Ni_2Mn_{1-x}Cr_xGa$ for x = 0, 0.25, 0.75 and 1.0: The formation energy decreases as the Cr concentration increases. (b) Probability of martensite transition shown for $Ni_2Mn_{1-x}Cr_xGa$: Equilibrium c/a values are expected to be around 1.25 to 1.3 for the whole composition range. The energy for the martensite phase has been normalized with respect to the energy of the austenite phase. The line joining the data points is just a guide to the eyes.

Calculated values of formation energy of the austenite phase with conventional Heusler alloy structure and ferromagnetic configuration, for all the substituted compounds, are presented in upper panels of Figures 4.1 to 4.4. The negative value of the formation energy indicates that the compound is more stable compared to the respective individual bulk components. More negativity indicates more stability. From these figures, it is clear that the formation energy as a function of x of all the compounds $A_2Mn_{1-x}B_xGa$ (with A = Pt, Ni; B = Cr, Fe; x = 0, 0.25, 0.75 and 1) is negative. The parent compounds Pt_2MnGa and Ni_2MnGa are found to be energetically the most stable ones and overall, Cr substitution gives rise to less stable compounds compared to the Fe substituted and parent Mn-based compounds. It is also observed from the figures that this trend is same for both cubic austenite and non-modulated tetragonal martensite phases. The tetragonal phase shows more negative formation energy compared to their respective cubic austenite phase and this result gives the indication that the tetragonal phase is the lower temperature phase for all the materials. This observation also corroborates with the results presented in lower panels of Figures 4.1 to 4.4 which give the plot of c/a versus the relative energy, *i.e.* energy of tetragonal phase normalized to the energy of the respective cubic phase; c being

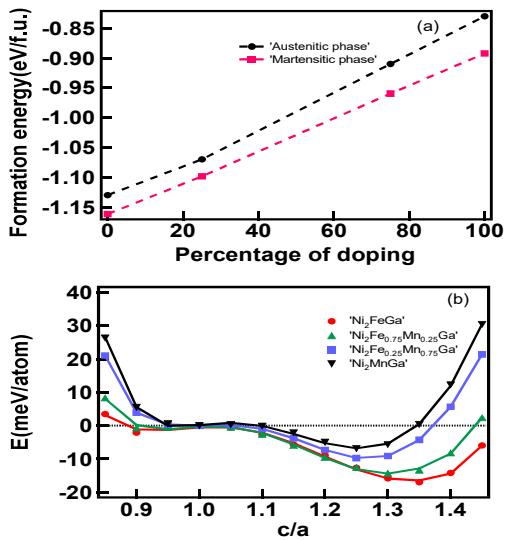

Figure 4.2: (a) Formation energy plotted for $Ni_2Mn_{1-x}Fe_xGa$ for x = 0, 0.25, 0.75 and 1.0: The formation energy decreases as the Fe concentration increases. (b) Probability of martensite transition shown for $Ni_2Mn_{1-x}Fe_xGa$: Equilibrium c/a values are expected to be around 1.25 to 1.35 for the whole composition range. The energy for the martensite phase has been normalized with respect to the energy of the austenite phase. The line joining the data points is just a guide to the eyes.

the lattice constant along the z-direction and a is the lattice constant along the x (and y)-direction. We find that as is seen in case of Pt_2MnGa, Ni_2MnGa, and Ni_2FeGa (observed in the literature), all the substituted alloys including the stoichiometric Pt_2CrGa, Pt_2FeGa and Ni_2CrGa show a stable tetragonal phase which is lower in energy compared to the respective cubic phase. It is worth noting that for the Pt-based alloys, ΔE (energy difference between cubic and tetragonal phases) is reasonably more compared to the Ni-based alloys. We also observe that ΔE systematically increases as Mn is substituted by Cr and Fe. The effect is more pronounced in Ni_2MnGa and its substituted alloys compared to the Pt-based alloys. We show later that the cubic and tetragonal phases have very close equilibrium volume. All these observations put together indicate that the materials studied here are likely to show martensite transition. This warrants a detailed study of the bulk mechanical, electronic and magnetic properties of these materials, since these materials may turn out to be interesting from both application and fundamental points of view.

For a given system, a comparison of the energies of the austenite and martensite phases, ΔE, may give an estimate of the trend of the martensite transition temperature,

Table 4.1: Calculated lattice parameter and trend of martensite transition temperature. Values from the literature are given along with the references which are shown in square brackets.

Material	a_{cubic}(Å)	$(c/a)_{eq}$	ΔE(meV/atom)	T_M(K)
Pt_2FeGa	6.18 6.19[139]	1.34	70.51	817.92
Pt_2MnGa	6.23 6.09[140], 6.23[141] 6.23[139]	1.30 1.30[141]	59.40	689.04
Pt_2CrGa	6.23 6.23[139]	1.30	60.23	698.67
Ni_2FeGa	5.76 5.77[142], 5.76[135] 5.77[143]	1.35 1.33[142], 1.33[135], 1.35[144]	17.04	197.66 142[143]
Ni_2MnGa	5.80 5.81[142], 5.81[92]	1.22 1.22[142],1.25[145]	6.18	71.69 210[146]
Ni_2CrGa	5.80 5.81[139]	1.26	14.88	172.61

T_M, for different systems, within a reasonable confidence interval.[18] Following this, we calculate and analyze ΔE and make a heuristic prediction of the values of T_M for Pt_2CrGa, Pt_2MnGa, Pt_2FeGa as well as Ni_2CrGa, Ni_2MnGa and Ni_2FeGa which are tabulated in Table 4.1. We wish to point out here that the trend in the T_M values over the absolute value of the martensite transition temperature is what is meaningful here and hence the trend only is considered for our further analysis related to the martensite transition.

We observe that all the materials, studied here, are likely to have higher T_M than Ni_2MnGa. The trend is as follows: Mn-derived alloys have lowest T_M, followed by Cr-derived and further followed by Fe-derived compounds for both A = Pt and Ni. Though the experimental value of martensite transition temperature of bulk Ni_2FeGa is lower than that of Ni_2MnGa, which is different from our predicted values (see Table 4.1), we wish to note here that the experimental samples may have inherent defects and that may be one of the reasons for this mismatch in the trend between our calculational result and the experimental value. As is observed from this table, the data are seen to be agreeing well with the literature. The $(c/a)_{eq}$ values of the c/a parameter for the optimized martensite phase for all the compounds are seen to be within the range of values of 1.22 to 1.35; this range matches with the same as is observed for most of the MSMAs found in the literature.

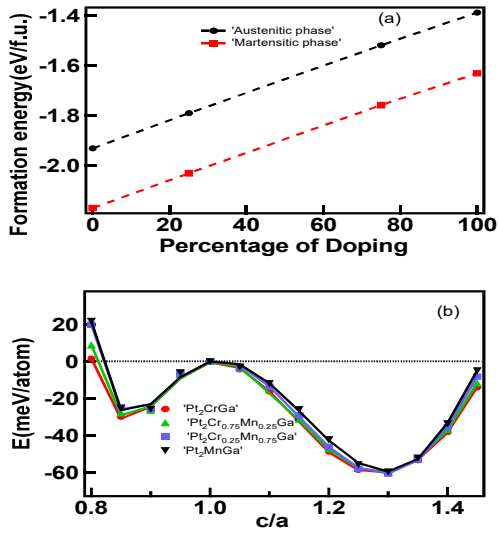

Figure 4.3: (a) Formation energy plotted for $Pt_2Mn_{1-x}Cr_xGa$ for x = 0, 0.25, 0.75 and 1.0: The formation energy decreases as the Cr concentration increases. (b) Probability of martensite transition shown for $Pt_2Mn_{1-x}Cr_xGa$: Equilibrium c/a values are expected to be around 1.3 for the whole composition range. The energy for the martensite phase has been normalized with respect to the energy of the austenite phase. The line joining the data points is just a guide to the eyes.

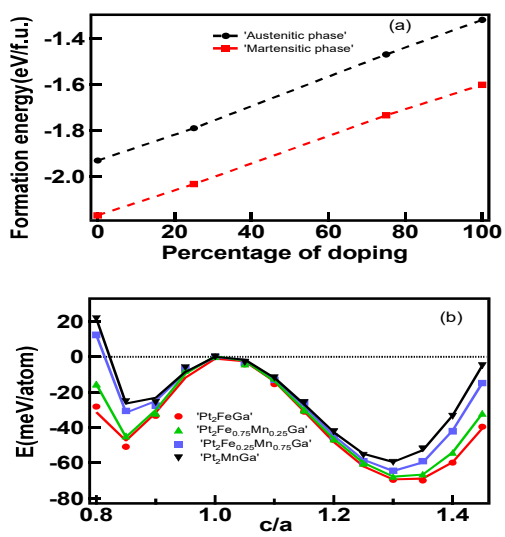

Figure 4.4: (a) Formation energy plotted for $Pt_2Mn_{1-x}Fe_xGa$ for x = 0, 0.25, 0.75 and 1.0: The formation energy decreases as the Fe concentration increases. (b) Probability of martensite transition shown for $Pt_2Mn_{1-x}Fe_xGa$: Equilibrium c/a values are expected to be around 1.3 to 1.35 for the whole composition range. The energy for the martensite phase has been normalized with respect to the energy of the austenite phase. The line joining the data points is just a guide to the eyes.

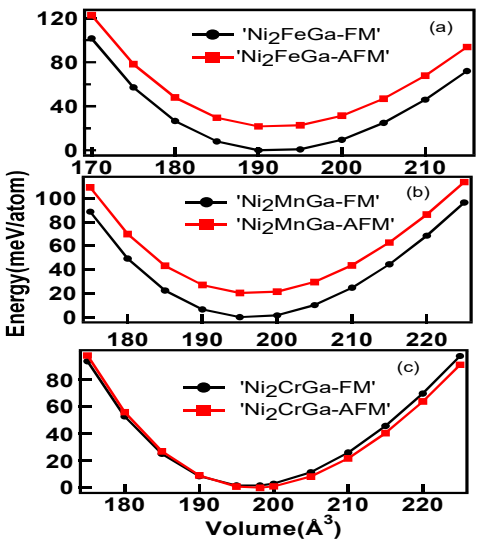

Figure 4.5: Energy versus volume plots for different magnetic configurations for the austenite phases of Ni_2BGa with B = (a) Fe, (b) Mn, (c) Cr. Value of the energy is normalized with respect to energy of ground state magnetic configuration. The lines are guide to the eyes only.

4.2.2 Magnetic Properties

In this subsection we discuss about the magnetic properties of all the systems studied here. First we probe the ground state magnetic configuration for their bulk austenite phase. In Figure 4.5 and Figure 4.6 we have plotted, for both FM and AFM configurations, the energy of the Ni-based and Pt-based systems, respectively, as a function of unit cell volume in their cubic phases. We have also carried out calculations of total energy in the phases with net zero magnetic moment. But the formation energies of these are found to be positive which implies that this type of magnetic configuration will subject the system to electronic instability and are not considered further and not shown in the figures as well. We have considered two types of anti-ferromagnetic configurations as starting magnetic configurations: AFM-I and AFM-II, which we describe now.

In all of our calculations, we have used P1 symmetry so there are four formula units corresponding to the conventional A_2BC structure in each case. In our considered supercell, there are eight A atoms and four B atoms. In the AFM-I type of configuration, spins of the A atoms are taken to be anti-parallel to the spins of the B atoms. So it is an *inter-sublattice* anti-ferromagnetic configuration. On the contrary, AFM-II type of spin configuration is an *intra-sublattice* anti-ferromagnetic configuration. In this, all the A

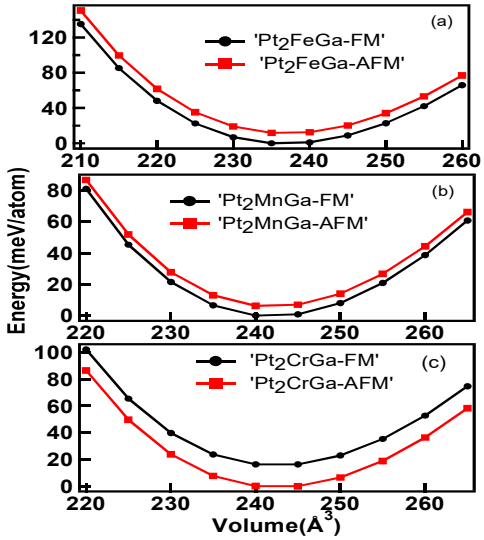

Figure 4.6: Energy versus volume plots for different magnetic configurations for the austenite phases of Pt_2BGa with B = (a) Fe, (b) Mn, (c) Cr. Value of the energy is normalized with respect to energy of ground state magnetic configuration. The lines are guide to the eyes only.

atoms have the same spin and ferromagnetic configuration. But out of the four B atoms, two are considered to have spin configurations parallel to the A atoms; and moments of the other two B atoms are taken to be anti-parallel to the other B atoms and consequently to all the A atoms. However, the AFM-I type of magnetic configuration is found to converge to the ferromagnetic configuration. Hence, we have not included the results corresponding to this magnetic structure in Figures 4.5 and 4.6. For A_2MnGa and A_2FeGa (A = Pt, Ni), AFM-II type of magnetic configuration has been found to be higher in energy though energetically very close to the FM configuration. However, for A_2CrGa (A = Pt, Ni) the AFM-II magnetic configuration is found to be lower in energy compared to the respective FM configuration. These indicate that for A_2MnGa and A_2FeGa, long-range ferromagnetic ordering is the ground state magnetic configuration whereas for A_2CrGa the ground state magnetic configuration is AFM-II. Following this finding related to the alloys having Cr as B atom, we have repeated all the calculations of A_2CrGa (A = Ni and Pt) taking into consideration the AFM-II magnetic configuration and considered the AFM-II phase only for all further calculations. We mention here that from this point onwards, AFM indicates AFM-II only (in Figure 4.5 and 4.6 as well).

First and foremost, we analyze the formation energy of the austenite and martensite

Table 4.2: Magnetic moments for the austenite and martensite phases; in brackets we provide the value of the partial moments; the first and second numbers correspond to the B and A atoms. Values from the literature are given along with the references which are shown in square brackets.

Materials	Austinitic phase (μ_B/f.u.)	Martensitic phase (μ_B/f.u.)
Pt_2FeGa	3.258(3.025, 0.088) 3.24[139]	3.401(2.970, 0.204)
Pt_2MnGa	4.169(3.671, 0.138) 4.15[139], 3.86[141]	4.173(3.627, 0.188)
Pt_2CrGa	0.000(±3.013, ±0.019)	0.000(±3.009, ±0.003)
Ni_2FeGa	3.343(2.812, 0.286) 3.27[139], 3.31[142]	3.349(2.656, 0.380) 3.36[142]
Ni_2MnGa	4.093(3.296, 0.357) 4.05[139], 4.17[142], 4.096[92]	4.155(3.231, 0.425) 4.23[142], 4.115[92]
Ni_2CrGa	0.000(±2.629, ±0.026)	0.000(±2.654, ±0.009)

phases of these two materials and find that the formation energy is consistently negative, implying the electronic stability. Further, in Figure 4.7, we plot the c/a versus ΔE (energy of the tetragonal phase is normalized with respect to the energy of the respective cubic phase). We find that for Ni_2CrGa as well as Pt_2CrGa, upon complete optimization of geometry (calculated from VASP[51, 52] and cross-checked using CASTEP[53] packages), the system always converges to at the tetragonal phase. This may be due to the much larger ΔE values in these materials in the AFM-II magnetic configuration, in comparison to the energy difference in their respective FM configuration. The equilibrium c/a values for both the materials fall in the range of 1.25 to 1.3 which indicates the possibility of a martensite transition though it is to be noted that these materials are not likely to exhibit ferromagnetic properties.

Next we discuss the change in magnetization of the systems as they undergo structural transition from cubic phase to the tetragonal phase. It is observed from Table 4.2 that, our results on the magnetic moments of the systems match well with the literature wherever available. We also observe that for both Mn and Fe-based alloys, total magnetic moment increases as the system undergoes the transition from cubic to tetragonal structure. On the other hand, the Cr-derived systems have anti-ferromagnetic configuration in both the austenite and martensite phases. In the Heusler alloys discussed here with general formula A_2BC (A = Pt, Ni; B = Fe, Mn, Cr; C = Ga), the main contribution to the total magnetic moment comes from the B element (Fe, Mn, Cr). One possible origin

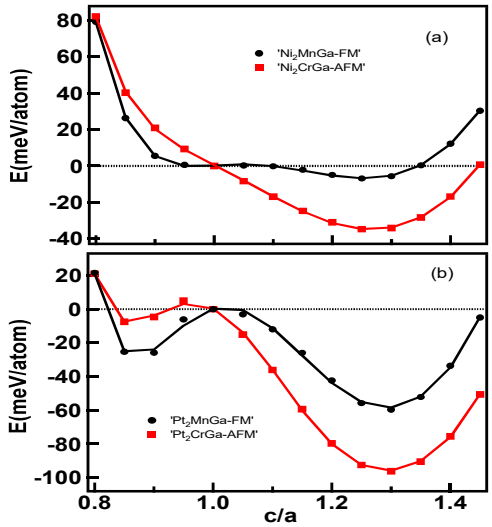

Figure 4.7: Probability of martensite transition shown for (a) Ni_2CrGa and (b) Pt_2CrGa: the energy for the martensite phase has been normalized with respect to the energy of the cubic austenite phase. The lines are just guide to the eyes.

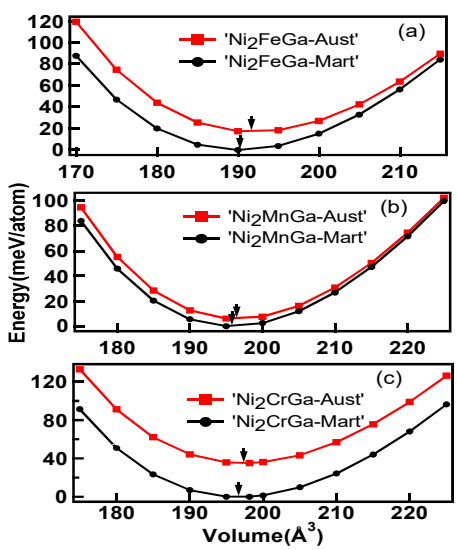

Figure 4.8: Energy versus volume plots for the optimized austenite and martensite phases of Ni_2BGa with B = (a) Fe, (b) Mn, (c) Cr for the respective lowest energy magnetic configurations. The volume conservation is highlighted using arrows at the equilibrium volumes for each of the phases. The lines are just guide to the eyes.

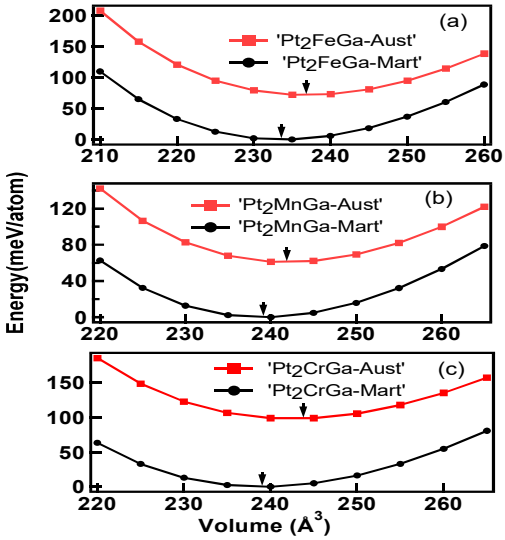

Figure 4.9: Energy versus volume plots for the optimized austenite and martensite phases of Pt_2BGa with B = (a) Fe, (b) Mn, (c) Cr for the respective lowest energy magnetic configurations. The volume conservation is highlighted using arrows at the equilibrium volumes for each of the phases. The lines are just guide to the eyes.

of magnetic moment of the A element is due to the induction from B atom as observed in the literature.[126] We see from Table 4.1 that the lattice parameters of the Pt-based systems are much larger compared to the Ni-based systems. This gives rise to a larger B-B distance and leads to the possibility of more localization of magnetic moments on the B sublattice. It is to be noted that Sosioglu et. al.[91] have studied a series of Heusler alloys Cu_2MnC and Pd_2MnC (C = In, Sn, Sb, Te). They have observed a very small induced moment in Cu and Pd, whereas the total moments of the systems were mostly contributed by the Mn sublattice. Further, the increased lattice parameter in Pt-based systems as observed by us causes a larger separation between A and B atoms. Hence we see from Table 4.2 that the partial moments of A atoms decrease in Pt-based alloys compared to the Ni-based ones. As a result, the total moment of the system depends on both the factors: moment of the B atom as well as the induced moment on the A atom.

Figures 4.8 and 4.9 give the energy versus volume plots for the optimized austenite and martensite phases of Ni_2BGa and Pt_2BGa, respectively (B = Fe, Mn, Cr) in their respective lowest energy magnetic configurations. The volume conservation in each case between the austenite and martensite phase is highlighted by marking the equilibrium volumes for each of the phases. The maximum change of volume being about 1.96%.

This indicates that while the Mn and Fe-based compounds are prone to be FSMA, the Cr-based alloys are likely to show AFSMA properties.

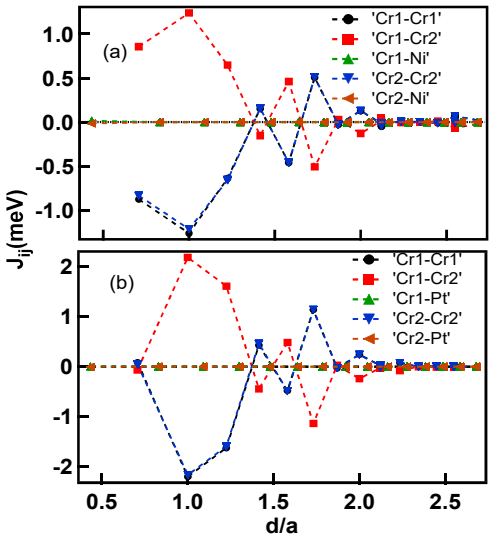

Figure 4.10: Heisenberg exchange parameters J_{ij} of Cr atom with its neighbours as a function of normalized distance d/a where a is the lattice constant of the austenitic phase for (a)Ni_2CrGa (b)Pt_2CrGa in their correct magnetic ground state (AFM) configuration in the cubic phase. The lines are just guide to the eyes.

4.2.3 Heisenberg exchange coupling constant of AFM Ni_2CrGa and Pt_2CrGa

In Figure 4.10, we show the variation of J_{ij} in their magnetic ground state (AFM configuration) of Ni_2CrGa and Pt_2CrGa. The calculations for *intra-sublattice* AFM configuration have been performed within coherent potential approximation implemented in the SPR-KKR code,[56] by considering that 50% of the body-centered site(fractional coordinates 0.5, 0.5, 0.5 and its fcc equivalent sites) is occupied by up spin Cr atom (Cr1) and rest 50% of the site is occupied by down spin Cr atom (Cr2). From Figure 4.10, as expected, we can see that Cr1-Cr1 interaction is almost identical with the Cr2-Cr2 interaction for the materials. Also the interaction is of RKKY type as is indicated by the J_{ij} plots. One more interesting point to note for these systems is that the magnetic interaction between Cr1-Cr1 (also Cr2-Cr2) is exactly cancelled by the Cr1-Cr2 (Cr2-Cr1) interaction. These two strong and mutually cancelling exchange interactions may have led to the intra-sublattice anti-ferromagnetic ordering as the ground state magnetic configuration for both of these

systems.

4.2.4 Density of states of cubic phases

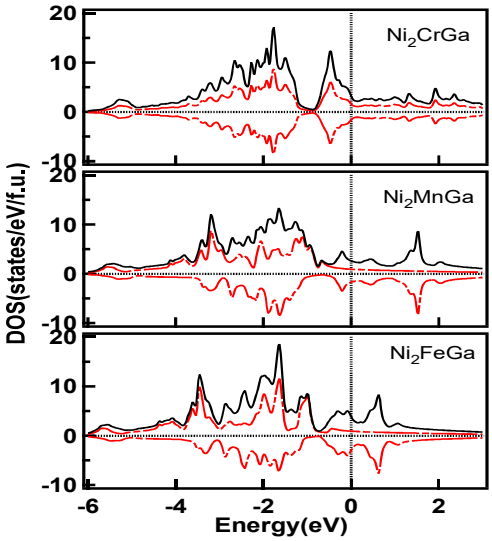

Figure 4.11: Total DOS and Spin polarized DOS for Ni-based materials; solid line represents the total DOS and the majority and minority spin DOS are shown by dash-dotted lines

First we discuss the density of states (DOS) of the Ni_2BGa (B = Cr, Mn, Fe) systems and we compare these results with the Pt_2BGa systems. Figure 4.11 shows the total DOS of all the Ni-based materials along with the spin polarized DOS. From the total DOS we can see that for Ni_2MnGa, there is a double peak structure very close to the Fermi level. The implication of this peak and also the peak in the minority DOS very close to Fermi level which plays a crucial role in favouring martensite transition have been discussed in detail in the literature and also in chapter 2 of this thesis.[118, 90] From Figure 4.11, it is clear that all the Ni-based materials are having a prominent Ni d-electron derived peak very close to (and also below) the Fermi level. While for Fe and Mn cases, the minority spin makes the major contribution, in case of Cr, both the spin densities of states show similar intensity. We note that it is expected from their respective DOS that the tetragonal distortion may lower the energy of these systems compared to their cubic structure, which can be very well explained by band Jahn-Teller distortion mechanism as has been observed in case of Ni_2MnGa in the literature.[35, 90, 104, 117] Similarly for

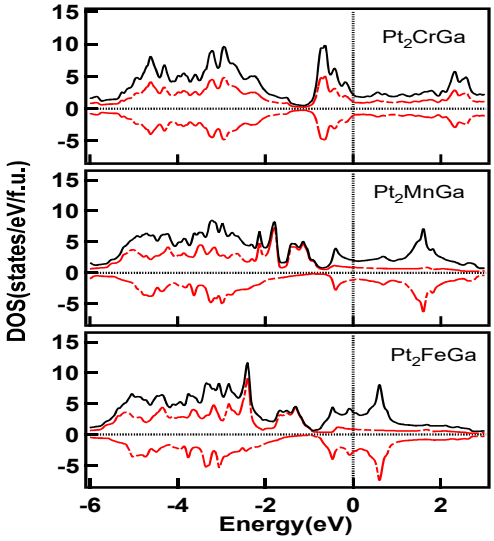

Figure 4.12: Total DOS and Spin polarized DOS for Pt-based materials; solid line represents the total DOS and the majority and minority spin DOS are shown by dash-dotted lines

Pt-based systems also, we can find from Figure 4.12, that such peaks in the DOS exist which are very close to the Fermi level.It is interesting to observe that the contributions of the majority and minority spin DOS close to Fermi level are similar in both the Pt and Ni-based systems.

4.2.5 Mechanical Properties

Mechanical Properties of the bulk Austenite phase

Now we discuss the mechanical properties of the cubic austenite phase of Pt_2MnGa, Ni_2MnGa and their substituted alloys. All the relevant parameters are listed in Table 4.3 and we observe that there is a good matching with the results available in the literature. As we discussed in the earlier section, the complete geometry optimization of Pt_2CrGa and Ni_2CrGa directly led to the more stable martensite phase. Therefore, in Table 4.3 we list the bulk mechanical parameters of the austenite phases of only Ni_2MnGa, Ni_2FeGa, Pt_2MnGa and Pt_2FeGa. For cubic lattices, only three independent elastic constants exist, C_{11}, C_{12} and C_{44}, where, symmetry dictates that: $C_{11} = C_{22} = C_{33}$; $C_{12} = C_{23} = C_{13}$ and $C_{44} = C_{55} = C_{66}$. The three experimentally measurable elastic constants are: C_{44}, $C' = 0.5*(C_{11}$ - $C_{12})$ and $C_L = 0.5*(C_{11} + C_{12} + 2C_{44})$.

Table 4.3: Bulk mechanical properties of austenite phase of materials. Values from the literature are given along with the references which are shown in square brackets.

Elastic constants	Pt_2FeGa	Pt_2MnGa	Ni_2FeGa	Ni_2MnGa
C_{11}(GPa)	151.75	145.75	162.41 162.2[142],166.0[135]	162.48 152.0[24]
C_{44}(GPa)	70.33	66.34	109.78 103.8[142],109.8[135]	108.91 103[24]
C_{12}(GPa)	210.86	193.22	177.51 165.5[142],168.9[135]	157.32 143[24]
B (GPa)	191.15	177.40	172.48 164.4[142],168.0[135]	159.04 146[24]
G_V (GPa)	30.37	30.31	62.85 61.62[142],65.3[135]	66.38 63.6[24]
G_R (GPa)	-199.91	-128.04	-21.03 -4.23[142],-3.70[135]	6.23 10.56[24]
G_V/B	0.16	0.17	0.36	0.42
C^p(GPa)	140.53	126.88	67.73	48.41
C'(GPa)	-29.56	-23.74	-7.56 -1.6[142],-1.5[135]	2.58 4.5[24]
Θ_D (K)	200	200	399	411
B/C'	-6.46	-7.47	-22.81	61.64
A	-2.37	-2.79	-14.52	42.21

These parameters are related to the experimental acoustic phonon modes TA_1, TA_2 and LA.[24] From Table 4.3, we compare our calculated elastic constants with the experimental and earlier theoretical results, wherever data are available in the literature. The mechanical stability of the cubic phase signifies the following conditions: (1) $C_{11} > 0$; (2) $C_{44} > 0$; (3) (C_{11}-C_{12}) > 0; (4) (C_{11}+2C_{12}) > 0.[78] We note that the third one is not met with most of the alloys studied here. For stable cubic crystals, the value of C_{11} is found to be much higher than that of C_{12}. However, we find from Table 4.3 that the values of C_{11} are either marginally higher or even lower than those of C_{12}. As a result of this, the tetragonal shear constant C' (= 0.5*(C_{11} - C_{12})) is seen to have either a value close to zero or a negative value. This implies that these materials are prone to a tetragonal distortion. The fact that the martensite phases possess more negative formation energy (see Figures 4.1 to 4.4) compared to the austenite phases for all the materials corroborates with this. The softening of the C' parameter is closely related to the possible martensite transition as is observed in the literature and also in this thesis.[24, 27]

The bulk modulus, B, is connected to the elastic constants in the following way: B = (1/3)*(C_{11} + 2 C_{12}). The calculated values of B have been listed in Table 4.3.

The isotropic shear modulus, G, is related to the resistance of a material to the plastic deformation. In literature, it has been shown[102] that the value of G lies in between the values of shear modulii given by formalisms of Voigt (G_V)[100] and Reuss (G_R)[101], which means $G = (G_V + G_R)/2$. We observe from Table 4.3, that for austenite phase of Ni_2MnGa, the experimental G value is close to the G_V value while G_R value is largely underestimated, which is due to the small positive or negative values of C'. Following this observation, we consider only the G_V value as the shear modulus (G) though it is generally considered to be the higher limit of the same. This particular aspect, in regard to this set of Heusler alloys, showing martensite transition, has been discussed in the literature and also in chapter 2.[118] Further, as discussed in detail in the previous chapter, a combination of a large value of G/B and a small value of Cauchy pressure (C^p) corresponds to a large ICB. In the present work, we observe that the trend of ICB goes as : ICB (Ni_2MnGa) > ICB (Ni_2FeGa) > ICB (Pt_2MnGa) > ICB (Pt_2FeGa). Further we have calculated the Debye temperature (Θ_D) from the averaged sound velocity which is dependent on the longitudinal and transverse elastic wave velocities of the material which are in turn derived from the bulk and shear modulii of a material.[27, 147] We observe that both the Pt-derived alloys have similar Θ_D values which is true for the Ni-derived alloys as well. The available experimental value for Ni_2MnGa has a much smaller value[112] which may be partly due to the somewhat larger value of shear modulus (G_V) used in our calculations. Furthermore, we calculate the anisotropy factors of the austenite phase.[148] The anisotropy factor for the austenite phase, A, has been defined as follows: $A = 2{*}C_{44}/(C_{11} - C_{12})$. If the material is completely isotropic, $A = 1$. On the other hand, values away from 1 (smaller or larger) give the measure of degree of elastic anisotropy. From our calculations the austenite phases of all the materials show large degree of elastic anisotropy. We wish to note here that, materials which undergo martensite transition possesses high value of A.[149]

Mechanical Properties of the bulk Martensite phase.

In this subsection, we discuss the bulk mechanical properties of the martensite phases of all the materials. All the relevant parameters are listed in Table 4.4 and we observe

Table 4.4: Bulk mechanical properties of martensite phase of materials. Values from the literature are given along with the references which are shown in square brackets.

Elastic constants	Pt_2FeGa	Pt_2MnGa	Pt_2CrGa	Ni_2FeGa	Ni_2MnGa	Ni_2CrGa
C_{11}(GPa)	271.68	237.68	244.58	225.31 248.5[135]	219.11 252[27]	221.11
C_{33}(GPa)	270.76	264.14	255.19	230.22 207.1[135]	200.94 194[27]	201.52
C_{44}(GPa)	65.50	66.30	80.23	93.49 104.8[135]	96.49 100[27]	104.98
C_{66}(GPa)	97.88	116.83	84.13	84.37 45.3[135]	86.49 55[27]	76.99
C_{12}(GPa)	181.52	171.73	156.00	142.90 96.0[135]	111.30 74[27]	108.13
C_{13}(GPa)	152.26	141.74	147.18	153.52 158.1[135]	144.48 144[27]	135.70
B (GPa)	198.20	183.32	182.78	175.51 169.8[135]	159.80 158[27]	155.94
G_V (GPa)	67.65	68.83	68.52	69.66	71.82	75.07
G_R (GPa)	63.67	58.66	64.09	58.47	55.68	61.53
G_H (GPa)	65.66	63.75	66.30	64.07	63.75	68.30
G_H/B (G_V/B)	0.33 (0.34)	0.35 (0.38)	0.36 (0.37)	0.37 (0.40)	0.40 (0.45)	0.44 (0.48)
C′(GPa)	45.08	32.98	44.29	41.21 76.3[135]	53.91 89[27]	56.49
B/C′	4.39	5.56	4.13	4.26	2.96	2.76
Θ_D (K)	291	287	294	403	403	411

that there is a good matching with the results available in the literature. The mechanical stability of the tetragonal phase signifies the following conditions: (1) All of C_{11}, C_{33}, C_{44}, $C_{66} > 0$; (2) (C_{11}-C_{12}) > 0; (3) (C_{11}+C_{33}-2C_{13}) > 0; (4) (2(C_{11}+C_{12})+C_{33}+4C_{13}) > 0.[78] We observe that for all the materials, the above-mentioned conditions are fulfilled and this indicates that the tetragonal phase is mechanically as also electronically (see Figures 4.1 to 4.4) stable. Next we analyze the results of the shear and bulk modulus and the ratio between these.

From the absolute values of G/B, which for the ease of comparison with the respective values of the austenite phase, taken as G_V/B, it is clear that for Ni-derived compounds, the values are close to the those of the austenite phase. On the other hand, for the Pt-based compounds, the G/B value is larger in the martensite phase compared to the austenite phase, indicating that the ICB is expected to be higher in this phase compared to that in the austenite phase. It is interesting to see that for all the 6 materials studied, values of the shear modulus given by the formalisms of Voigt and Reuss are similar and

the G_R is not underestimated in the martensite phase as observed in case of the austenite phase of the same material. Consequently, in the martensite phase, the ratios G_V/B, G_R/B and G_H/B are quite close to each other. Since the tetragonal phase is the lower energy state for all the materials studied here, probably for the ground state of a Heusler alloy material, the ratios of shear and bulk modulus, given by Hill[102], Voigt[100] and Reuss[101], are close to each other as has been observed for the cubic half-metallic Heusler alloys.[107–110]

The Debye temperature (Θ_D) values for the martensite phase for all the compounds are calculated and tabulated in Table 4.4. It is observed that for the Ni-based alloys the Θ_D values are similar to each other as well as to the values for the austenite phase. On the contrary, for Pt_2MnGa and Pt_2FeGa, the Θ_D values are clearly much larger compared to the values obtained for their respective cubic phase. In this context, it is to be noted that the Θ_D values are derived from G and B values.[27, 147] In case of Ni_2BGa (B = Fe, Mn and Cr), not only the values of bulk modulus are similar between the two phases, but also the G (G_V for austenite phase) values are close to each other (Ni_2BGa, B = Fe, Mn and Cr). As a consequence, the Θ_D values are similar for austenite and martensite phases in case of Ni-based alloys. Also we observe that all the three materials have values which are very close to each other. For Pt_2BGa (B = Fe, Mn and Cr) the shear modulus in the cubic austenite phase has lower value, implying that the resistance to a plastic deformation is lower in these materials compared to their Ni-derived counter-parts. On the other hand, the values of shear modulus in the martensite phase are much comparable in Ni and Pt derived systems. As a consequence, higher Θ_D values result as is observed from our calculations.

4.3 Conclusion

Using first-principles density functional theory based calculations, we investigate the effects of Fe and Cr doping at the Mn site on mechanical, electronic, and magnetic properties of Pt_2MnGa as well as Ni_2MnGa for comparison. We find that these substitutions are likely to yield stable compounds. Contrary to the Fe substitution, the Cr substitution at the Mn site leads to lowering of energy for an *intra-sublattice* anti-ferromagnetic

configuration compared to the ferromagnetic ordering. In this work, we predict two *intra-sublattice* anti-ferromagnetic alloys, namely, Pt_2CrGa and Ni_2CrGa, which are likely to show martensite transition.

Chapter 5

Probing the Possibility of Coexistence of Martensite Transition and Half-metallicit in Ni and Co-based Full Heusler Alloys

5.1 Introduction

It is clear from the literature, that in terms of different physical, including, structural, electronic and magnetic properties, the full Heusler alloys show a rich variety. Among the full Heusler alloys (FHA), both conventional and inverse Heusler structures have been observed. In terms of the electronic structure, there are various categories among the FHAs. While some of these alloys prefer to be in a metallic state, some are found to be semiconducting in nature, and some are having a large spin-polarization at the Fermi level.[1, 3, 150, 151] If the FHAs are magnetic in nature, their properties may change when a magnetic field is applied which can be of interest in terms of potential technological application. Hence, specially, magnetic Heusler alloys are gaining increasing interest among the researchers. In the literature, various magnetic ground state configurations are observed in case of full Heusler alloys. While some alloys carry net zero magnetic moment, many of these exhibit a long-range ferromagnetic ordering and are expected to show magnetic shape memory alloy (MSMA) property. Further, it has also been observed that some of these alloys including Mn_2NiGa, Mn_2NiIn even show long-range ferrimagnetism and also some alloys even exhibit anti-ferromagnetism[11, 12, 66, 152–154] or as shown in this thesis (previous chapter) few alloys may possess intra-sublattice anti-ferromagnetism.

It is of particular interest that, as it has been shown in the literature as well as in some of the earlier chapters of this thesis, that, out of all the full Heusler alloys, only a few undergo the martensite transition. These alloys are prone to a cubic to non-cubic distortion when temperature is lowered, and the volume is practically conserved in this transition; these alloys are generally likely to exhibit the technologically important SMA property. These FHAs in general are found to be metallic in nature. On the other hand, it has been observed that there is another group of full Heusler alloys which are half-metallic-like in nature, with a much reduced density of states (DOS) at the Fermi level in case of one of the spin channels. These materials generally do not show the tendency of undergoing a tetragonal distortion. However, an application in the field of spintronics is a possibility for these materials. From both the points of view of fundamental understanding as well as technological application, it can be interesting to probe the similarities and differences in magnetic, bulk mechanical, and electronic properties of these two categories of materials. It will also be interesting to see if there is any FHA which has a tendency to undergo a tetragonal transition and at the same time possesses a high spin polarization at the Fermi level.

Keeping these aims in mind, in the present chapter, we systematically probe the magnetic, bulk mechanical, and electronic properties of a series of Ni and Co-based full Heusler alloys (in total forty materials) using density functional theory (DFT) based electronic structure calculations. The choice of these two systems (Ni and Co-based FHAs) is due to the following facts. First and foremost, it has been observed in literature that typically, a large amount of studies dedicated to the FHAs are on Ni and Co-based compounds. It is found that while quite a few of the Ni-based FHAs tend to undergo martensite transition, many of the Co-based FHAs exhibit a large spin-polarization at the Fermi level. It has also been pointed out in the literature, that while the magnetic interactions are somewhat different in the Ni and Co-based FHAs, the total energy variation for an austenite to martensite phase transition is similar.[88] Hence, a comparative study may be interesting and also important for detailed understanding of various physical properties of these alloys. The primary interest is to study the possibility of co-existence of tetragonal transition versus a high spin polarization at the Fermi level. Further, we look

for new ferromagnetic materials so that the realization of MSMA property in these may be a possibility.

5.2 Results and Discussion

In this section we discuss our observed results. As is well-known, the full Heusler alloys, as for example, the prototype Ni_2MnGa, commonly assume an ordered A_2BC structure, where typically A, B are elements with d-electrons and C are elements with s, p electrons. Here, we have carried out calculations on Ni and Co-based systems. So Ni and Co are taken as A atom and C = Ga as well as Sn. As for the B atom, we have taken into consideration and consequently tested the electronic stability of the first five atoms of the first as well as second rows of the transition metal atoms, Sc, Ti, V, Cr and Mn as well as Y, Zr, Nb, Mo and Tc are considered as the B atom. All the systems studied here possess conventional Heusler alloy structure.

5.2.1 Geometry Optimization and Electronic Stability

Lattice parameter and Atomic number Z of B atom - For the cubic phase, the $L2_1$ structure has been assumed for all the structures studied here, namely, Ni_2BC and Co_2BC (B = Sc, Ti, V, Cr and Mn as well as Y, Zr, Nb, Mo and Tc; C = Ga and Sn). The geometry has been optimized to obtain the converged lattice parameter, using VASP code.[51, 52] Figure 5.1 and Figure 5.2 show the variation of this lattice parameter as a function of Z of B elements of A_2BC alloy (A = Ni, Co; C = Ga, Sn). The B atoms correspond to the period IV of the periodic table (first row transition metal atoms; Sc etc) and the period V (second row transition metal atoms; Y etc). Therefore, in Figure 5.1 and Figure 5.2, we have mentioned the period numbers IV and V in the legends.

For the Ni_2BC materials, it is observed, as the atomic number of B elements increases, with a saturating trend towards higher Z, lattice parameters of the materials decrease for a fixed row of the periodic table (Figure 5.1). This may happen due to the increasing electro-negativity and decreasing atomic radius of atoms across the column. Further, for these materials we observe (in the left panel of Figure 5.1) a sudden increase in the lattice parameter value for Z of B = 24 (i.e. Cr atom). It is to be noted that out of

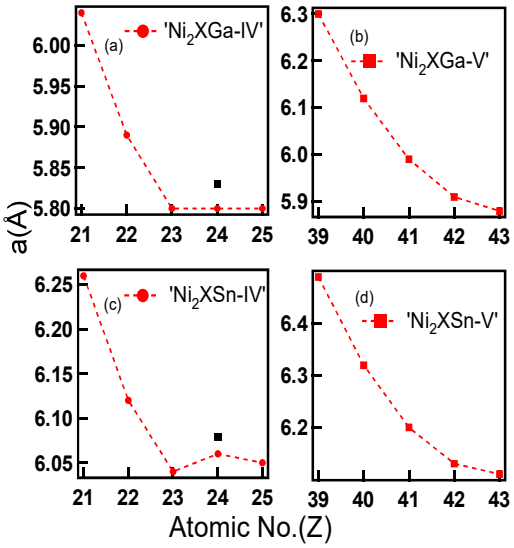

Figure 5.1: Variation of lattice parameter as a function of Z of B elements for Ni_2BC alloy (C = Ga, Sn); X=B atoms being first five transition metal elements of period IV (left panel) and V (right panel). The lines are just guide to the eyes.

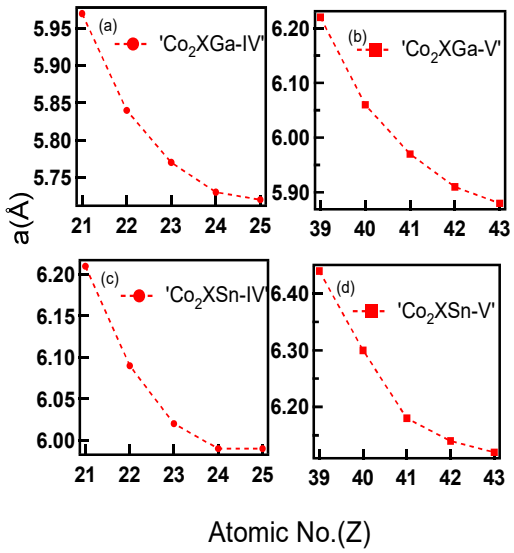

Figure 5.2: Variation of lattice parameter as a function of Z of B elements for Co_2BC alloy (C = Ga, Sn); X=B atoms being first five transition metal elements of period IV (left panel) and V (right panel). The lines are just guide to the eyes.

all the materials studied here, a deviation from the ferromagnetic nature is expected for Ni_2CrSn as well as Ni_2CrGa as described in an earlier chapter (chapter 4).[154] These two materials have lower energy for a long-range *intra-sublattice* anti-ferromagnetic (AFM) ordering compared to the ferromagnetic (FM) one. This difference in the long-range magnetic interaction between the FHAs with B = Cr and the other B atoms indicates that the Cr-based materials are possibly of a different class compared to the rest of the FHAs, considered here and this may be the reason behind the deviation from the observed trend. It is to be further noted that for the AFM ordering, the lattice parameter (shown by a black square) is even larger compared to the corresponding FM phase. However, the long-range magnetic interaction in all the materials with A = Co is ferromagnetic. It is worth-noting that for these Co-based materials the lattice parameters show a smooth decrease as we increase the Z of the B atom (Figure 5.2). As discussed above for Ni-based systems, this may, again, be due to the increase of electronegativity and decrease of atomic radius across the column which may have led to the shrinkage of the electron cloud around the B atom, and consequently, of the whole unit cell. It has been observed that there is an increase in the lattice parameter values when we go from period IV to period V, for both Ni and Co-based materials. Increase of atomic radius is observed across the row, going from period IV to V, and the above-mentioned trend may be attributed to this increase.

Formation energy and Atomic number Z of B atom - Figure 5.3 as well as Figure 5.4 suggest that the formation energy (E_{form}) is negative for all of the materials with C atom = Ga, except Ni_2TcGa which is having a marginally positive formation energy. It is to be noted that Co_2TcGa has a marginally negative formation energy and hence in reality these materials may not turn out to be electronically stable. It is well-known that negative formation energy signifies ease of formation of the material and in turn, may indicate energetic stability; more negativity indicates more stability of the material. A few of the materials, A_2BC, where C = Sn, like Ni_2MoSn, Ni_2TcSn, Co_2CrSn, Co_2MoSn and Co_2TcSn, are having positive formation energy. These calculated values and the prediction that these particular materials are electronically unstable, matches with the results wherever available in the literature.[139] The AFM phases for Ni_2CrGa

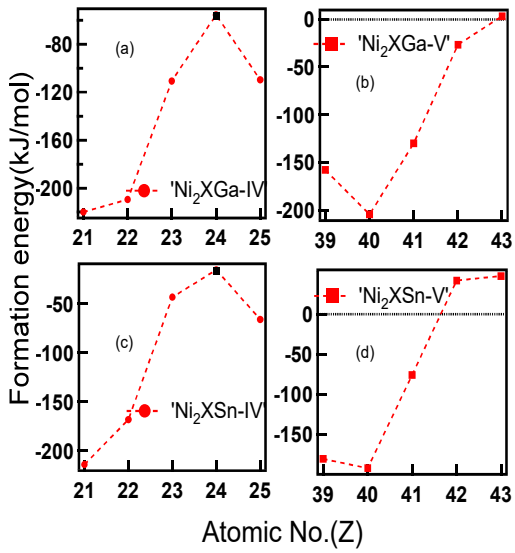

Figure 5.3: Variation of formation energy as a function of Z of B elements for Ni_2BC alloy (C = Ga, Sn); X=B atoms being first five transition metal elements of period IV (left panel) and V (right panel). The lines are just guide to the eyes.

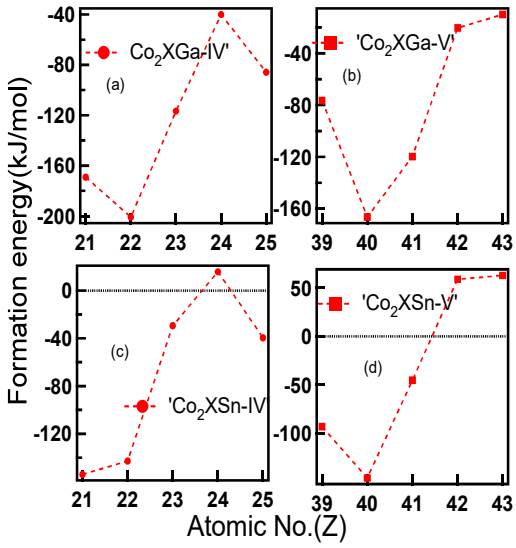

Figure 5.4: Variation of formation energy as a function of Z of B elements for Co_2BC alloy (C = Ga, Sn); X=B atoms being first five transition metal elements of period IV (left panel) and V (right panel). The lines are just guide to the eyes.

and Ni_2CrSn have very close but slightly smaller E_{form} compared to the respective FM case. It is observed from both the figures that, overall, there is a trend of electronic stability decreasing as Z of B atom increases. However, for B = Mn, the stability has increased compared to the previous B element. This suggests an interesting preference for the Mn atom in the B position for the Heusler alloys with $L2_1$ structure in both the cases when A atom is Ni or Co. Similar is the case with B = Zr. It is seen that, for Y, i.e. the first atom of the second row of the transition metal atoms (period V) at the B position, the formation energy is somewhat unfavorable compared to the next case of B = Zr. The origin of this has been found to be electronic in nature - analysis of the density of states for B = Zr, presented later in this chapter, indicates a lowering of binding energy in this material compared to the B = Y case. For our further discussions, we concentrate only on the materials which, from our calculations, are found to be electronically stable.

Electronic Stability of the Tetragonal phase - We calculate the difference between the energy of the cubic (E_C) and tetragonal (E_T) phases of all the electronically stable materials. Figure 5.5 shows this energy difference, ΔE = E_T - E_C (in units of meV per atom), as a function of the ratio of lattice constants c and a for some typical materials. From our calculations, we find that only a few of the materials, among all the electronically stable and magnetic FHAs we study here, exhibit the tetragonal phase as a lower energy state. Among all the Ni-based alloys, we find that Ni_2MoGa, Ni_2CrGa and Ni_2CrSn possess a lower energy for the tetragonal phase over the cubic phase similar to Ni_2MnGa, which have a tetragonal ground state, as has already been established in the literature. From Figure 5.5, we also observe that Ni_2VGa and Ni_2VSn have very flat energy curves with no clear minimum in the E_T - E_C versus c/a curve. Further, we observe that though in case of Ni_2MnSn, there is a cubic ground state, there is also a very subtle signature of a tetragonal phase which is evident from the clear asymmetric nature of the E_T - E_C versus c/a curve for this material (Figure 5.5). It is observed that Ni_2MoGa does not carry any magnetic moment in its ground state. Further, Ni_2CrGa and Ni_2CrSn are found to possess an *intra-sublattice* AFM phase as a ground state. It is to be noted that, in this present study our concentration will be only on the alloys which will have a FM phase in its ground state. So, for Ni-based alloys, further on, we will discuss only about

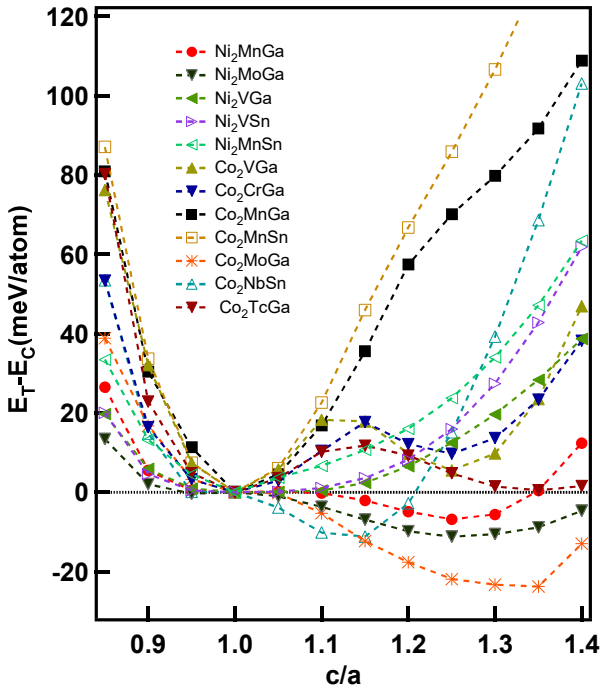

Figure 5.5: Energy difference between the crystal structures with tetragonal (T) and cubic (C) symmetries, of some typical materials represented as $E_T - E_C$ (in units of meV per atom), as a function of the ratio of lattice constants c and a. The energies have been normalized with respect to the energy of the respective cubic austenite phase of each material. The lines are just to guide the eyes.

Ni_2MnGa and Ni_2MnSn.

Out of all the Co-based alloys studied here, we observe that only two alloys are likely to show energetically lower martensite phase over the cubic austenite phase. Out of these two, while Co_2NbSn is already known in the literature[35], Co_2MoGa is not reported till date. From Figure 5.5, it is clearly seen that for Co_2MoGa a significant energy difference exists between the cubic and tetragonal phases. This indicates that a martensite phase transition is possible in this material. It is expected that the martensite transition temperature for Co_2MoGa will be higher than Ni_2MnGa since the energy difference between the austenite and martensite phase of the former is evidently much larger than that of the latter. This expectation is because it is argued in the literature, that, relative values of ΔE can be indicative of the relative values of martensite transition temperatures of two alloys.[18, 88] A cubic ground state is observed for most of the Co-based alloys, including the two well-known Co-based half-metallic-like materials Co_2MnSn[155] and Co_2MnGa.[156] It is interesting to note that there are three more alloys which show

Table 5.1: Martensite transition temperature of the four ferromagnetic materials. Values from the literature are given along with the references which are shown in square brackets.

Material	$(c/a)_{eq}$	ΔE(meV/atom)	T_M(K)	$\|\Delta V\|$/V(%)
Ni_2MnGa	1.22 1.22[154], 1.22[142]	6.05 6.18[154]	70.18 70.51[154], 210[146]	0.30
Ni_2MoGa	1.27	11.08	128.58	0.36
Co_2MoGa	1.37	19.58	227.13	1.96
Co_2NbSn	1.11	10.63	123.33 233[157]	0.08

a state of cubic symmetry having a lowest energy while the tetragonal phases of these materials are energetically very close (within 25 meV) to the respective austenite phases. The ΔE versus c/a plots of these materials, namely, Co_2VGa, Co_2CrGa and Co_2TcGa are included in Figure 5.5 which clearly depict this energetic aspect.

In Table 5.1 we report the calculated tetragonal transition temperature (T_M) of those materials which are expected to exhibit tetragonal transition among the materials studied here. These are calculated based on the values of ΔE using the conversion factor 1 meV = 11.6 K. As discussed above, these T_M values are not to be considered as the absolute values of the transition temperature. These values are listed here to only give a trend of the expected transition temperatures for different materials as has been done in the literature earlier.[18, 88] Out of the four ferromagnetic materials (magnetic aspect of the materials is discussed in detail in the next subsection) showing the possibility of a tetragonal transition, we find that Ni_2MnGa has the lowest T_M value; on the other hand, Co_2MoGa is expected to have the highest transition temperature. The optimized c/a values for all the four materials are given in Table 5.1. Co_2MoGa is found to have the highest value of about 1.4. Furthermore, volume conservation between the cubic and the tetragonal phases (Table 5.1) as well as an energetically lower tetragonal phase (Figure 5.5) which are observed here are generally indicative of the martensite transition. Therefore, from the present study, among the materials studied here, two Ni-based and two Co-based FHAs are likely to exhibit SMA property. Out of which one Ni and one Co-based alloys are well-known MSMA materials, namely Ni_2MnGa and Co_2NbSn. On the other hand, Co_2MoGa and Ni_2MoGa are two new materials which are predicted in this work to exhibit martensite transition.

5.2.2 Magnetic Properties

Table 5.2: Magnetic properties of austenite phase of Co-based materials Z_t is the total number of valence electrons. P denotes the spin polarization at the Fermi level. Values from the literature are given along with the references which are shown in square brackets.

Material	μ_t (μ_B)	Z_t-24	$\mu_A(\mu_B)$	$\mu_B(\mu_B)$	$\mu_C(\mu_B)$	T_C(K)	P(%)
Co_2ScGa	0.00 0.25[158]	0	0.00	0.00	0.00	-	-
Co_2TiGa	1.00 0.75[159] 0.82[160]	1	0.62 0.40[158] 0.40[159]	−0.14	−0.01	161 130[159] 128[160]	97
Co_2VGa	2.00 1.92[161] 2.00[31]	2	0.95 0.91[31]	0.18	−0.01	356 352[161] 368[31]	100
Co_2CrGa	3.03 3.01[162]	3	0.77 0.9[162]	1.59 1.28[162]	−0.05 −0.07[162]	418 419[162] 495[162]	92
Co_2MnGa	4.10 4.0[32]	4	0.77	2.73	−0.07	586 700[32]	68
Co_2YGa	0.00	0	0.00	0.00	0.00	-	-
Co_2ZrGa	1.00	1	0.61	−0.11	−0.01	166	94
Co_2NbGa	2.00 1.39[163] 2.00[34]	2	1.04	−0.01	0.00	397	100
Co_2MoGa	2.93	3	1.22	0.51	−0.01	180	86
Co_2TcGa	3.95	4	1.37	1.26	−0.04	711	71
Co_2ScSn	1.05	1	0.67	−0.14	−0.02	207	80
Co_2TiSn	2.00 1.96[161]	2	1.07	−0.06	0.00	409 371[161]	100
Co_2VSn	3.00 1.21[161] 1.80[31]	3	1.08	0.89	−0.02	291 95[161] 103[31]	100
Co_2MnSn	5.03 5.02[31]	5	0.98 0.885[31]	3.23 3.25[31]	−0.06	897 899[31]	76
Co_2YSn	1.05	1	0.67	−0.10	−0.02	162	79
Co_2ZrSn	2.00 1.46[161]	2	1.10	−0.09	0.01	449 448[161]	100
Co_2NbSn	1.98 0.69[161]	3	0.97	0.07	0.01	37 105[161]	66

Total and Partial Magnetic Moments - Table 5.2 gives the total and partial moments for the electronically stable Co-based materials. The values available from the literature are also listed in the table for a few materials, wherever available and we note that the matching is very good with the existing calculated data. With the experimental results the matching is reasonably good as well. It is seen that each of Ga and Sn atoms

has negligible moments in all cases. We observe that, as opposed to the materials with A = Ni atom, those with A = Co atom have significant contribution from the A atom to the total moment. However, when the B atom is non-magnetic, in a few cases, the moment on the Co atom is either zero or much less compared to its bulk moment. As the moment on the B atom increases, the moment of the Co atom gets larger but always largely underestimated compared to the value of its bulk moment (about $1.7\mu_B$). This is expected due to the delocalized-like common d-band between the A and B atoms.[38] For period IV, when B = Cr and Mn, there is a slight decrease in the partial moment of the Co atom, but not in the total moment value of the respective systems. For all the Co-based alloys, the moments are very close to an integer value and this is generally the signature of a half-metallic material. Further, from Table 5.2, we note that these FHAs follow the Slater-Pauling rule as is seen earlier in case of many Co-based FHAs.[34, 164] As a consequence of this rule, we get an almost linear variation of the magnetic moment with the atomic number of B elements for all the Co-based materials. It is seen that there is a deviation from the Slater-Pauling rule only for Co_2NbSn which has been observed and explained in the literature.[34] Due to their typical electronic structure, all the Co-based compounds are seen to exhibit (Table 5.2) a high spin polarization at the Fermi level (E_F) in comparison to the Ni-based compounds. It is worth-noting that from our calculations, Ni_2MnGa and Ni_2MnSn have spin-polarization of ∼28 and ∼21%, respectively which are much lower compared to the values of Co-based alloys, as expected.

Heisenberg Exchange Coupling Parameters - To gain insight into the magnetic interactions in detail, using SPR-KKR programme package[56], we calculate and present the results of our calculation of the Heisenberg exchange coupling parameters, J_{ij}, (i and j being pairs (A, A) and (A, B)) only for the alloys which are magnetic and likely to favor tetragonal distortion and consequently exhibit martensite transition. We also show the same parameters for some other related alloys for the purpose of comparison. Most of the materials chosen for presentation have relatively large moment on the B atom so that the (A, B) exchange interactions are always significant. In the left panels of Figure 5.6, 5.7 and 5.8, the J_{ij} parameters for different compounds are plotted. The right panels give the interaction parameters, J_{ij}^{bare}, which are J_{ij} parameters, divided by the product

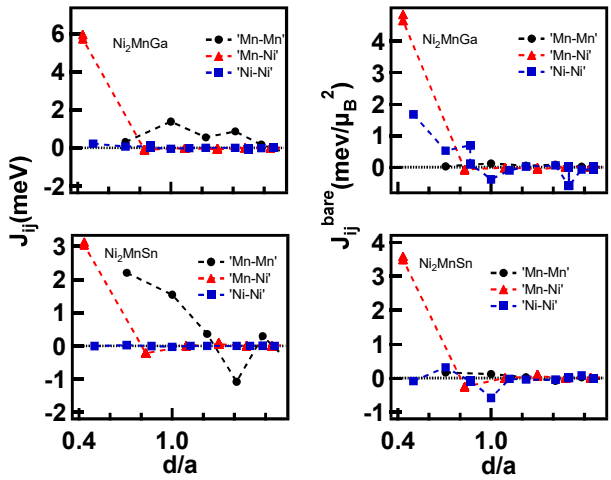

Figure 5.6: J_{ij} parameters between different atoms of Ni_2MnGa and Ni_2MnSn as a function of distance between the atoms i and j (normalized with respect to the respective lattice constant). Lines are just guide to the eyes.

of the moments of the i and j atoms.

Figure 5.6 gives the Heisenberg coupling parameters for Ni_2MnGa and Ni_2MnSn which exhibit the effect of the change of the C atom, and consequently the lattice parameter. Figure 5.7 contains the values for Co_2MnGa and Co_2MoGa to understand what is the role of the B = Mn over the Mo atom. Similarly, we plot the exchange parameters for alloys Co_2MnSn and Co_2NbSn in Figure 5.8. The results match well with the literature wherever the data are available.[92, 165] It is seen that there is a RKKY[40] type of interaction for the (A, A) and (B, B) pairs.[38, 91] The oscillatory behaviour of the J_{ij} parameters as a function of distance between the atoms i and j (normalized with respect to the lattice constant), is a well-known signature of the same. Further, it is seen that between the A and the B atoms there is a signature of a significant direct interaction whenever B atom has a strong moment. From Figure 5.6, we observe that the direct interaction between Ni-B atom is stronger in case of Ni_2MnGa compared to the case of Ni_2MnSn. This is due to the increased lattice constant and hence weak coupling in case of the latter. It is also found that the direct interaction is somewhat stronger than the RKKY interaction in case of both the materials, though it is quite clear that, as expected and observed in the literature[91, 38], both these types of magnetic interactions are important in these materials.

The magnetic interactions in the Co-based materials shown here exhibit a somewhat

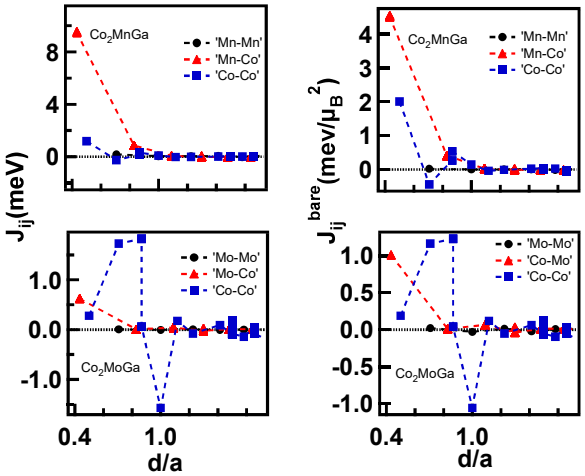

Figure 5.7: J_{ij} parameters between different atoms of Co_2MnGa and Co_2MoGa as a function of distance between the atoms i and j (normalized with respect to the respective lattice constant). Lines are just guide to the eyes.

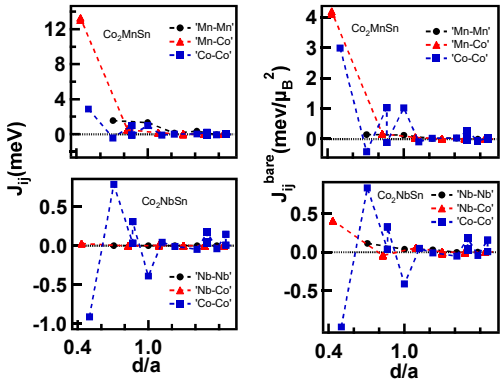

Figure 5.8: J_{ij} parameters between different atoms of Co_2MnSn and Co_2NbSn as a function of distance between the atoms i and j (normalized with respect to the respective lattice constant). Lines are just guide to the eyes.

similar trend. It is found that for the materials favouring tetragonal transition, Co_2MoGa (Figure 5.7) and Co_2NbSn (Figure 5.8), the direct A-B magnetic interaction is small and to some extent comparable to the indirect RKKY-type interaction between A atoms. In the former material, as is evident from Table 5.2, the moment on Mo atom is somewhat larger compared to that on the Nb atom in case of the latter material. Consequently, the strength of the direct interaction in the former alloy, between B atom (Mo) and A atom (Co) is found to be slightly stronger. From Figure 5.7 and 5.8, we observe that for the materials Co_2MnGa and Co_2MnSn, having high magnetic moments (4.10 and 5.03 μ_B, respectively), which are of the order of the moments possessed by the two Ni-based materials discussed above, the direct A-B interaction is much stronger compared to the RKKY-type indirect interactions (A-A or B-B). A decrease of partial moment of the Mn atom is observed in case of Co_2MnGa over Ni_2MnGa (2.73 in Co_2MnGa versus 3.41 μ_B in Ni_2MnGa). But due to larger moment on the A = Co over Ni atom, the direct interaction strength between Mn and the respective A atoms, is much larger in the former material, as seen from the top left panels of Figure 5.6 and 5.7. Hence, the delocalized-like common $3d$ band between Mn and Co atom in case of Co_2MnGa is expected to be more effective compared to the case of Ni_2MnGa. We observe from Figure 5.6, 5.7 and 5.8 that, relatively, the RKKY-type indirect interactions are slightly stronger for the C = Sn over the C = Ga case. It is to be noted here that Sn has one valence electron more than Ga.

It is known that the magnetic interactions in the Heusler alloy materials having a large moment on B atom, comprise of a large contribution from the A-B direct interaction. At the same time, contribution of the A-A and B-B indirect RKKY type of interaction is important as well. The materials, which have high moment on the B atom, typically exhibit a large A-B direct interaction when compared to the strength of RKKY-type interaction. However, when the J_{ij}^{bare} parameters are analyzed, for the majority of the materials, it is seen that, both the direct A-B interaction and RKKY-type interaction between i and j (i and j being A and B) atoms, are somewhat similar in strength. This observation reiterates the fact that the magnetic exchange interactions are not only the function of i-j distances (as is evident from Figure 5.6 to 5.8), but also of the individual magnetic moments of the i and j atoms which becomes clear when we present the J_{ij}^{bare}

plots versus d/a.

Based on the J_{ij} parameters of the six materials discussed above, the Curie temperatures of the materials within a mean field approximation[81] have been calculated to probe further into the possible MSMA property. For Ni_2MnGa and Ni_2MnSn, the Curie Temperature (T_C) values are 410 and 365 K, respectively. These values as well as the J_{ij} parameters match quite well with both experimental and calculated values reported in the literature[92, 165] as well as from our work. We note that the experimental values are generally underestimated compared to the theoretical values. This is because of the mean field approximation used for the calculation as discussed in chapter 3. For some of the Co-based materials T_C values are presented in Table 5.2. We observe that the calculated values match very well with the previously reported data, wherever these results are available. It is interesting to note that due to the small values of J_{ij} for Co_2NbSn the value of the Curie temperature for this material is very low and this is consistent with the experimentally observed room-temperature paramagnetism of this material.[166] Similarly, due to weak RKKY-type interaction of pair (A, A) with a somewhat comparable A-B direct interaction, the T_C value for another Co-based material, which has been predicted from our present work, namely, Co_2MoGa, is expected to be low (below room temperature) as well.

5.2.3 Bulk Mechanical Properties

Table 5.3: Bulk mechanical properties of austenite phase of Ni-based materials. Values from the literature are given along with the references which are shown in square brackets.

Material	C_{11} (GPa)	C_{12} (GPa)	C_{44} (GPa)	C' (GPa)	B (GPa)	G_V (GPa)	G_R (GPa)	G_V/B
Ni_2VGa	193.20	183.32	109.36	4.94	186.62	67.59	11.56	0.36
Ni_2MnGa	165.41 152.0[24]	159.45 143[24]	113.67 103[24]	2.98 4.5[24]	161.44 146[24]	69.39 63.6[24]	7.16	0.43
Ni_2MoGa	197.36	206.36	103.40	-4.5	203.36	60.24	-12.04	0.30
Ni_2MnSn	161.02 158.1[167]	137.46 128.5[167]	92.56 81.3[167] 87[104]	11.78 14.8[167] 8[104]	145.31 138.4[167] 140[104]	60.25	24.73	0.41

After presenting the results of magnetic properties of the austenite phase of the materials, now, we discuss about the bulk mechanical properties of the same phase since from

Table 5.4: Bulk mechanical properties of austenite phase of Co-based materials. Values from the literature are given along with the references which are shown in square brackets.

Material	C_{11} (GPa)	C_{12} (GPa)	C_{44} (GPa)	C' (GPa)	B (GPa)	G_V (GPa)	G_R (GPa)	G_V/B
Co_2VGa	266.52	162.12	126.83	52.20	196.92 198[168]	96.98	80.68	0.49
Co_2CrGa	233.02	182.82	136.77	25.1	199.56	92.10	49.20	0.46
Co_2MnGa	254.87	165.27	142.69	44.80	195.14 199[104]	103.53	76.14	0.53
Co_2MoGa	180.92	163.60	114.10	8.66	169.38	71.92	19.44	0.42
Co_2TcGa	249.54	186.10	123.87	31.72	207.25	87.01	57.29	0.42
Co_2MnSn	234.63	136.75	119.05	48.94	169.38	91.01	75.68	0.54
Co_2NbSn	164.95	184.99	80.80	-10.02	178.31	44.47	-30.77	0.25

the point of view of technological application, these properties are important. For demonstrating the similarities and differences, we concentrate on eight typical FM materials and present the detailed results of the same. Three of these FM materials are likely to favour a tetragonal distortion at low temperature and these materials are Ni_2MnGa, Co_2MoGa, Co_2NbSn. The other group of alloys consists of materials having a cubic ground state. Among these alloys, the following compounds have been considered - Co_2VGa, Co_2CrGa, Co_2MnGa, Co_2MnSn and Ni_2MnSn, which are expected to have a cubic symmetry at the lowest temperature. Tables 5.3 and 5.4 contain the bulk mechanical properties of these above-mentioned Ni and Co-based alloys, respectively. Values of few other materials are also listed in Tables 5.3 and 5.4, for comparison. It is observed that the overall agreement with the values from the literature is reasonably good.

There are three independent elastic constants for a cubic structure. These are C_{11}, C_{12} and C_{44}. $C_{11} > 0$, $C_{44} > 0$, $C_{11}-C_{12} > 0$ and $C_{11}+2C_{12} > 0$. From the tables containing elastic constants we can see that first, second and fourth conditions are satisfied for all the materials listed here, but the third condition is not satisfied by some of the materials. These mechanical properties of the materials are now discussed in detail below.

Tetragonal shear constant (C') - This is defined as $0.5\times(C_{11}-C_{12})$. A value of C' which is close to zero or negative indicates that the material is prone to tetragonal distortion. It is clear from Table 5.3, that for Ni_2MnGa, as expected, the tetragonal shear constant is rather close to zero. For Ni_2MoGa the value of C' is found to be negative, which indicates that it has a mechanically unstable cubic austenite phase, which corroborates

the result presented in Figure 5.5. It is interesting to note that Ni_2VGa has a value of C′ close to that of Ni_2MnGa. From Figure 5.5, we observe that it has a flat region near $c/a = 1$, in the energy versus c/a curve. Hence, in this case the ground state symmetry can not be properly ascertained as is evident from our elastic constants and energetics results. It is important to mention here that the stoichiometric Ni_2MnSn is a material which is not known to undergo martensite transition and we find that the tetragonal shear constant has a slightly larger positive value (about 12 GPa) compared to Ni_2MnGa.

From Table 5.4, it is observed that two Co-based materials show a negative or close to zero value for C′. Out of these, Co_2NbSn is known to be prone to the non-cubic distortion.[35] Among the materials, namely, Co_2MoGa, Co_2VGa, Co_2CrGa, Co_2CrGa, Co_2MnSn, Co_2TcGa, except the first alloy all the others have a large positive value for the C' constant. It is also observed from Figure 5.5 that, while for Co_2MoGa, there is a clear indication of the tetragonal phase being the lowest energy state, this is not the case for the other materials. So the combined study of energetics and bulk mechanical properties of all the materials indicates that the only two Co_2BC materials which are likely to undergo tetragonal transition and exhibit MSMA property are Co_2NbSn and Co_2MoGa.

Inherent Crystalling Brittleness (ICB) - The calculated values of bulk modulus, B, have been listed in Tables 5.3 and 5.4 for Ni and Co-based materials, respectively. The isotropic shear modulus, G, is related to the resistance of the material to the plastic deformation. In literature, it has been shown[102] that the value of G lies in between the values of shear modulii given by formalisms of Voigt (G_V)[100] and Reuss (G_R)[101], which means $G = (G_V + G_R)/2$. As has been discussed for austenite phase of Ni_2MnGa in chapter 2[118] the experimental G value is close to the calculated G_V value while G_R value remains largely underestimated. This occurs due to the small positive value of C'. This particular aspect, observed for similar FHAs which are prone to martensite transition, has been discussed in detail in the chapter 2.[118] Following this observation, we consider G_V value as the value of shear modulus (G) though it is generally considered to be the higher limit of the same.[102] Further, as discussed in chapter 2, a simple and empirical relationship, given by S. F. Pugh[28], proposes that the plastic property of a material is

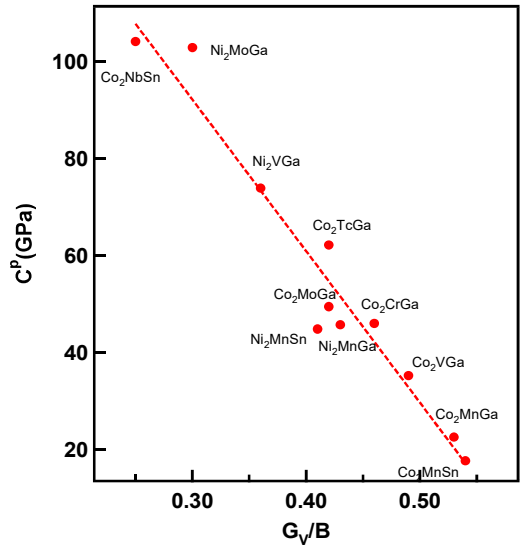

Figure 5.9: Cauchy pressure, C^p, versus G_V/B; a linear fitting of the data is carried out and shown here. An inverse linear-type relation is seen to exist between the two parameters (see text). The line is just guide to the eyes.

related to the ratio of the shear and bulk modulus of that particular material. A high value (greater than ~ 0.57) of ratio of shear and bulk modulus, namely, G/B, is related to the inherent crystalline brittleness of a bulk material. A value below this critical number phenomenologically signifies that the material's ICB is low. From Table 5.3, we find that the values for Ni-based materials are below this critical value and hence the ICB of these materials is low though the well-known FHA, Ni_2MnGa, has a somewhat higher value compared to the materials containing platinum in place of Ni as shown in the chapter 2. We note that Ni_2MoGa shows a negative value of C$'$, as well as the lowest value of G/B among all the materials and hence it is expected to have a low ICB. Therefore, it appears from the points of view of energetics (Figure 5.5) and the bulk mechanical properties, it is a promising material, though not so when the magnetic properties are considered. Table 5.4 lists the bulk mechanical properties for some of the Co-based FHAs studied here. The two materials which are likely to show a tetragonal ground state, namely, Co_2NbSn and Co_2MoGa, are expected to exhibit ICB smaller or comparable to that of Ni_2MnGa; the corresponding G/B values are 0.25 and 0.42 GPa, respectively. All the Co_2BC alloys have G/B values comparable to or larger than that of Co_2NbSn.

Cauchy Pressure - We now focus on the value of Cauchy Pressure, C^p, which is defined as $C^p = C_{12}$ - C_{44}. In Figure 5.9, we plot the available data for C^p versus G_V/B

calculated in case of some of the Ni and Co-based materials. We find that overall, there is a clear trend of inverse (linear) relationship between G_V/B and C^p. Interestingly, this type of nearly-linear inverse relationship between the Cauchy pressure and the G/B ratio seems to be a rather general observation as it is observed in the literature for various types of materials.[114, 118]

Finally, after analyzing the bulk mechanical as well as the magnetic properties and the energetics, out of all the materials studied, only two new materials, namely, Ni_2MoGa and Co_2MoGa, emerge to be promising in terms of application as an SMA material. However, due to the absence of any magnetic moment in Ni_2MoGa, this material is not expected to be suitable as an MSMA material. Further, the problem with Co_2MoGa is that a low T_C indicates an absence of ferromagnetism in Co_2MoGa at room temperature as is observed in case of Co_2NbSn as well.

5.2.4 Electronic Properties: Density of States

Analysis of Total and Atom-Projected Partial DOS

After discussing the energetics, magnetic and bulk mechanical property of the cubic austenite phase, we now analyze the electronic property in terms of the total and partial density of states of different atoms of various materials. We have carried out calculations on all the eletronically stable materials but here we concentrate on and present the results of the austenite phases of eight typical FM materials as discussed above. These materials are Ni_2MnGa, Co_2MoGa, Co_2NbSn, which are to exhibit a tetragonal symmetry as well as Co_2VGa, Co_2CrGa, Co_2MnGa, Co_2MnSn and Ni_2MnSn, which are to possess a cubic symmetry, at the lowest possible temperature. First we will discuss the total and atom-projected DOS of these systems in the cubic phase.

Total DOS: It is seen that the valence band width for all the materials is about the same, which is roughly about 6 eV (Figure 5.10 to 5.13). Now we discuss in detail about the hybridization observed in the total DOS and the trend of the corresponding formation energy for a few typical materials. The two-peak structure in the down DOS at the Fermi level for both Ni and C atoms indicating about substantial hybridization among these atoms is evident from Figure 5.10. This covalent interaction between the Ga $4p$ and Ni

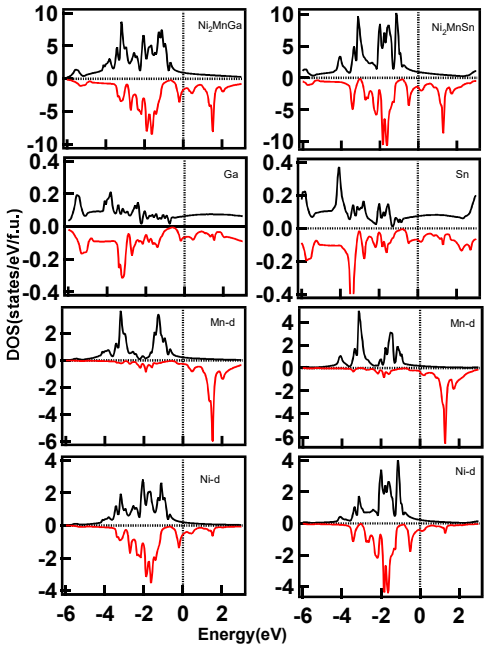

Figure 5.10: The left and right set of panels depict the density of states of Ni_2MnGa and Ni_2MnSn materials, respectively. From top to bottom panel, first the total density of states as a function of energy has been plotted. Next panel shows the partial density of states of the Ni atom. Partial density of states of the Mn atom and the C atom are shown in the third and the fourth panels. The Fermi level is at 0 eV.

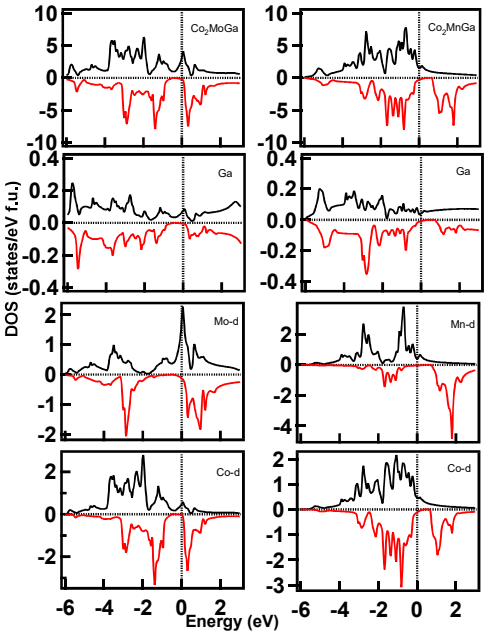

Figure 5.11: The left and right set of panels depict the density of states of Co_2MoGa and Co_2MnGa materials, respectively. From top to bottom panel: first the total density of states as a function of energy has been plotted. Next panel shows the partial density of states of the Co atom. Partial density of states of the B atom and the Ga atom are shown in the third and the fourth panels. The Fermi level is at 0 eV.

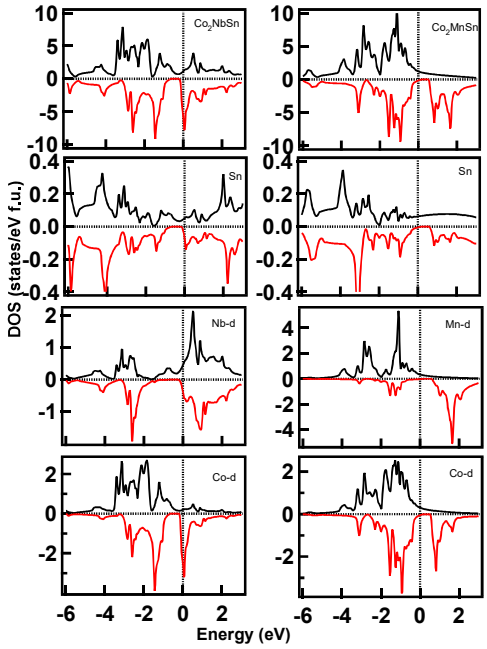

Figure 5.12: The left and right set of panels depict the density of states of Co_2NbSn and Co_2MnSn materials, respectively. From top to bottom panel: first the total density of states as a function of energy has been plotted. Next panel shows the partial density of states of the Co atom. Partial density of states of the B atom and the Sn atom are shown in the third and the fourth panels. The Fermi level is at 0 eV.

$3d$ minority electrons plays a crucial role in the stability of the material. We note here that the overlapping and the two-peak structure of the DOS is also prominent in case of A and C atoms of Co_2ZrGa, which has a highly negative formation energy (Figure 5.4). On the other hand, in Co_2CrGa, the two-peak structure and the overlapping of DOS for both the A and C atoms are not quite substantial below the Fermi level and the formation energy is found to be low as well (Figure 5.4). Further, Figure 5.13 depicts the DOS for B = Y and Zr. These plots indicate a lowering of binding energy (less negative value of formation energy) in the B = Y material compared to the B = Zr case. This corroborates with the trend of the formation energy values of these materials. It is to be noted that the contribution from the A atom plays a crucial role in this. Zayak et. al.[89] have earlier shown that the stability of the Ni_2MnGa type Heusler alloys is closely related to the minority DOS and the hybridization at and around the Fermi level; this has been argued in other cases as well.[23]

When the total DOS is analyzed, a large exchange splitting has clearly been observed for systems which have Mn as the B atom. From Figure 5.10 to 5.12, we observe that for

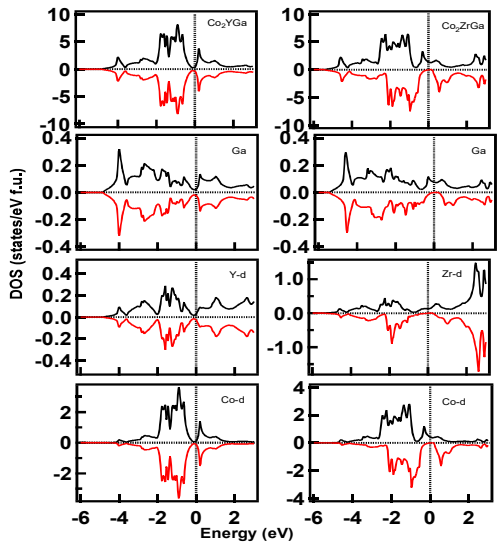

Figure 5.13: The left and right set of panels depict the density of states of Co_2YGa and Co_2ZrGa materials, respectively. From top to bottom panel: first the total density of states as a function of energy has been plotted. Next panel shows the partial density of states of the Co atom. Partial density of states of the B atom and the Ga atom are shown in the third and the fourth panels. The Fermi level is at 0 eV.

A_2BC systems (A = Ni, Co; B = Mn; C = Ga; Sn), the occupied DOS of the B atom is dominated by the majority spin whereas the unoccupied DOS is dominated by the minority spin. For Ni_2MnGa and Ni_2MnSn, the majority DOS of the Mn atom is centred around -1.2 eV and -1.5 eV, whereas the minority DOS of the same atom is centred around 1.5 eV and 1.3 eV for the respective systems. For Co_2MnGa and Co_2MnSn, the position of the occupied majority spin DOS for Mn atom is at about -0.7 eV and -1.1 eV, respectively, while the position of the unoccupied minority DOS peak is at about 1.8 eV and 1.6 eV. For Co_2CrGa also, we observe a large separation between the occupied majority DOS peak (at about -0.1 eV) of Cr atom and unoccupied minority DOS peak (at about 1.7 eV).

Partial DOS: Now we analyze the partial DOS of few of the important A and B atoms, to understand the nature of DOS close to the Fermi level.

Ni Atom - The DOS in case of the two Ni-based alloys are similar (Figure 5.10). However, since Sn atom contains one extra valence electron compared to the Ga atom in the C position, the peak positions of the total DOS of the Mn atom are shifted towards lower energy in case of the materials with C = Sn. At this point, it is worth-mentioning that it has already been discussed in the literature that a rigid band model is a suitable

model to understand the trends when the C atom is changed.[104] We observe that a similar situation is seen to arise when the A atom is changed from Ni to Co, which is discussed below.

Co Atom - Co has one valence electron less than Ni. Hence, a larger contribution of Co-derived levels compared to the Ni-derived levels in the unoccupied part of the respective DOS is expected. When DOS of Ni_2MnC is compared with that of Co_2MnC, this is clearly evident (Figure 5.10, 5.11 and 5.12). Among the materials with C = Ga and A = Co, only Co_2MoGa is a material which is likely to show a martensite transition (Figure 5.5). It is seen that it has the first unoccupied DOS peak very close to the E_F (Figure 5.11). Among the materials studied here with C = Sn and A = Co, only Co_2NbSn is known to be prone to non-cubic distortion[35] and it has an unoccupied DOS peak close to E_F as well. On the contrary, when we analyze the DOS of Co_2MnGa (Figure 5.11) and Co_2MnSn (Figure 5.12), which do not show the tendency of a tetragonal distortion as well as are known to possess high spin polarization at the Fermi level, we observe that the first unoccupied DOS peak is further away from E_F compared to the materials which are prone to tetragonal distortion, namely Co_2MoGa (Figure 5.11) and Co_2NbSn (Figure 5.12).

Mn Atom - There are four out of eight materials analyzed in detail in this chapter which contain Mn atom in the B position. When we compare the total DOS of the Mn atom at the B position, in all the four materials considered here, it is clearly seen that majority of the DOS of the down spin occupies the unoccupied region above the Fermi level, while the up spin electrons primarily have negative binding energies. As opposed to the down spin DOS, which has one major peak in all the four cases, the up spin electrons typically occupy two energy ranges, one around 1 and one around 3 eV below E_F. Due to one extra electron in Sn atom compared to the Ga atom in the C position, the peak positions of the total DOS of the Mn atom are shifted towards lower energy in case of the materials with C = Sn. To elaborate, first we compare the DOS of the down spin of Mn in the four alloys Ni_2MnGa, Ni_2MnSn, Co_2MnGa and Co_2MnSn in the cubic phase. While, for Ni-derived alloys, DOS of Mn atom in the unoccupied part peaks at about 1.5 eV in case of C = Ga, it peaks around 1.2 eV when C = Sn. The corresponding peak

positions for Co_2MnGa and Co_2MnSn are at about 1.8 and 1.6 eV, respectively. In case of the up spin DOS, there are two ranges of predominant DOS in all the four materials. For the first such range, which is closer to the Fermi energy, the peak positions are at about -1.3, -1.5, -0.7 and -1.1 for Ni_2MnGa, Ni_2MnSn, Co_2MnGa and Co_2MnSn, respectively. For the range which is at a much higher binding energy, the peak positions are at about -3.2, -3.2, -2.5 (also one slightly weaker one at -2.8) and -2.5 (also one slightly weaker one at -2.8) eV for Ni_2MnGa, Ni_2MnSn, Co_2MnGa and Co_2MnSn, respectively. It is observed that these peaks of the DOS are not sharp but broad ones, with shoulders on either or one of the sides.

Electronic Stability of the Tetragonal phase from DOS

After discussing the electronic property of the cubic austenite phase, we now analyze the electronic property in terms of the density of states of different materials as a function of c/a. We concentrate on the eight typical FM materials as mentioned above. A tetragonal distortion has been imposed on all these eight materials. To highlight the difference between the two symmetries, we will concentrate on the detailed results of cases only with a few typical cases of c and a ratio (c/a = 1.00, 1.05 and 1.10). The aim is to understand the electronic stability or instability of the tetragonal phase of these compounds from the DOS results, which is discussed below for selected eight materials.

Ni_2MnGa versus Ni_2MnSn :

Figure 5.14 contains the density of states of the cubic and tetragonal phases, with c/a varying from 1.00 to 1.10 in steps of 0.05 for materials Ni_2MnGa and Ni_2MnSn. First we analyze Figure 5.14 for the cubic phase. We observe that there is a peak at around -0.2 eV for Ni_2MnGa and at around -0.5 eV for Ni_2MnSn, respectively. This peak is derived from the $3d$ electrons of the Ni atoms with down spin having e_g symmetry and is known to play a crucial role in the stabilization of the tetragonal phase in case of Ni_2MnGa.[104] The density of states of the down spin $3d$ electrons with t_{2g} symmetry of these A atoms corresponds to the peaks with reasonably higher binding energy. This is the case for both the materials. On the other hand, detailed investigation suggests that the B atom = Mn has negligible contribution near the Fermi level; both for the up and down spin. The up

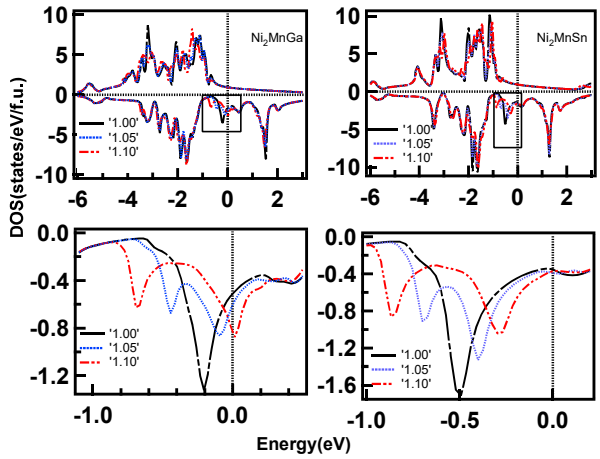

Figure 5.14: The density of states as a function of energy has been plotted for the cubic and tetragonal phases, with c/a varying from 1 to 1.10 in steps of 0.05 for materials Ni_2MnGa and Ni_2MnSn in left and right panels, respectively. Panels below show the down spin density near the Fermi level derived from e_g states of the $3d$ electrons of the A atom, for the respective materials. The Fermi level is at 0 eV.

spin electrons of A atom also do not significantly contribute to the DOS at around -0.2 and -0.5 eV (as mentioned above) for Ni_2MnGa and Ni_2MnSn, respectively.

As c/a is increased , some systematic changes in the density of states are clearly visible from the lower panels of Figure 5.14 to 5.17. For Ni_2MnGa, it is seen that the peak near the Fermi level, at about -0.2 eV, derived from the down spin DOS, has been split into two peaks when c/a is changed. This has been observed and argued about in detail in the literature.[104, 169, 170] As a result of the tetragonal distortion, the degeneracy of the sub-bands near the Fermi level is lifted. As a consequence, a redistribution of the density of states of the $3d$ electrons and in turn a reduction of the free energy occurs. This is the so-called band Jahn-Teller effect which is known to result in the lowering of energy under tetragonal distortion and it is observed in many of the FHAs including Ni_2MnGa.[104, 169] For Ni_2MnSn as well, it is seen that the most prominent change is the splitting of the peak at about -0.5 eV[104] upon the tetragonal distortion as seen from Figure 5.14. However, it is well-known that stoichiometric Ni_2MnSn is not expected to have tetragonal ground state. It has been argued in the literature that the band Jahn-Teller effect is sensitive to the DOS at the E_F in the cubic phase. The closeness of the degenarate peak for Ni_2MnGa (at about -0.2 eV with respect to E_F) over Ni_2MnSn (at about -0.5 eV with respect to E_F) is an indication of the possibility of lowering of energy as a function of tetragonal

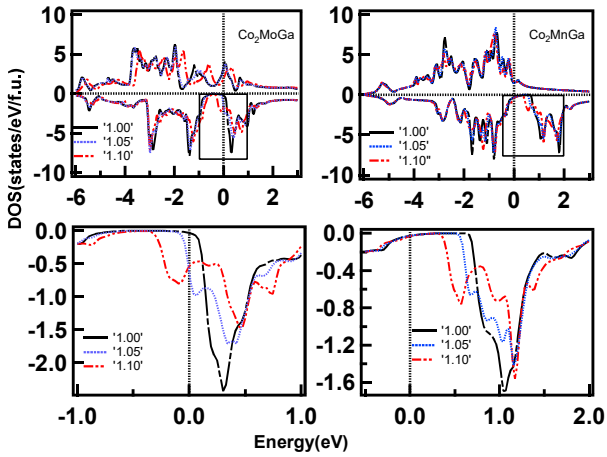

Figure 5.15: The density of states as a function of energy has been plotted for the cubic and tetragonal phases, with c/a varying from 1 to 1.10 in steps of 0.05 for materials Co_2MoGa and Co_2MnGa in left and right panels, respectively. Panels below show the down spin density near the Fermi level derived from e_g states of the $3d$ electrons of the A atom, for the respective materials. The Fermi level is at 0 eV.

distortion in the former.[104, 169] We find that the density of states at the Fermi level in case of cubic phase of Ni_2MnGa is relatively more in comparison to Ni_2MnSn, which is evident from the relative position of the peak due to the e_g states of the $3d$ electrons near the Fermi level in the two materials (Figure 5.14).

Co_2MoGa versus Co_2MnGa:

Figure 5.15 gives the plot of DOS with different c/a values for Co_2MoGa versus Co_2MnGa. In case of Co_2MoGa there is a large peak in the minority DOS just above the Fermi level (at about +0.3 eV with respect to E_F). Detailed analysis shows that this peak at the minority DOS has contributions from all three atoms i.e. (Co, Mo, Ga), but the major contribution comes from the e_g levels of $3d$ electrons of Co atom. We find that these e_g levels of Co atom have a major role to play in the stabilization of the tetragonal phase, similar to the e_g levels of $3d$ electronsof Ni atom in case of Ni_2MnGa. It is observed that, in case of Co_2MoGa also, band Jahn-Teller distortion plays a significant role in stabilizing the tetragonal phase. The DOS of down spin electrons close to the Fermi level is high, which leads to the instability of the cubic phase of this material while it is not the case in Co_2MnGa. In case of the latter material, the minority DOS almost vanishes at E_F. Further, here, the e_g levels of $3d$ electrons of Co atom are located farther away from the Fermi level (at about +1.0 eV with respect to E_F). For both the materials the

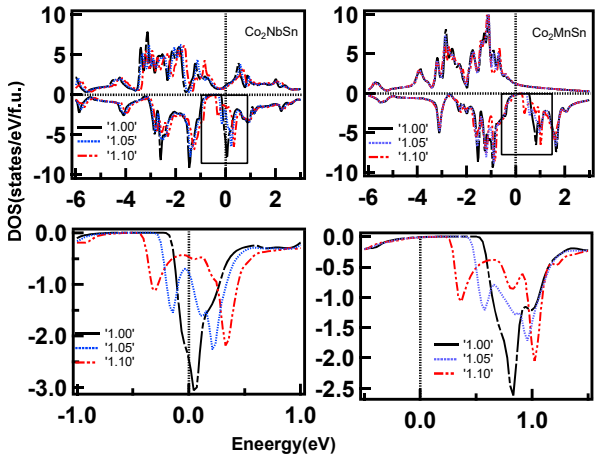

Figure 5.16: The density of states as a function of energy has been plotted for the cubic and tetragonal phases, with c/a varying from 1 to 1.10 in steps of 0.05 for materials Co_2NbSn and Co_2MnSn in left and right panels, respectively. Panels below show the down spin density near the Fermi level derived from e_g states of the $3d$ electrons of the A atom, for the respective materials. The Fermi level is at 0 eV.

B atom does not contribute to the minority DOS at the Fermi level but it contributes significantly to the large DOS observed for the up spin electrons at the Fermi level in case of Co_2MoGa. The peak positions of the DOS in the unoccupied part of the energy for Co_2MoGa and Co_2MnGa are different due to the difference in hybridization of Co atom with the Mo and Mn atoms, respectively.

Co_2NbSn versus Co_2MnSn :

Figure 5.16 gives the plot of DOS with different c/a values. As in case of Ni_2MnGa, for Co_2NbSn also we can find same type of evolution of density of states as a function of c/a and e_g states of $3d$ electrons of Co atom play the key role in the tetragonal transition. In austenite phase of Co_2NbSn the e_g peak of $3d$ electrons of Co atom is just above Fermi level (at about +0.05 eV). Under tetragonal distortion this peak is split into two: one part being above the Fermi level and another one being below the Fermi level. This splitting lowers the overall energy of the system and the tetragonal phase tends to be the ground state structure compared to the cubic structure. In the literature[35], it has been observed that at the Fermi energy, the contribution to DOS mainly comes from the $3d$ bands of Co and Nb. We observe from Figure 5.12 that Sn atoms also contribute. In the cubic phase, Co atom has a single large peak just above the E_F. But under tetragonal distortion, this single peak is split into two and the energy of the tetragonal phase is

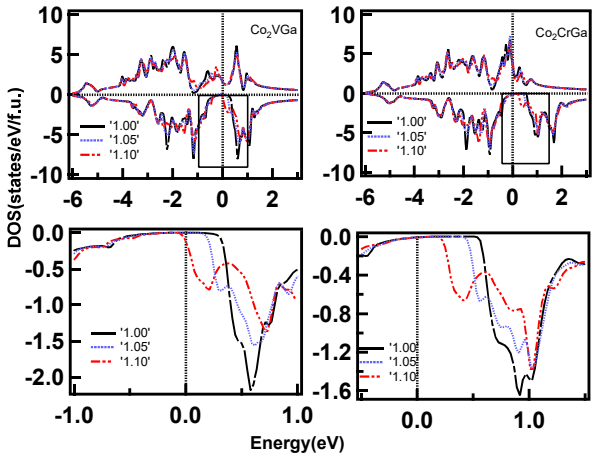

Figure 5.17: The density of states as a function of energy has been plotted for the cubic and tetragonal phases, with c/a varying from 1 to 1.10 in steps of 0.05 for materials Co_2VGa and Co_2CrGa in left and right panels, respectively. Panels below show the down spin density near the Fermi level derived from e_g states of the $3d$ electrons of the A atom, for the respective materials. The Fermi level is at 0 eV.

lower compared to the cubic phase. It has been observed[35] that the band Jahn-Teller distortion is the cause of the structural transition in this material. On the other hand, as seen from Figure 5.12 and 5.16, for Co_2MnSn, the peak due to e_g levels of $3d$ electrons of Co atom is located at a higher energy (at about +0.8 eV) compared to Co_2NbSn. After the application of the tetragonal distortion this single peak is split into two for Co_2MnSn as well(Figure 5.16). However, after splitting both the peaks lie above E_F which does not yield to overall lowering of energy of the system.

Co_2CrGa versus Co_2VGa:

From Figure 5.17, it is observed that the single peak of the e_g levels of the $3d$ electrons of Co atom above E_F is split for Co_2VGa as observed in the other cases. However, after splitting both the peaks lie above E_F. Consequently, there is no lowering of energy of the system possible under the tetragonal deformation. For Co_2CrGa, the single peak corresponding to the e_g states in the cubic phase is located at an even higher (positive) energy with respect to the Fermi level. Therefore, in this case also lowering of energy under tetragonal deformation is not possible, which is consistent with the results presented in Figure 5.5.

Finally, we find that in all the materials, as a result of tetragonal distortion, the degeneracy is lifted for the $3d$ sub-bands in the minority spin channel of A atoms, which

is present close to the Fermi level. Subsequently, as a result of this band Jahn-Teller effect, a redistribution of the density of states of these $3d$ electrons takes place. In all the materials,[35, 83] which favour a tetragonal deformation, a substantial density of states very close to the Fermi level has been observed. As a result of the redistribution of the DOS, under tetragonal distortion, due to closeness of the peak in DOS to the Fermi level, the energy gets lowered in these materials. Consequently, the possibility of martensite transition is found to be high. In other words, the band Jahn-Teller effect is found to be, as expected, quite sensitive to the DOS at or very close to the E_F in the cubic phase. Further, for these materials, a negative or very close to zero value of tetragonal shear constant, C′, has also been observed, as is expected.[35, 83] For the set of materials, which have cubic phase in their lowest energy phase, under tetragonal distortion, the splitting of the levels of minority spin $3d$ electrons is observed as well but the peaks are away from the E_F, resulting in a reduced density of states at E_F. Therefore, in these systems, the lowering of free energy as a function of tetragonal distortion is not possible, which renders the tetragonal transition unlikely. This observation is corroborated by the relatively large and positive values of C' for all these materials.

5.3 Conclusion

In this chapter, we present our results on the bulk mechanical, magnetic and electronic properties of a series of Ni and Co-based full Heusler alloys, namely, Ni_2BC and Co_2BC (B = Sc, Ti, V, Cr and Mn as well as Y, Zr, Nb, Mo and Tc; C = Ga and Sn). After full geometry optimization and establishing the electronic stability from the formation energy, we carry out the calculation of different properties to probe and understand, the similarities and differences in the properties of these materials. Out of all the electronically stable compounds of the total forty Ni and Co-based materials, most of the Ni-based materials are expected to show a non-magnetic ground state. On the other hand, Ni_2MnGa and Ni_2MnSn as well as all the Co-based materials are ferromagnetic in nature (except Co_2ScGa and Co_2YGa). Further, from the Heisenberg exchange interaction parameters, it is seen that the materials exhibit similar nature in terms of the relative contributions of the direct and RKKY-type nature of the magnetic interactions. The trend of the calcu-

lated values of Curie temperature for various materials, obtained from the J_{ij} parameters, matches reasonably well with the literature. From the point of view of bulk mechanical properties, the values of tetragonal shear constant show consistent trend: high positive for materials not prone to tetragonal distortion and low or negative for others. A general trend of nearly-linear inverse relationship between the Cauchy pressure and the G/B ratio is predicted for both the Ni and Co-based materials.

It is observed that the Ni-based materials are typically metallic in nature. However, all the Co-based alloys exhibit a significant spin polarization at the Fermi level. Most of the Ni-based materials have a $3d$ band of the minority spin of the A atoms close to and below the E_F. On the other hand, the peak position of the same is above the E_F for most of the Co-based materials. We observe that, in both the cases of Ni and Co-based materials, the $3d$ levels of the Ni and Co atoms play an important role in deciding the ground state. Further, the results of DOS following, the replacements of the A, B, C sites of the A_2BC materials by different atoms, indicate that in general a rigid band model explains the differences in the electronic structure of both the Ni and Co-based materials to a large extent. This model along with the hybridization between atoms, further supports the results of partial and total moments of these systems. The relationship between the closeness of the peak corresponding to the e_g levels of the $3d$ down spin electrons of the A atom to the Fermi level and the tendency of lowering of energy upon tetragonal distortion is consistent across all the Ni and Co-based materials.

Finally, from our study on the two categories of materials, it is clear that out of all the materials which we study here, only four FHAs show a tendency of undergoing martensite transition. Out of these four materials, which have a conventional Heusler alloy structure and exhibit a clear possibility of finding a tetragonal phase as their ground state, three of them, namely, Ni_2MnGa, Ni_2MoGa and Co_2NbSn have a metallic nature as is observed in case of majority of the MSMA material. On the other hand, from our calculations, Co_2MoGa is predicted to be a shape memory alloy with a reasonably high spin polarization at the Fermi level.

Chapter 6

Study of Effect of Co Substitution on the Magnetic Properties of Ni and Pt-based Heusler Alloys

6.1 Introduction

In the literature, as well as in the earlier chapters of this thesis, the possibility of two types of application of the full Heusler alloys (FHA) has already been discussed. One category of Heusler alloys is likely to be used as shape memory alloys and these are metallic in nature whereas another category is likely to be used as spin-injector materials due to the high spin polarization at the Fermi level. Both these types of Heusler alloys have generated immense interest among the researchers, theoreticians and experimentalists alike, because of the wide diversity of physical properties of these materials. In this chapter, we concentrate on some aspects of the magnetic properties of these materials. The full Heusler alloys may have ferromagnetic, ferrimagnetic, anti-ferromagnetic and also non-magnetic (net and partial atomic moments being zero or negligible) configurations, depending on their chemical composition. Along with these long-range orderings present in these systems, it may be interesting to study the similarities and differences between the various magnetic interactions present in the above-mentioned two categories of FHAs. In most of the full Heusler alloys, A_2BC, B is the primary moment carrying atom. In many of the Heusler alloys, A_2BC, there is the presence of a delocalized-like common d-band formed by the d-electrons of the A and B atoms, which are both typically first-row transition metal atoms.[38] Additionally, there is also an indirect RKKY-type exchange mechanism[40] between the B atoms, primarily mediated by the electrons of the C atoms, which also

plays an important role in defining the magnetic properties of these materials.[38, 91] In the literature, Staunton et. al.[171] have discussed the role of RKKY interaction behind the origin of magnetic anisotropy of a system.

In the previous chapter, we have shown in detail the similarities and differences between the Heusler alloys which are likely to show martensite transition and which are not, in terms of some aspects of the electronic, magnetic as well as mechanical properties. In this chapter, we focus our interest on how the magnetic exchange interactions, mainly the RKKY type of interaction between the B atoms itself of the A_2BC systems evolve as a function of substitution: we consider that at one end there are materials which are prone to martensite transition (generally metallic in nature) and at the other end there are materials which are not prone (typically half-metallic in nature) to it. Here, we present the results of our study on the nature of RKKY type of interaction present in four sets of materials: $Ni_{2-x}Co_xMnGa$, $Ni_{2-x}Co_xFeGa$, $Pt_{2-x}Co_xMnGa$, $Pt_{2-x}Co_xMnSn$ where x = 0.00, 0.25, 0.50, 0.75, 1.25, 1.50, 1.75, 2.00. In all the cases the material is likely to show SMA property at one ends (for x = 0.00) and is predicted to be half-metallic at the other (for x = 2.00).

6.2 Results and Discussion

The Heusler alloys (A_2BC) studied here possess $L2_1$ structure that consists of four interpenetrating face-centered-cubic (fcc) sub-lattices with origin at fractional positions, (0.25, 0.25, 0.25), (0.75, 0.75, 0.75), (0.5, 0.5, 0.5), and (0.0, 0.0, 0.0). As mentioned in the earlier chapters, for the conventional Heusler alloy structure, the first two sub-lattices are occupied by A atom and the third by B and fourth by C atom. While we study the Co substitution in four A_2BC systems (Ni_2MnGa, Ni_2FeGa, Pt_2MnGa and Pt_2MnSn), the Co atom substitutes the A atom only. First, we carry out full geometry optimization of all the materials corresponding to x = 0.00, 0.25, 1.75, 2.00, using the 16 atom cell (with P1 symmetry). After obtaining the equilibrium lattice constants of the four above-mentioned materials using VASP[51, 52], we plot the same. A linear variation of the lattice constant is observed. We deduce the lattice constants of the other materials, corresponding to x = 0.50, 0.75, 1.25, 1.50 by the method of interpolation. As mentioned above, we studied here

four sets of materials, $Ni_{2-x}Co_xMnGa$, $Ni_{2-x}Co_xFeGa$, $Pt_{2-x}Co_xMnGa$, $Pt_{2-x}Co_xMnSn$ with x = 0.00, 0.25, 0.50, 0.75, 1.25, 1.50, 1.75, 2.00. At the two ends of the composition, i.e. for x = 0.00 and x = 2.00, all the materials except Pt_2MnSn are already reported in the literature. We predict in this work, that Pt_2MnSn also possesses conventional Heusler alloy structure and ferromagnetic ordering in its ground state as well as is likely to exhibit the martensite transition.

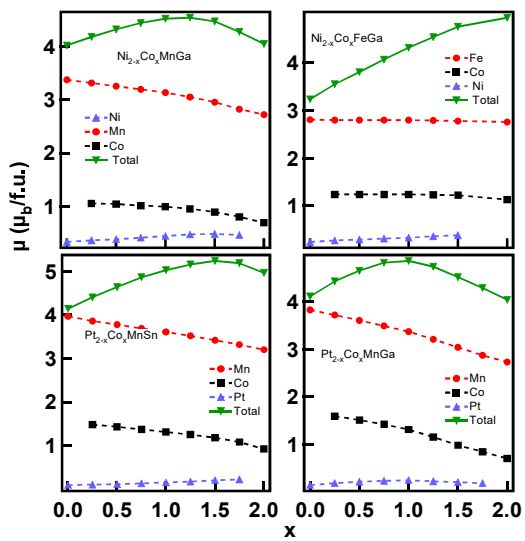

Figure 6.1: x dependence of magnetic moments for $Ni_{2-x}Co_xMnGa$, $Ni_{2-x}Co_xFeGa$, $Pt_{2-x}Co_xMnSn$, $Pt_{2-x}Co_xMnGa$. The line is only guide to the eyes.

Total and partial moments- We observe from Figure 6.1 that for the three sets of materials namely, $Ni_{2-x}Co_xMnGa$, $Pt_{2-x}Co_xMnGa$, $Pt_{2-x}Co_xMnSn$ the variation of total moment (μ_T) follows the same trend, which is as follows: for lower value of x, μ_T increases and then starts to fall at a higher x value, attaining a maximum value in between the range of x = 0.00 to x = 2.00. For $Ni_{2-x}Co_xMnGa$, the nature of variation of the moment as a function of x matches with the existing literature.[172] The variation of the total moment as a function of x can be well understood from the variation of the partial atomic moments for the respective systems. We find that for $Ni_{2-x}Co_xMnGa$, $Pt_{2-x}Co_xMnGa$, $Pt_{2-x}Co_xMnSn$, the partial moment of Co and Mn-atom decreases linearly as a function of x. This may be because, as we move towards the higher value of x, the lattice parameter of the systems decreases which leads to decrease of the Mn and Co partial moment. But as the absolute value of moment of Co-atom is much larger compared to that of Ni or Pt,

the total moment increases initially with increasing value of x. However, this increasing factor has to compete with the continuous reduction of the partial moments of Co and Mn-atom, which dominates at higher value of x. This results in a fall of the total value of the moment. Because of these two competing factors, initially we get a maximum value of μ_T and then it falls, finally it reaches a value which is very close to an integer value following the Slater Pauling rule.[34] On the contrary, the total magnetic moment of $Ni_{2-x}Co_xFeGa$ system increases linearly as a function of x. This type of linear variation may arise due to the following factors: (1) the partial moments of Fe and Co atom over the entire range of x remain almost constant which is probably due to the fact that the lattice parameters for the two end materials Ni_2FeGa (a = 5.76 Å) and Co_2FeGa (a = 5.73 Å) are very close, (2) hence, the only controlling factor in this case is the change of moment of the whole system due to the substitution of Ni atom by Co atom, which is always positive and proportional to the substitution and thus, effectively results in a linear increase of the total moment of this system.

Energy vs c/a ***curve-*** We have applied a tetragonal distortion on the cubic phase

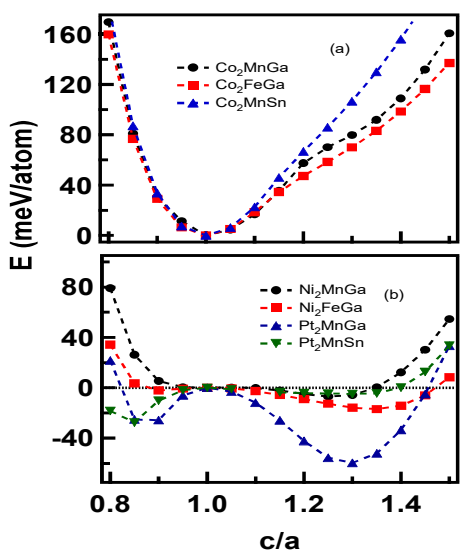

Figure 6.2: Variation of the total energy of (a) Co_2MnGa, Co_2FeGa, Co_2MnSn (b) Ni_2MnGa, Ni_2FeGa, Pt_2MnGa, Pt_2MnSn in their respective ground state magnetic configurations as a function of c/a. Energy E in the Y-axis signifies the energy difference between the cubic and tetragonal phase. Some results of these figures are part of published literature.[117, 173] Estimated values of T_M for Ni_2MnGa, Ni_2FeGa, Pt_2MnGa,Pt_2MnSn are 70 K, 197 K, 817 K, 56 K respectively, which match well with literature.[18] The dashed line is only guide to the eyes.

of all the stoichiometric (end) materials to probe whether those are prone to undergo tetragonal distortion or not. In the upper panel of Figure 6.2, we find that for some materials there is no lowering of energy under tetragonal distortion. For this set of materials (with x = 2.0), namely Co_2MnGa, Co_2MnSn, Co_2FeGa, the cubic phase is the lowest energy state ($c/a = 1$) and therefore, these are not likely to undergo martensite transition.[117, 118, 141] In the lower panel of Figure 6.2 we observe that for all the materials shown here (i.e. Ni_2MnGa, Ni_2FeGa, Pt_2MnGa, Pt_2MnSn), energy of the systems is lowered under tetragonal distortion which indicates a possibility of martensite transition in these materials. Except Pt_2MnSn, which is predicted in this thesis for the first time, the other three materials, namely Ni_2MnGa, Ni_2FeGa and Pt_2MnGa are already reported to undergo martensite transition.[4, 143, 169]

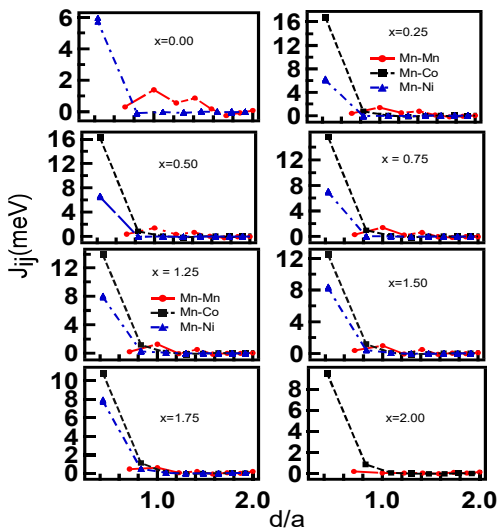

Figure 6.3: J_{ij} of Mn atom with its neighbours as a function of normalized distance d/a for $Ni_{2-x}Co_xMnGa$ system. a is the lattice parameter for x=0.00, 0.25, 0.50, 0.75, 1.25, 1.50, 1.75, 2.00. The lines are only guide to the eyes.

Direct exchange interaction- Now we discuss (Figure 6.3 to Figure 6.6) the Heisenberg exchange coupling parameters (J_{ij}) between Mn or Fe with other magnetic atoms of $Ni_{2-x}Co_xMnGa$, $Ni_{2-x}Co_xFeGa$, $Pt_{2-x}Co_xMnGa$, $Pt_{2-x}Co_xMnSn$ systems (x = 0.00, 0.25, 0.50, 0.75, 1.25, 1.50, 1.75, 2.00), as a function of interatomic spacing in the units of lattice parameter (a). Calculation of Heisenberg exchange coupling parameters has been carried out using SPR-KKR package.[56] We study the evolution of the magnetic

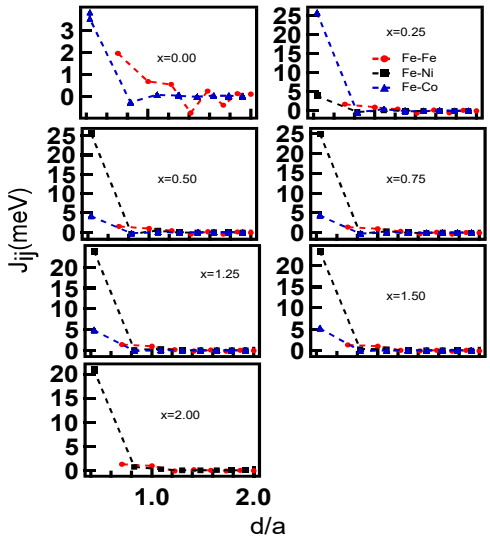

Figure 6.4: J_{ij} of Fe atom with its neighbours as a function of normalized distance d/a for $Ni_{2-x}Co_xFeGa$ system. a is the lattice parameter for x=0.00, 0.25, 0.50, 0.75, 1.25, 1.50, 2.00 (x=1.75 case has not converged). The lines are only guide to the eyes.

exchange interaction in going from a material which may show the SMA property (x = 0.00) to another which is not likely to show the SMA property (x = 2.00). We will first probe the inter-sublattice exchange interactions present in the system. We know that for conventional Heusler alloy structure (A_2BC), A atom is the nearest neighbour of the B atom. Therefore, the magnetic exchange interactions between the A and B atom will be of direct type.[38, 91, 130, 126] From Figure 6.3 we observe that, for the off stoichiometric systems where both Ni and Co are equidistant atoms from the Mn atom, the Heisenberg exchange coupling constant is much weaker between Mn and Ni compared to that between the Mn and Co atoms, as a direct consequence of the lower magnetic moment of Ni atom compared to that of Co atom. For $Ni_{2-x}Co_xFeGa$ (Figure 6.4), we observe the same, i.e. the direct exchange coupling constant between Co and Fe atom is much stronger compared to that between Ni and Fe. Similarly, from Figure 6.5 and Figure 6.6, we observe that in case of Pt-based systems, the exchange coupling constant between Mn and Co is much higher compared to that of between Mn and Pt, as a consequence of much lower magnetic moment of Pt atom compared to Co atom. In case of direct exchange, the interaction energy is sizable only between the nearest neighbors. It dies very fast with distance. Figure 6.7 shows how the nearest neighbor exchange interaction energy varies with the Co

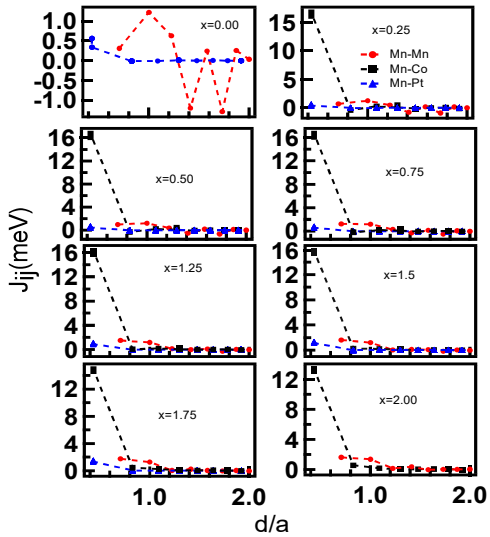

Figure 6.5: J_{ij} of Mn atom with its neighbours as a function of normalized distance d/a for $Pt_{2-x}Co_xMnSn$ system. a is the lattice parameter for x=0.00, 0.25, 0.50, 0.75, 1.25, 1.50, 1.75, 2.00. The lines are only guide to the eyes.

substitution. For $Ni_{2-x}Co_xMnGa$ we observe that, the direct exchange coupling constant between Mn and Co atom is maximum (16.94 meV) at x = 0.25, then falls almost linearly to its minimum value (9.57 meV) at x = 2.00. But the exchange coupling constant between Mn and Ni atom increases linearly as a function of Co substitution for the same system. For the rest of the systems i.e. $Ni_{2-x}Co_xFeGa$, $Pt_{2-x}Co_xMnSn$, $Pt_{2-x}Co_xMnGa$, the direct exchange interaction energy between B and Co atom varies in the same way as found in case of $Ni_{2-x}Co_xMnGa$. In all the cases, the exchange coupling constant decreases almost linearly with increasing x. For $Ni_{2-x}Co_xFeGa$ and $Pt_{2-x}Co_xMnSn$ the nearest neighbour exchange interaction energy between B atom and Ni or Pt, (depending on the system) increases almost linearly as a function of Co substitution. To understand the trend of the variation of nearest neighbour direct exchange interaction, we show how the product of the magnetic moments of A and B atom varies as function of Co substitution, in Figure 6.8. Here we find that the product $\mu_B * \mu_{Co}$ varies in the same way as that of exchange coupling energy between B and Co atom as shown in the Figure 6.7. This is also true for the Ni (or Pt) and Co atom. In case of $Pt_{2-x}Co_xMnGa$, we find that the direct exchange interaction energy between Mn and Pt atom increases first for lower value of x, then falls, after attaining a maximum value in between x = 0.00 and x

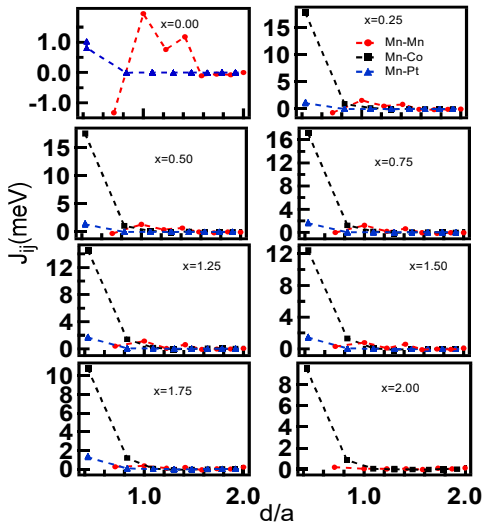

Figure 6.6: J_{ij} of Mn atom with its neighbours as a function of normalized distance d/a for $Pt_{2-x}Co_xMnGa$ system. a is the lattice parameter for x=0.00, 0.25, 0.50, 0.75, 1.25, 1.50, 1.75, 2.00. The lines are only guide to the eyes.

= 2.00. The same trend has been observed for the product $\mu_{Mn} * \mu_{Pt}$. This observation shows that there is a strong dependence of the direct exchange interaction between two magnetic moments on the product of the interacting moments.

Curie temperature from Heisenberg coupling constant- We have calculated the ferromagnetic transition temperature (T_C) for all the stoichiometric and off-stoichiometric materials, studied here. T_C has been calculated from the exchange coupling parameters as has been done earlier in the literature.[175] A stronger ferromagnetic coupling yields higher value of T_C. Figure 6.9 shows the variation of calculated T_C as a function of Co substitution. For the stoichiometric cases (x = 0.00, x = 2.00), we compare our calculated T_C, with the existing literature. The experimental values of T_C are shown as black square in Figure 6.9, wherever available. We observe that the calculated and the experimentally measured T_C values are quite close for the stoichiometric materials. We observe that with increasing percentage of Co doping, T_C increases, which can be attributed to the much stronger direct exchange coupling between B and Co atoms compared to that of the B and Ni or Pt atoms. Kanomata et. al.[172] have shown experimentally how T_C varies with x for $Ni_{2-x}Co_xMnGa$ system. We notice that there is a discrepancy between our calculated and experimental values[172] of T_C in the nonstoichiometric region of $Ni_{2-x}Co_xMnGa$,

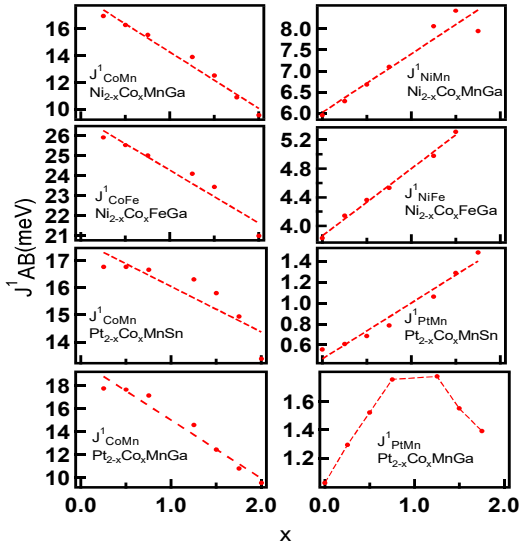

Figure 6.7: In panels from top to bottom, nearest neighbour direct exchange interaction, $J^1{}_{AB}$ (A=Co, Ni or Pt; B=Mn or Fe depending on the system) as a function of Co doping, x for $Ni_{2-x}Co_xMnGa$, $Ni_{2-x}Co_xFeGa$, $Pt_{2-x}Co_xMnSn$, $Pt_{2-x}Co_xMnGa$, respectively. Dashed line is a guide to the eye.

which may be because of our consideration of ideal $Pm\bar{3}m$ symmetry of the materials without the presence of any kind of defects or disorder.

RKKY type indirect exchange interaction- RKKY type of interaction plays a very important role in the systems where the localized moments are far apart to have any direct exchange interaction. There are studies on the RKKY interactions in various dilute magnetic systems, where the magnetic atoms like Mn or Fe are present in a very low concentration in a nonmagnetic metallic host material,[176] and the presence of RKKY interaction between the localized-like moments (Mn or Fe) was reported. This interaction was via the conduction electrons of the host material, which may be from atoms, Au, Ag, Mo, Zn etc. Not only in metallic systems, RKKY interaction has been seen to play a crucial role in determining the magnetic property of dilute magnetic semiconductor also.[177] Experimentally the presence of long range oscillatory type of magnetic exchange interaction between the localized Mn moments of Ni_2MnSn and Pd_2MnSn was confirmed by Noda et. al.[178] using neutron spin wave scattering method.

In this chapter, all the systems studied contain either Mn or Fe atom as the B atom, and the magnetic moments are mainly confined to these atoms. As all the systems studied here possess conventional Heusler alloy structure (A_2BC), the separation between the

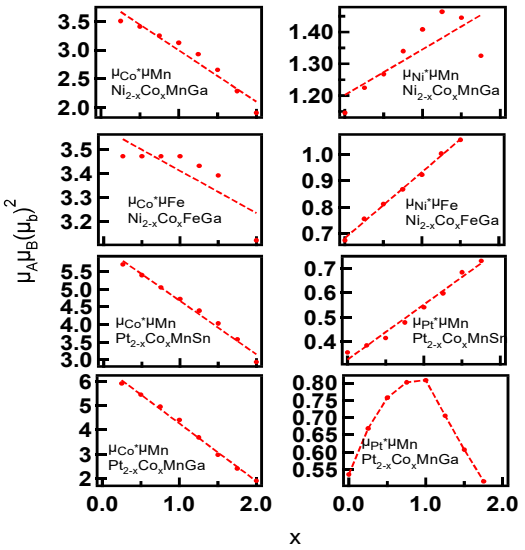

Figure 6.8: In panels from top to bottom, x dependence of product of magnetic moments of A and B atom (μ_A*μ_B)for $Ni_{2-x}Co_xMnGa$, $Ni_{2-x}Co_xFeGa$, $Pt_{2-x}Co_xMnSn$, $Pt_{2-x}Co_xMnGa$, respectively. Dashed line is a guide to the eye.

B atoms (Mn or Fe depending on the system) is too large to have a direct exchange interaction between them. For this kind of Heusler alloy structure, B atom is surrounded by eight A atoms, which makes the A atoms play a very important role in determining the magnetic exchange interactions between B atoms themselves. The localized-like nature of the magnetic moment of the B atoms spin-polarizes the free-like electrons present in the system and these spin-polarized conduction electrons effectively couple the B atoms.[95] Previously in the literature[38] it was mentioned for A_2MnC systems (A = Cu, Pd; C = Al, In, Sb), that the conduction electrons of the C atom take part in the coupling between Mn atoms. In a recent study[91] the role of conduction electron of A atom has also been confirmed for a number of Mn-based Heusler alloys. In the systems studied here, C-atom is fixed (when x is varied), which is Ga for $Ni_{2-x}Co_xMnGa$, $Ni_{2-x}Co_xFeGa$, $Pt_{2-x}Co_xMnGa$ and Sn for $Pt_{2-x}Co_xMnSn$. However with the substitution, nature of the atom at A site changes. Here we will discuss only about the role of A-atom in the RKKY interaction between B atoms themselves. It is to be noted that the spin polarization of the conduction electron will depend on the value of partial magnetic moment of the B atom and the number of the conduction electrons present in the system. Now as we move from Ni_2MnGa to Co_2MnGa we are effectively reducing the number of conduction

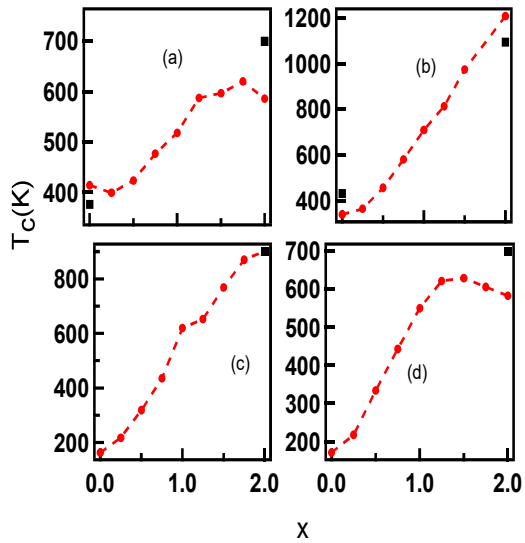

Figure 6.9: x dependence of Curie temperature (T_C) for (a)$Ni_{2-x}Co_xMnGa$, experimental values of T_C for Ni_2MnGa and Co_2MnGa have been taken from Ref[1] and Ref[32], respectively (b)$Ni_{2-x}Co_xFeGa$, experimental values of T_C for Ni_2FeGa and Co_2FeGa have been taken from Ref[143] and Ref[174], respectively (c)$Pt_{2-x}Co_xMnSn$, experimental value of T_C for Co_2MnSn has been taken from Ref[32] (d)$Pt_{2-x}Co_xMnGa$, experimental value of T_C for Co_2MnGa has been taken from Ref[32]. Dashed line is a guide to the eye.

electrons of the system, as Ni has one more d-electron compared to Co-atom. This may cause a weaker coupling between the Mn atoms themselves. From Figure 6.10(a) we find that for Ni_2MnGa (x = 0.00) the Mn-Mn interaction is the most oscillatory in nature (Heisenberg exchange coupling constant varies between 1.39 meV ($d/a = 1$) to -0.25 meV ($d/a = 1.73$)) whereas for Co_2MnGa the oscillation is minimal (varies between 0.2 meV ($d/a = 0.71$) to -0.02 meV ($d/a = 1.58$)). It is to be noted that the oscillatory nature gets reduced gradually as we move from Ni_2MnGa to Co_2MnGa. For $Ni_{2-x}Co_xFeGa$ system also, we observe the same kind of variation for Fe-Fe interaction as we move from x = 0.00 to x = 2.00. For x = 0.00 i.e. for Ni_2FeGa the amplitude of Fe-Fe RKKY interaction varies between 1.96 meV ($d/a = 0.71$) and -0.76 meV ($d/a = 1.41$) which is the strongest among the $Ni_{2-x}Co_xFeGa$ series.

In going from Pt-based systems to Co-based systems (Figure 6.10(c) and Figure 6.10(d)) also, we are reducing the number of conduction electrons. One more factor which we must consider when we discus about $Pt_{2-x}Co_xMnSn$ and $Pt_{2-x}Co_xMnGa$ is, the change in lattice parameter between the compounds corresponding to x = 0.00 and 2.00. On the other hand, for $Ni_{2-x}Co_xMnGa$ and $Ni_{2-x}Co_xFeGa$ this change is nominal

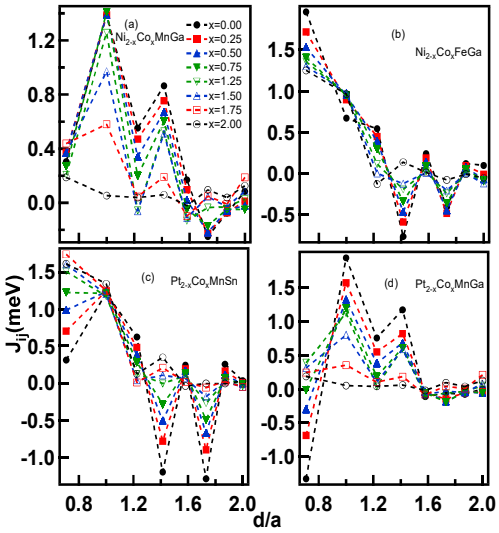

Figure 6.10: J_{B-B} (B=Mn or Fe depending on the systems) as a function of normalized distance d/a for (a)$Ni_{2-x}Co_xMnGa$ (b) $Ni_{2-x}Co_xFeGa$ (c)$Pt_{2-x}Co_xMnSn$ (d)$Pt_{2-x}Co_xMnGa$. a is the lattice parameter for different values of x. The lines are only guide to the eyes.

as both Ni and Co has very close values of atomic radius. As we move from Pt_2MnSn (a = 6.46 Å) to Co_2MnSn (a = 5.98 Å) there is a contraction of lattice parameter of about 0.48 Å. For Pt_2MnGa (a = 6.23 Å) to Co_2MnGa (a = 5.72 Å), a contraction of about 0.51 Å takes place. This larger lattice parameter for Pt-based systems causes more localization of the Mn partial magnetic moment (3.97 μ_B and 3.82 μ_B in Pt_2MnSn and Pt_2MnGa, respectively) compared to the values in the Co-based systems (3.19 μ_B and 2.73 μ_B in case of Co_2MnSn and Co_2MnGa, respectively). Bose et. al.[130] have mentioned that the strength of exchange interaction between two interacting magnetic moments also depends on the values of the respective magnetic moments. Therefore, if we focus on Figure 6.10(c) we observe that the Mn-Mn exchange interaction energy for x = 0.00 (Pt_2MnSn) oscillates between a maximum value of 1.21 meV (d/a = 1.00) and minimum value of -1.29 meV (d/a = 1.73) but oscillation becomes weaker gradually as we increase x and for Co_2MnSn it varies between 1.61 meV (d/a = 0.71) and 0.03 meV (d/a = 0.58). It indicates RKKY type of interaction is stronger in Pt_2MnSn compared to Co_2MnSn, which may be because of the more localized-like Mn-moments in Pt_2MnSn. For $Pt_{2-x}Co_xMnGa$ system also we find that for x = 0.00, RKKY type of interaction between Mn-Mn is the most oscillatory (for Pt_2MnGa it varies between -1.33 meV and 1.94 meV

at d/a = 0.71 and 1.00, respectively) and gradually with increasing x, the interaction becomes less oscillatory in nature.

Density of states for $Ni_{2-x}Co_xMnGa$ and $Pt_{2-x}Co_xMnSn$ - Figure 6.11, depicts the spin polarized and atom projected density of states (DOS) of $Ni_{2-x}Co_xMnGa$ for some representative values of x (0.00, 0.50, 1.50, 2.00). We observe that the spin polarization at the Fermi level is maximum for x = 2.00, i.e. for Co_2MnGa, as minority density of states almost vanishes there. Majority density of states is found to move towards the higher energy side with increasing Co substitution at Ni site and this supports a rigid band model.

For all the cases, we observe a large exchange splitting in the density of states of Mn atom. For Mn atom, the occupied density of states is dominated by the majority spin whereas the unoccupied region is dominated by the minority spin. In case of Ni_2MnGa (x = 0.00), the majority peak of DOS corresponding to the Mn atom is centred around -1.1 eV whereas its minority peak is centred around +1.3 eV. This exchange splitting for Mn atom decreases gradually with increasing value of x and becomes minimum for x = 2.00, where the majority peak is centred around -0.6 eV and minority peak is centered around +1.5 eV. In going from Ni_2MnGa to Co_2MnGa, the localized nature of the Mn magnetic moment is reduced, which effectively causes an weaker RKKY type of indirect coupling between them for the latter, which has been observed earlier.

From Figure 6.11(a), we observe a peak in the minority DOS, which is very close to the Fermi level. A detailed analysis shows that this peak is derived from the e_g states of $3d$ electrons of Ni atom. In literature, the role of this peak in assisting the martensite transition has been extensively discussed. Here we observe that, this peak diminishes gradually as we move towards the Co_2MnGa end, and the DOS of minority spin electrons gets reduced at the Fermi level. Complete substitution of Ni by Co atom makes the system half metallic-like but the majority density of states of Ni atom changes hardly near the Fermi level as a function of substitution of Co at Ni site. The reduction of the minority carriers with increasing Co substitution at the Ni site effectively reduces the conduction electrons present in the system, causing a weaker exchange coupling between the localized-like Mn moments, which we observe in Figure 6.10. For Co atom, DOS for

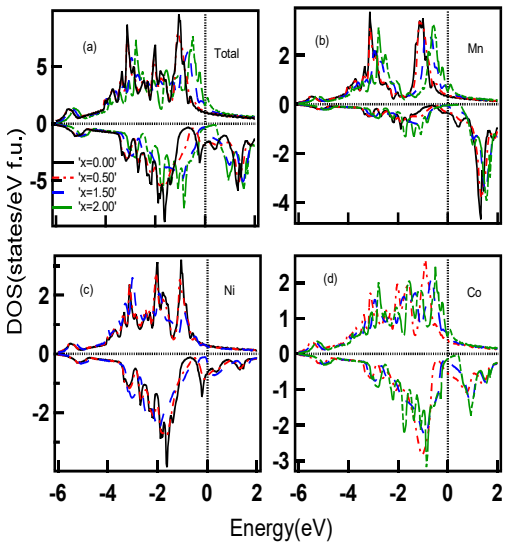

Figure 6.11: Spin polarized and atom projected density of states of (a)$Ni_{2-x}Co_xMnGa$ (b)Mn (c)Ni (d)Co, for x=0.00, 0.50, 1.50, 2.00 (We have not shown the density of states for all values of x for better clarity of the figure).

both majority and minority spin channels move to the lower binding energy side with increasing value of x.

Figure 6.12 shows the spin polarized total and partial density of states for $Pt_{2-x}Co_xMnSn$ for the same representative x values (x = 0.00, 0.50, 1.50, 2.00). From Figure 6.12(a), we observe that the systems become rather close to half-metallic for x = 2.00, i.e. for Co_2MnSn, whereas Pt_2MnSn (x = 0.00) is a metallic system. We find that there a clear shift of the majority density of states towards the higher binding energy with increasing value of x. Similar to the $Ni_{2-x}Co_xMnGa$ case, the exchange splitting of the Mn atom is maximum for x = 0.00 and minimum in the case of x = 2.00. For x = 0.00 and x = 2.00, the peaks corresponding to the majority spin are centred around -1.9 eV and -1.0 eV, whereas the corresponding minority peaks are centred around +1.2 eV and +1.4 eV, respectively. It suggests that the magnetic moment of Mn atom is much more localized-like in case of Pt_2MnSn in comparison to the Co_2MnSn system. This may be because of the much larger lattice parameter of the former one. Next we focus on the DOS of Co and Pt atoms. We observe that the increase in the majority DOS of Co atom with increasing value of x is almost counterbalanced by the decrease of the majority DOS of Pt atom at the Fermi level. But the minority DOS decreases gradually with increasing

value of x for both Pt and Co atoms at the Fermi level. As a result, the effective number of conduction electrons of the system seems to decrease as we move from x = 0.00 to x = 2.00. In going from Pt_2MnSn to Co_2MnSn we observe a gradual decrease in the strength of RKKY type of interaction (Figure 6.10(c)) mainly due to two facts: *(a) magnetic moment of the Mn atom become more delocalized-like, (b) continuous reduction of the number of conduction electrons*, with increasing value of x. For the other two sets of systems, namely, $Ni_{2-x}Co_xFeGa$ and $Pt_{2-x}Co_xMnGa$, we observe the same kind of evolution of the electronic structure as a function of x as in case of the other two systems discussed above. Both $Ni_{2-x}Co_xFeGa$ and $Pt_{2-x}Co_xMnGa$ seem to be metallic for x = 0.00 and become almost half-metal for x = 2.00, as the minority spin DOS diminishes gradually with the increase of Co substitution.

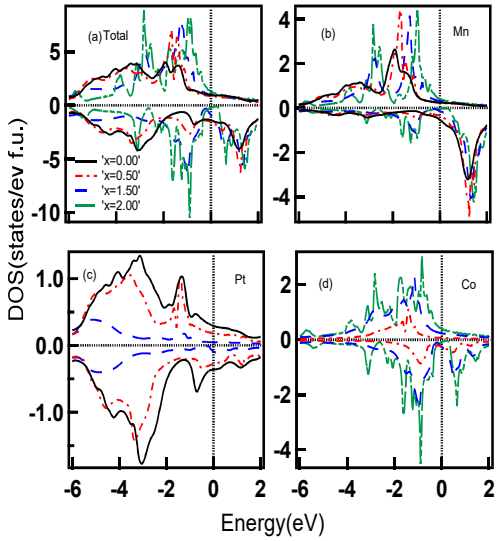

Figure 6.12: Spin polarized total and atom projected density of states of (a)$Pt_{2-x}Co_xMnSn$ (b)Mn (c)Pt (d)Co, for x=0.00, 0.50, 1.50, 2.00 (We have not shown the density of states for all values of x for better clarity of the figure).

6.3 Conclusion

Using density functional theory based calculations we study the effects of Co substitution in Ni and Pt-based Heusler alloys which are likely to show SMA. Our results suggest that there is a decrease in strength of the RKKY interaction as we increase the Co doping at Ni or Pt site. It indicates about the dominant role played by the d-electrons of A atoms in

the formation of coupling between localized-like moments of B atom in the A_2BC systems studied here. We also report the dependence of the strength of the RKKY interaction on the localized-like nature magnetic moment of B atom. Our study signifies the implicit and important presence of RKKY interaction in the magnetic Heusler alloys which are likely to show martensite transition.

Chapter 7

Summary and Conclusion

7.1 Summary

The well known prototype magnetic shape memory Heusler alloys Ni_2MnGa and Mn_2NiGa undergo a structural transition (martensite transition) from cubic to non-cubic symmetry below a certain transition temperature, which is below the room temperature. In the literature[10], copper doping at the Mn site of Ni_2MnGa is shown to result in an increase in the martensite transition temperature (T_M), compared to the parent material Ni_2MnGa. This has motivated us to probe the effects of the copper substitution partially or even completely, at the different sites of Ni_2MnGa and Mn_2NiGa. It has been observed that substitution at Ni site stabilizes the cubic phase, while that at Ga and Mn sites tends to favor tetragonal distortion in both the systems. Overall, it has been observed that despite the presence of differences in terms of crystal structures and ground state magnetic configurations between these two systems, the physics of effects of Cu substitution on the tetragonal transition is rather similar.

Further, it is known that, Ni_2MnGa possesses poor mechanical property. Since, both bulk Cu and Pt have high ductility, the effects of Pt, Cu and Pd substitution at the Ni site of Ni_2MnGa have been probed on the bulk mechanical, as well as electronic and magnetic properties. On the basis of our studies, it can be conjectured that, some amount of Pt substitution at the Ni site, along with Cu substitution at the Mn site in Ni_2MnGa may lead to a promising magnetic shape memory alloy, with possible martensite transition temperature above the room temperature and reduced inherent crystalline brittleness. But, as Pt is substituted at the Ni site of the Ni_2MnGa, Curie temperature is predicted to decrease significantly (for Pt_2MnGa, T_C=176K) with respect to the parent material Ni_2MnGa (T_C= 414K).

Hence, in order to screen Heusler alloy materials for which T_C will lie above the room temperature, we probe Co-based full Heusler alloys (FHA), which are known to exhibit high T_C. The Co-based FHAs are generally half metallic in nature and do not show a possibility of martensite transition (except for a very few materials, e.g. Co_2NbSn). Recently, Co_2NiGa has been reported to undergo martensite transition. Further, our calculated results and the existing literature suggest that Pt substitution at the Ni site of Ni_2MnGa, leads to improvement of mechanical property and results in a T_M which is above the room temperature. These above-mentioned findings motivate us to probe a hitherto unexplored material, which is Co_2PtGa. Further, as the number of valence electrons per atom is known to play an important role in deciding the electronic properties of these systems, we carry out a comparative study of Cr_2PtGa, Mn_2PtGa, Fe_2PtGa and Co_2PtGa. We predict that all these materials are likely to undergo martensite transition. For Mn_2PtGa the same has already been theoretically shown in the literature. Among the studied materials, Co_2PtGa is likely to possess the highest spin polarization at the Fermi level for both the cubic phase (80%) and tetragonal phase ((71%)). Among all the materials we studied in this thesis, this novel material is expected to exhibit among the studied materials the lowest inherent crystalline brittleness as well as the highest martensite transition temperature (880K), and high melting (1380K) and Curie temperatures (580K). All of these predicted temperatures being well above the room temperature render Co_2PtGa interesting from the application as well as fundamental points of view.

The family of Heusler alloys is well known to exhibit a wide diversity in terms of magnetic configuration which include ferromagnetic, ferrimagnetic and anti-ferromagnetic. In this regard, as both Mn and Cr are antiferromagnetic in bulk form, the effects of Mn substitution by Cr (and also Fe) in Ni_2MnGa and Pt_2MnGa have been probed. From this study we predict that, Ni_2CrGa and Pt_2CrGa are two novel Heusler alloys, which may possess intra-sublattice anti-ferromagnetic configuration in the ground state and these materials show the possibility of undergoing martensite transition as well.

Apart from predicting possible novel magnetic shape memory alloys with better properties, in this thesis, study has also been carried out on the differences and similarities

in terms of the electronic, bulk mechanical and magnetic properties between following two classes of FHAs, based mainly on Ni and Co-atoms, (1) which are likely to undergo martensite transition (generally metallic in nature) (2) which are not likely to undergo martensite transition (generally half metallic in nature). It is also probed that, if there is any possibility of existence of magnetic full Heusler alloy systems which exhibit high spin polarization at Fermi level (E_F) as well as show tendency to undergo martensite transition. Studying around forty full Heusler alloy systems (A_2BC, A = Ni,Co; B = Sc, Ti, V, Cr, and Mn as well as Y, Zr, Nb, Mo, and Tc; C = Ga and Sn), it has been observed that, contrary to the second set, in case of the first set of materials, there is a softening of tetragonal shear constant and a high density of states (DOS) at or very close to E_F. The outermost e_g levels of the $3d$ (minority spin) electrons of the A atom is found to mainly contribute to this DOS. This closeness of the e_g levels to E_F indicates a lowering of overall energy as a result of an applied tetragonal distortion in the first set of materials. During this course of study, the system Co_2MoGa has been predicted as a novel ferromagnetic Heulser alloy, which is likely to undergo martensite transition (T_M = 886K) and exhibit high spin polarization at the Fermi level in both cubic ($\sim$ 80 %) and tetragonal ($\sim$ 72 %) phases.

In the ferromagnetic full Heusler alloy systems (A_2BC), RKKY interaction plays an important role in deciding the magnetic properties of the system. The partial moments of the primary-moment-carrying B atoms are coupled mainly by the RKKY interaction. We study the evolution of RKKY interaction for the systems $Ni_{2-x}Co_xMnGa$, $Ni_{2-x}Co_xFeGa$, $Pt_{2-x}Co_xMnSn$, $Pt_{2-x}Co_xMnGa$ as a function of x (x=0.00, 0.25, 0.50, 0.75, 1.25, 1.50, 1.75, 2.00), where at one end (x = 0.00), the material is likely to favor tetragonal transition and at the other end (x = 2.00) the material is likely to exhibit cubic ground state. It has been observed that there is a decrease in the strength of RKKY interaction as we increase Co substitution at the Ni or Pt site of the Ni and Pt-based alloys. Our study indicates about the dominant role played by the valence d-electrons of the A atom in the formation of coupling between the localized-like partial moments of B atom in the A_2BC systems studied here. The dependence of the strength of this RKKY interaction on the magnetic moment of B atom has also been probed. This study signifies the implicit and important

presence of RKKY interaction in the magnetic FHAs which favor martensite transition.

7.2 Conclusion

The first aspect of the present thesis is to search for the novel magnetic shape memory alloys in a systematic way, aiming at betterment of properties from the application point of view. From literature it is well known that the properties of these systems can be tuned by means of substitution. In this work, it has been predicted that partial Ni substitution by Pt, combined with partial Mn substitution by Cu in prototype Heusler alloy Ni_2MnGa may lead to some interesting magnetic material which has a significantly high martensite transition temperature and better mechanical properties. causes a significant increase in martensite transition temperature and improvement of mechanical property. However, in this case, the major drawback is that, with increasing Pt substitution, the Curie temperature decreases and comes down well below the room temperature for Pt_2MnGa. After an intuitive search and optimized selection of the substituent element and the substituting site, Co_2PtGa has been predicted as a probable promising high temperature magnetic shape memory alloy. This novel material is expected to possess low inherent crystalline brittleness as well as high Curie, melting and martensite transition temperatures. Along with these properties, Co_2PtGa is shown to exhibit high spin polarization in both the cubic and tetragonal phases as well. Further, based on DFT based first principles calculations, we predict two novel alloys with intra-sublattice anti-ferromagnetic configuration, namely Pt_2CrGa and Ni_2CrGa for the first time. Both these systems are expected to favor martensite transition. Experimental validation of all these novel materials is awaited.

The second aspect of the present thesis is to study the differences and similarities between two classes of FHAs: (1) which are likely to undergo martensite transition (with typically metallic nature), (2) which are not likely to undergo martensite transition (generally with half-metallic nature). It has been observed that, for the first set of materials, the presence of high density of states at or very close to the E_F, especially for the outermost e_g levels of 3d electrons (minority spin) of the A atom is observed, which leads to a lowering of overall energy as a result of an applied tetragonal distortion. This observation is associated with a softening of tetragonal shear constant in the cubic phase. Both these

observations put together indicate that the tetragonal phase is energetically favorable for the studied first set of A_2BC systems. Further, an implicit and important presence of a stronger RKKY interaction has been observed for the first set in contrast to the second set of materials.

7.3 Future outlook

The present work suggests following directions for future studies.

(1) In this thesis, Co_2PtGa, has been predicted as a promising magnetic shape memory alloy with reasonably high Curie, melting and martensite transition temperatures and improved mechanical properties. The well known shape memory alloys e.g. Ni_2MnGa, Mn_2NiGa accommodate significant amount of magnetic field induced strain, and these systems are well known to possess modulated structure in the martensite phase. So it will be interesting for us to probe the possibility of existence of modulated structure for Co_2PtGa, which is a prerequisite for a MFIS.

(2) There is a major part in this work, where we have suggested probable shape memory alloys. We have compared the stability of austetenite and martensite phases, based on the energy difference between the cubic austenite phase and the non modulated tetragonal phase of the systems. All these calculations are a zero temperature calculation, hence, the effects of finite temperature has not been included. It will be very much interesting to compare the free energy differences between the austenite and martensite phases as a function of temperature. This approach may yield a better prediction of T_M for the probable novel shape memory alloys.

(3) We wish to study in detail the magnetic properties of Mn_2YZ systems (Y=Co, Ni; Z= s, p elements) based on first principles calculations as Mn_2YZ series is less explored compared to the Ni_2YZ systems.

Bibliography

[1] Webster, P. J.; Ziebeck, K. R. A.; Town, S. L.; Peak, M. S. *Philos. Mag. B* **1984**, *49*, 295.

[2] Ullakko, K.; Huang, J. K.; Kantner, C.; OHandley, R. C.; Kokorin, V. V. *Appl. Phys. Lett.* **1996**, *69*, 1966.

[3] de Groot, R. A.; Mueller, F. M.; Engen, P. G. v.; Buschow, K. H. J. *Phys. Rev. Lett.* **1983**, *50*, 2024.

[4] Siewert, M.; Gruner, M. E.; Dannenberg, A.; Chakrabarti, A.; Herper, H. C.; Wuttig, M.; Barman, S. R.; Singh, S.; Al-Zubi, A.; Hickel, T.; Neugebauer, J.; Gillessen, M.; Dronskowski, R.; Entel, P. *Appl. Phys. Lett.* **2011**, *99*, 191904.

[5] Brown, P. J.; Crangle, J.; Kanomata, T.; Matsumoto, M.; Neumann, K.-U.; Ouladdiaf, B.; Ziebeck, K. R. A. *J. Phys.: Condens. Matter* **2002**, *14*, 10159.

[6] Kaufmann, S.; Rößler, U. K.; Heczko, O.; Wuttig, M.; Buschbeck, J.; Schultz, L.; Fähler, S. *Phys. Rev. Lett.* **2010**, *104*, 145702.

[7] Sozinov, A.; Likhachev, A. A.; Lanska, N.; Ullakko, K. *Appl. Phys. Lett.* **2002**, *80*, 1746.

[8] Pasquale, M.; Sasso, C.; Lewis, L.; Giudici, L.; Lograsso, T.; Schlagel, D. *Physical Review B* **2005**, *72*, 094435.

[9] Radelytskyi, I.; Pkaa, M.; Szymczak, R.; Gawryluk, D.; Berkowski, M.; Fink-Finowicki, J.; Diduszko, R.; Dyakonov, V.; Szymczak, H. *J. Magn. Magn. Mater.* **2017**, *430*, 16.

[10] Roy, S.; Blackburn, E.; Valvidares, S. M.; Fitzsimmons, M. R.; Vogel, S. C.; Khan, M.; Dubenko, I.; Stadler, S.; Ali, N.; Sinha, S. K.; Kortright, J. B. *Phys. Rev. B* **2009**, *79*, 235127.

[11] Liu, G. D.; Chen, J. L.; Liu, Z. H.; Dai, X. F.; Wu, G. H.; Zhang, B.; Zhang, X. X. *Appl. Phys. Lett.* **2005**, *87*, 262504.

[12] Barman, S. R.; Banik, S.; Shukla, A. K.; Kamal, C.; Chakrabarti, A. *Europhys. Lett.* **2007**, *80*, 57002.

[13] Barman, S. R.; Chakrabarti, A. *Phys. Rev. B* **2008**, *77*, 176401.

[14] Singh, S.; Esakki Muthu, S.; Senyshyn, A.; Rajput, P.; Suard, E.; Arumugam, S.; Barman, S. *Appl. Phys. Lett.* **2014**, *104*, 051905.

[15] Lanska, N.; Sderberg, O.; Sozinov, A.; Ge, Y.; Ullakko, K.; Lindroos, V. K. *J. Appl. Phys.* **2004**, *95*, 8074.

[16] Jin, X.; Marioni, M.; Bono, D.; Allen, S. M.; OHandley, R. C.; Hsu, T. Y. *J. Appl. Phys.* **2002**, *91*, 8222.

[17] Hu, Q.; Luo, H.; Li, C.; Vitos, L.; Yang, R. *Sci. China. Tech. Sci.* **2012**, *55*, 295.

[18] Barman, S. R.; Chakrabarti, A.; Singh, S.; Banik, S.; Bhardwaj, S.; Paulose, P. L.; Chalke, B. A.; Panda, A. K.; Mitra, A.; Awasthi, A. M. *Phys. Rev. B* **2008**, *78*, 134406.

[19] Chakrabarti, A.; Biswas, C.; Banik, S.; Dhaka, R. S.; Shukla, A. K.; Barman, S. R. *Phys. Rev. B* **2005**, *72*, 073103.

[20] Kataoka, M.; Endo, K.; Kudo, N.; Kanomata, T.; Nishihara, H.; Shishido, T.; Umetsu, R. Y.; Nagasako, M.; Kainuma, R. *Phys. Rev. B* **2010**, *82*, 214423.

[21] Khan, M.; Dubenko, I.; Stadler, S.; Ali, N. *J. Phys.: Condens. Matter* **2004**, *16*, 5259.

[22] Khan, M.; Gautam, B.; Pathak, A.; Dubenko, I.; Stadler, S.; Ali, N. *J. Phys.: Condens. Matter* **2008**, *20*, 505206.

[23] Li, C.-M.; Luo, H.-B.; Hu, Q.-M.; Yang, R.; Johansson, B.; Vitos, L. *Phys. Rev. B* **2011**, *84*, 024206.

[24] Worgull, J.; Petti, E.; Trivisonno, J. *Phys. Rev. B* **1996**, *54*, 15695.

[25] Stenger, T. E.; Trivisonno, J. *Phys. Rev. B* **1998**, *57*, 2735.

[26] Bungaro, C.; Rabe, K. M.; Corso, A. D. *Phys. Rev. B* **2003**, *68*, 134104.

[27] Kart, S. O.; Cagn, T. *J. Alloys Compd.* **2010**, *508*, 177.

[28] Pugh, S. *Philos. Mag.* **1954**, *45*, 823.

[29] Pons, J.; Cesari, E.; Seguí, C.; Masdeu, F.; Santamarta, R. *Mater. Sci. Eng. A* **2008**, *481*, 57.

[30] Hosoda, H.; Takeuchi, S.; Inamura, T.; Wakashima, K. *Science and Technology of Advanced Materials* **2004**, *5*, 503, 21st Century COE Program, Tokyo Institute of Technology, Nanomaterials 2004.

[31] Kübler, J.; Fecher, G. H.; Felser, C. *Phys. Rev. B* **2007**, *76*, 024414.

[32] Varaprasad, B.; Rajanikanth, A.; Takahashi, Y.; Hono, K. *Acta Mater.* **2009**, *57*, 2702.

[33] Singh, S.; Ziebeck, K. R. A.; Suard, E.; Rajput, P.; Bhardwaj, S.; Awasthi, A. M.; Barman, S. R. *Appl. Phys. Lett.* **2012**, *101*, 171904.

[34] Kandpal, H. C.; Fecher, G. H.; Felser, C. *J. Phys. D: Appl. Phys.* **2007**, *40*, 1507.

[35] Fujii, S.; Ishida, S.; Asano, S. *J. Phys. Soc. Jpn.* **1989**, *58*, 3657.

[36] Siewert, M.; Gruner, M. E.; Dannenberg, A.; Hucht, A.; Shapiro, S. M.; Xu, G.; Schlagel, D. L.; Lograsso, T. A.; Entel, P. *Phys. Rev. B* **2010**, *82*, 064420.

[37] Arryave, R.; Junkaew, A.; Chivukula, A.; Bajaj, S.; Yao, C.-Y.; Garay, A. *Acta Mater.* **2010**, *58*, 5220.

[38] Kübler, J.; William, A. R.; Sommers, C. B. *Phys. Rev. B* **1983**, *28*, 1745.

[39] Wollmann, L.; Chadov, S.; Kübler, J.; Felser, C. *Phys. Rev. B* **2015**, *92*, 064417.

[40] Ruderman, M. A.; Kittel, C. *Phys. Rev.* **1954**, *96*, 99.

[41] Born, M.; Oppenheimer, R. *Annalen der Physik* **1927**, *389*, 457.

[42] Hohenberg, P.; Kohn, W. *Phys. Rev.* **1964**, *136*, B864.

[43] Kohn, W.; Sham, L. J. *Phys. Rev.* **1965**, *140*, A1133.

[44] Dirac, P. A. M. On the theory of quantum mechanics. 1926.

[45] Ceperley, D. M.; Alder, B. J. *Phys. Rev. Lett.* **1980**, *45*, 566.

[46] Vosko, S. H.; Wilk, L.; Nusair, M. *Can. J. Phys.* **1980**, *58*, 1200.

[47] Perdew, J. P.; Wang, Y. *Phys. Rev. B* **1992**, *45*, 13244.

[48] Perdew, J. P.; Burke, K.; Ernzerhof, M. *Phys. Rev. Lett.* **1996**, *77*, 3865.

[49] Blaha, P.; Schwarz, K.; Madsen, G. K. H.; Kvasnicka, D.; Luitz, J. *WIEN2K, An Augmented Plane Wave + Local Orbitals Program for Calculating Crystal Properties*; Karlheinz Schwarz, Techn. Universität Wien, Austria, 2001.

[50] Blöchl, P. E. *Phys. Rev. B* **1994**, *50*, 17953.

[51] Kresse, G.; Furthmüller, J. *Phys. Rev. B* **1996**, *54*, 11169.

[52] Kresse, G.; Joubert, D. *Phys. Rev. B* **1999**, *59*, 1758.

[53] Clark, S. J.; Segall, M. D.; Pickard, C. J.; Hasnip, P. J.; Probert, M. I.; Refson, K.; Payne, M. C. *Zeitschrift für Kristallographie-Crystalline Materials* **2005**, *220*, 567.

[54] Perdew, J. P. *Electronic structure of solids 91*; Akademie Verlag, Berlin, 1991; Vol. 11.

[55] Liechtenstein, A.; Katsnelson, M.; Antropov, V.; Gubanov, V. *J. Magn. Magn. Mater.* **1987**, *67*, 65.

[56] Ebert, H.; Kdderitzsch, D.; Minr, J. *Reports on Progress in Physics* **2011**, *74*, 096501.

[57] Meinert, M.; Schmalhorst, J.-M.; Reiss, G. *J. Phys.: Condens. Matter* **2011**, *23*, 036001.

[58] Gautam, B. R.; Dubenko, I.; Mabon, J. C.; Stadler, S.; Ali, N. *J. Alloys Compd.* **2009**, *472*, 35.

[59] Stadler, S.; Khan, M.; Mitchell, J.; Ali, N.; Gomes, A. M.; Dubenko, I.; Takeuchi, A. Y.; Guimares, A. P. *Appl. Phys. Lett.* **2006**, *88*, 192511.

[60] ed, V. A. C. *Advances in Magnetic Shape Memory Materials.*; Trans Tech Publications, Switzerland, 2011.

[61] Jiang, C.; Wang, J.; Li, P.; Jia, A.; Xu, H. *Appl. Phys. Lett.* **2009**, *95*, 012501.

[62] Wang, J.; Bai, H.; Jiang, C.; Li, Y.; Xu, H. *Mater. Sci. Eng. A* **2010**, *527*, 1975.

[63] Wang, J.; Jiang, C. *Scr. Mater.* **2010**, *62*, 298.

[64] Murray, S. J.; Marioni, M.; Allen, S. M.; OHandley, R. C.; Lograsso, T. A. *Appl. Phys. Lett.* **2000**, *77*, 886.

[65] Banik, S.; Rawat, R.; Mukhopadhyay, P. K.; Ahuja, B. L.; Chakrabarti, A.; Paulose, P. L.; Singh, S.; Singh, A. K.; Pandey, D.; Barman, S. R. *Phys. Rev. B* **2008**, *77*, 224417.

[66] Chakrabarti, A.; Barman, S. R. *Appl. Phys. Lett.* **2009**, *94*, 161908.

[67] Gao, Z.; Liu, C.; Wu, D.; Ma, W.; Zhang, J.; Cai, W. *J. Magn. Magn. Mater.* **2010**, *322*, 2488.

[68] Luo, H.; Meng, F.; Feng, Z.; Li, Y.; Zhu, W.; Wu, G.; Zhu, X.; Jiang, C.; Xu, H. *J. Appl. Phys.* **2010**, *107*, 013905.

[69] Ma, L.; Wang, W. H.; Zhen, C. M.; Hou, D. L.; Tang, X. D.; Liu, E. K.; Wu, G. H. *Phys. Rev. B* **2011**, *84*, 224404.

[70] Singh, S. et al. *Phys. Rev. Lett.* **2012**, *109*, 246601.

[71] Gao, Z.; Dong, G.; Cai, W.; Sui, J.; Feng, Y.; Li, X. *J. Alloys Compd.* **2009**, *481*, 44.

[72] Ma, Y.; Yang, S.; Liu, Y.; Liu, X. *Acta Mater.* **2009**, *57*, 3232.

[73] Moya, X.; Mañosa, L.; Planes, A.; Krenke, T.; Acet, M.; Morin, M.; Zarestky, J. L.; Lograsso, T. A. *Phys. Rev. B* **2006**, *74*, 024109.

[74] Sui, J.; Zhang, X.; Gao, L.; Cai, W. *J. Alloys Compd.* **2011**, *509*, 8692.

[75] Tsuchiya, K.; Tsutsumi, A.; Ohtsuka, H.; Umemoto, M. *Mater. Sci. Eng. A* **2004**, *378*, 370, European Symposium on Martensitic Transformation and Shape-Memory.

[76] Wang, H.; Chen, F.; Gao, Z.; Cai, W.; Zhao, L. *Mater. Sci. Eng. A* **2006**, *438440*, 990, Proceedings of the International Conference on Martensitic Transformations.

[77] Wang, Y.; Cong, D.; Peng, R. L.; Zetterstrm, P.; Zhang, Z.; Zhao, X.; Zuo, L. *J Mater Res* **2006**, *21*, 691.

[78] Wu, Z.; Hao, X.; Liu, X.; Meng, J. *Phys. Rev. B* **2007**, *75*, 054115.

[79] Singh, S.; D'Souza, S. W.; Mukherjee, K.; Kushwaha, P.; Barman, S. R.; Agarwal, S.; Mukhopadhyay, P. K.; Chakrabarti, A.; Sampathkumaran, E. V. *Appl. Phys. Lett.* **2014**, *104*, 231909.

[80] Kishi, Y.; Yajima, Z.; Shimizu, K.; Wuttig, M. *Mater. Sci. Eng. A* **2004**, *378*, 361, European Symposium on Martensitic Transformation and Shape-Memory.

[81] Meinert, M.; Schmalhorst, J.-M.; Reiss, G. *J. Phys.: Condens. Matter* **2011**, *23*, 036001.

[82] Murnaghan, F. *Proc. Natl. Acad. Sci.* **1944**, *30*, 244.

[83] Enkovaara, J.; A.,; Nordstrm, L.; Nieminen, R. M. *J. Appl. Phys.* **2002**, *91*, 7798.

[84] Uijttewaal, M. A.; Hickel, T.; Neugebauer, J.; Gruner, M. E.; Entel, P. *Phys. Rev. Lett.* **2009**, *102*, 035702.

[85] Chen, X. Q.; Yang, F. J.; Lu, X.; Qin, Z. X. *Phys. Stat. Solidi B* **2007**, *244*, 1047.

[86] Li, C.-M.; Hu, Q.-M.; Yang, R.; Johansson, B.; Vitos, L. *Appl. Phys. Lett.* **2011**, *98*, 261903.

[87] Li, C.-M.; Luo, H.-B.; Hu, Q.-M.; Yang, R.; Johansson, B.; Vitos, L. *Phys. Rev. B* **2011**, *84*, 174117.

[88] Siewert, M.; Gruner, M. E.; Hucht, A.; Herper, H. C.; Dannenberg, A.; Chakrabarti, A.; Singh, N.; Arryave, R.; Entel, P. *Adv. Eng. Mat.* **2012**, *14*, 530.

[89] Zayak, A. T.; Entel, P.; Rabe, K. M.; Adeagbo, W. A.; Acet, M. *Phys. Rev. B* **2005**, *72*, 054113.

[90] Barman, S. R.; Banik, S.; Chakrabarti, A. *Phys. Rev. B* **2005**, *72*, 184410.

[91] Şaşıoğlu, E.; Sandratskii, L. M.; Bruno, P. *Phys. Rev. B* **2008**, *77*, 064417.

[92] Chakrabarti, A.; Siewert, M.; Roy, T.; Mondal, K.; Banerjee, A.; Gruner, M. E.; Entel, P. *Phys. Rev. B* **2013**, *88*, 174116.

[93] Li, C.-M.; Luo, H.-B.; Hu, Q.-M.; Yang, R.; Johansson, B.; Vitos, L. *Phys. Rev. B* **2010**, *82*, 024201.

[94] Roy, T.; Chakrabarti, A. *Physics Letters A* **2017**, *381*, 1449.

[95] Stearns, M. B. *J. Appl. Phys.* **1979**, *50*, 2060.

[96] D'Souza, S. W.; Roy, T.; Barman, S. R.; Chakrabarti, A. *J. Phys.: Condens. Matter* **2014**, *26*, 506001.

[97] Galanakis, I.; Özdoğan, K.; Şaşıoğlu, E.; Aktaş, B. *Phys. Rev. B* **2007**, *75*, 172405.

[98] Vasil'Ev, A.; Kokorin, V.; Savchenko, Y.; Chernenko, V. *Zhurnal Eksperimental'noi i Teoreticheskoi Fiziki* **1990**, *98*, 1437.

[99] Jian-Tao, Z.; Kun, Z.; Jia-Jia, W.; Xin-Quan, Y.; Jin, Y.; San-Xie, W. **2012**,

[100] Voigt, W. *Annalen der Physik* **1889**, *274*, 573.

[101] Reuss, A. *Z. Angew. Math. Mech.* **1929**, *9*, 49.

[102] Hill, R. *Proceedings of the Physical Society. Section A* **1952**, *65*, 349.

[103] Godlevsky, V. V.; Rabe, K. M. *Phys. Rev. B* **2001**, *63*, 134407.

[104] Ayuela, A.; Enkovaara, J.; Ullakko, K.; Nieminen, R. M. *J. Phys.: Condens. Matter* **1999**, *11*, 2017.

[105] Zayak, A. T.; Entel, P.; Enkovaara, J.; Ayuela, A.; Nieminen, R. M. *Phys. Rev. B* **2003**, *68*, 132402.

[106] MacLaren, J. M. *J. Appl. Phys.* **2002**, *91*, 7801.

[107] Amari, S.; Mebsout, R.; Mabih, S.; Abbar, B.; Bouhafs, B. *Intermetallics* **2014**, *44*, 26.

[108] Kanchana, V.; Vaitheeswaran, G.; Ma, Y.; Xie, Y.; Svane, A.; Eriksson, O. *Phys. Rev. B* **2009**, *80*, 125108.

[109] Kong, B.; Chen, X.-R.; Yu, J.-X.; Cai, C.-L. *J. Alloys Compd.* **2011**, *509*, 2611.

[110] Wu, Y.; Wang, J.; Mao, F.; Kwong, F. Y. *Chemistry An Asian Journal* **2014**, *9*, 26.

[111] Pettifor, D. G. *Mat. Sci. Tech.* **1992**, *8*, 345.

[112] Chernenko, V.; Fujita, A.; Besseghini, S.; Prez-Landazabal, J. *J. Magn. Magn. Mater.* **2008**, *320*, e156, {VIII} Latin American Workshop on Magnetism, Magnetic Materials and their Applications.

[113] Entel, P.; Siewert, M.; Gruner, M. E.; Herper, H. C.; Comtesse, D.; Arróyave, R.; Singh, N.; Talapatra, A.; Sokolovskiy, V. V.; Buchelnikov, V. D.; Albertini, F.; Righi, L.; Chernenko, V. A. *Eur. Phys. J. B* **2013**, *86*, 65.

[114] Niu, H.; Chen, X.-Q.; Liu, P.; Xing, W.; Cheng, X.; Li, D.; Li, Y. *Scient. Rep.* **2012**, *2*, 718.

[115] Canadinc, D.; Dadda, J.; Maier, H. J.; Karaman, I.; Karaca, H. E.; Chumlyakov, Y. I. *Smart Materials and Structures* **2007**, *16*, 1006.

[116] Dai, X. F.; Liu, G. D.; Liu, Z. H.; Wu, G. H.; Chen, J. L.; Meng, F. B.; Liu, H. Y.; Yan, L. Q.; Qu, J. P.; Li, Y. X.; Wang, W. G.; Xiao, J. Q. *Appl. Phys. Lett.* **2005**, *87*, 112504.

[117] Roy, T.; Pandey, D.; Chakrabarti, A. *Phys. Rev. B* **2016**, *93*, 184102.

[118] Roy, T.; Gruner, M. E.; Entel, P.; Chakrabarti, A. *J. Alloys Compd.* **2015**, *632*, 822.

[119] Dutta, B.; Hickel, T.; Entel, P.; Neugebauer, J. *J. Phase Equlib. Diffus.* **2014**, *35*, 695.

[120] Nayak, A. K.; Nicklas, M.; Chadov, S.; Khuntia, P.; Shekhar, C.; Kalache, A.; Baenitz, M.; Skourski, Y.; Guduru, V. K.; Puri, A.; Zeitler, U.; Coey, J. M. D.; Felser, C. *Nat Mater* **2015**, *14*, 679, Letter.

[121] Nayak, A. K.; Nicklas, M.; Chadov, S.; Shekhar, C.; Skourski, Y.; Winterlik, J.; Felser, C. *Phys. Rev. Lett.* **2013**, *110*, 127204.

[122] Nayak, A. K.; Sahoo, R.; Mejia, C. S.; Nicklas, M.; Felser, C. *J. Appl. Phys.* **2015**, *117*, 17D715.

[123] Burch, T. J.; Litrenta, T.; Budnick, J. I. *Phys. Rev. Lett.* **1974**, *33*, 421.

[124] von Ranke, P. J.; de Oliveira, N. A.; Alho, B. P.; Plaza, E. J. R.; de Sousa, V. S. R.; Caron, L.; Reis, M. S. *J. Phys.: Condens. Matter* **2009**, *21*, 056004.

[125] Liechtenstein, A.; Katsnelson, M.; Antropov, V.; Gubanov, V. *J. Magn. Magn. Mater.* **1987**, *67*, 65.

[126] Şaşıoğlu, E.; Sandratskii, L. M.; Bruno, P. *Phys. Rev. B* **2005**, *71*, 214412.

[127] Şaşıoğlu, E.; Sandratskii, L. M.; Bruno, P.; Galanakis, I. *Phys. Rev. B* **2005**, *72*, 184415.

[128] Rusz, J.; Bergqvist, L.; Kudrnovský, J.; Turek, I. *Phys. Rev. B* **2006**, *73*, 214412.

[129] Khovailo, V. V.; Novosad, V.; Takagi, T.; Filippov, D. A.; Levitin, R. Z.; Vasil'ev, A. N. *Phys. Rev. B* **2004**, *70*, 174413.

[130] Bose, S. K.; Kudrnovský, J.; Drchal, V.; Turek, I. *Phys. Rev. B* **2011**, *84*, 174422.

[131] Luo, H.; Meng, F.; Liu, G.; Liu, H.; Jia, P.; Liu, E.; Wang, W.; Wu, G. *Intermetallics* **2013**, *38*, 139.

[132] Mañosa, L.; Gonz'alez-Comas, A.; Obradó, E.; Planes, A.; Chernenko, V. A.; Kokorin, V. V.; Cesari, E. *Phys. Rev. B* **1997**, *55*, 11068.

[133] Gu, X.; Poon, S. J.; Shiflet, G. J.; Widom, M. *Acta Mater.* **2008**, *56*, 88 – 94.

[134] Fine, M.; Brown, L.; Marcus, H. *Scr. Metall.* **1984**, *18*, 951.

[135] Soykan, C.; zdemir Kart, S.; Sevik, C.; an, T. *J. Alloys Compd.* **2014**, *611*, 225.

[136] Oikawa, K.; Ota, T.; Ohmori, T.; Tanaka, Y.; Morito, H.; Fujita, A.; Kainuma, R.; Fukamichi, K.; Ishida, K. *Appl. Phys. Lett.* **2002**, *81*, 5201.

[137] Santamarta, R.; Font, J.; Muntasell, J.; Masdeu, F.; Pons, J.; Cesari, E.; Dutkiewicz, J. *Scr. Mater.* **2006**, *54*, 1105, Viewpoint set no. 40: Grain boundary engineering.

[138] Zhang, H. R.; Ma, C.; Tian, H. F.; Wu, G. H.; Li, J. Q. *Phys. Rev. B* **2008**, *77*, 214106.

[139] Gillessen, M. *Ph.D. thesis,University of Aachen,* **2009**,

[140] Feng, L.; Liu, E.; Zhang, W.; Wang, W.; Wu, G. *J. Magn. Magn. Mater.* **2015**, *377*, 40.

[141] Alonso, J. A. *Ph.D. thesis,University of Duisburg-Essen,* **2011**,

[142] Sahariah, M. B.; Ghosh, S.; Singh, C. S.; Gowtham, S.; Pandey, R. *J. Phys.: Condens. Matter* **2013**, *25*, 025502.

[143] Liu, Z. H.; Zhang, M.; Cui, Y. T.; Zhou, Y. Q.; Wang, W. H.; Wu, G. H.; Zhang, X. X.; Xiao, G. *Appl. Phys. Lett.* **2003**, *82*, 424.

[144] Qawasmeh, Y.; Hamad, B. *J. Appl. Phys.* **2012**, *111*, 033905.

[145] Entel, P.; Dannenberg, A.; Siewert, M.; Herper, H. C.; Gruner, M. E.; Comtesse, D.; Elmers, H.-J.; Kallmayer, M. *Metall. Mater. Trans. A* **2012**, *43*, 2891.

[146] Biswas, C.; Rawat, R.; Barman, S. R. *Appl. Phys. Lett.* **2005**, *86*, 202508.

[147] Wu, D.-H.; Wang, H.-C.; Wei, L.-T.; Pan, R.-K.; Tang, B.-Y. *Journal of Magnesium and Alloys* **2014**, *2*, 165.

[148] Mahlangu, R.; Phasha, M.; Chauke, H.; Ngoepe, P. *Intermetallics* **2013**, *33*, 27 – 32.

[149] Planes, A.; Mañosa, L.; Ríos-Jara, D.; Ortín, J. *Phys. Rev. B* **1992**, *45*, 7633.

[150] Amari, S.; Mebsout, R.; Mabih, S.; Abbar, B.; Bouhafs, B. *Intermetallics* **2014**, *44*, 26.

[151] Pickett, W. E.; Moodera, J. S. *Phys. Today* **2001**, *54*, 39.

[152] Galanakis, I.; aolu, E. *Appl. Phys. Lett.* **2011**, *98*, 102514.

[153] Priolkar, K. R.; Bhobe, P. A.; Lobo, D. N.; D'Souza, S. W.; Barman, S. R.; Chakrabarti, A.; Emura, S. *Phys. Rev. B* **2013**, *87*, 144412.

[154] Roy, T.; Chakrabarti, A. *J. Magn. Magn. Mater.* **2016**, *401*, 929.

[155] Baral, M.; Banik, S.; Chakrabarti, A.; Phase, D.; Ganguli, T. *J. Alloys Compd.* **2015**, *645*, 112.

[156] Kurtulus, Y.; Dronskowski, R.; Samolyuk, G. D.; Antropov, V. P. *Phys. Rev. B* **2005**, *71*, 014425.

[157] Antonov, V. N.; Harmon, B. N.; Bekenov, L. V.; Shpak, A. P.; Yaresko, A. N. *Phys. Rev. B* **2005**, *71*, 174428.

[158] Carbonari, A.; Saxena, R.; Pendl, W.; Filho, J. M.; Attili, R.; Olzon-Dionysio, M.; de Souza, S. *J. Magn. Magn. Mater.* **1996**, *163*, 313 – 321.

[159] Ziebeck, K.; Webster, P. *Journal of Physics and Chemistry of Solids* **1974**, *35*, 1.

[160] Sasaki, T.; Kanomata, T.; Narita, T.; Nishihara, H.; Note, R.; Yoshida, H.; Kaneko, T. *J. Alloys Compd.* **2001**, *317318*, 406, The 13th International Conference on Solid Compounds of Transition Elements.

[161] van Engen, P.; Buschow, K.; Erman, M. *J. Magn. Magn. Mater.* **1983**, *30*, 374.

[162] Umetsu, R. Y.; Kobayashi, K.; Fujita, A.; Oikawa, K.; Kainuma, R.; Ishida, K.; Endo, N.; Fukamichi, K.; Sakuma, A. *Phys. Rev. B* **2005**, *72*, 214412.

[163] Buschow, K.; van Engen, P. *J. Magn. Magn. Mater.* **1981**, *25*, 90.

[164] Galanakis, I.; Dederichs, P. H.; Papanikolaou, N. *Phys. Rev. B* **2002**, *66*, 174429.

[165] Şaşıoğlu, E.; Sandratskii, L. M.; Bruno, P. *Phys. Rev. B* **2004**, *70*, 024427.

[166] Neumann, K.-U.; Kanomata, T.; Ouladdiaf, B.; Ziebeck, K. R. A. *J. Phys.: Condens. Matter* **2002**, *14*, 1371.

[167] Aduk, S.; Gkolu, G. *J. Alloys Compd.* **2012**, *511*, 9.

[168] Kanomata, T.; Chieda, Y.; Endo, K.; Okada, H.; Nagasako, M.; Kobayashi, K.; Kainuma, R.; Umetsu, R. Y.; Takahashi, H.; Furutani, Y.; Nishihara, H.; Abe, K.; Miura, Y.; Shirai, M. *Phys. Rev. B* **2010**, *82*, 144415.

[169] Brown, P. J.; Bargawi, A. Y.; Crangle, J.; Neumann, K.-U.; Ziebeck, K. R. A. *J. Phys.: Condens. Matter* **1999**, *11*, 4715.

[170] Suits, J. *Solid State Commun.* **1976**, *18*, 423 – 425.

[171] Staunton, J. B.; Gyorffy, B. L.; Poulter, J.; Strange, P. *J. Phys. C: Solid State Phys.* **1988**, *21*, 1595.

[172] Kanomata, T.; Kitsunai, Y.; Sano, K.; Furutani, Y.; Nishihara, H.; Umetsu, R. Y.; Kainuma, R.; Miura, Y.; Shirai, M. *Phys. Rev. B* **2009**, *80*, 214402.

[173] Roy, T.; Chakrabarti, A. *J. Magn. Magn. Mater.* **2017**, *423*, 395.

[174] Kobayashi, K.; Umetsu, R.; Fujita, A.; Oikawa, K.; Kainuma, R.; Fukamichi, K.; Ishida, K. *J. Alloys Compd.* **2005**, *399*, 60.

[175] Meinert, M.; Schmalhorst, J.-M.; Reiss, G. *J. Phys.: Condens. Matter* **2011**, *23*, 036001.

[176] Smith, F. W. *Phys. Rev. B* **1976**, *14*, 241.

[177] Priour, D. J.; Hwang, E. H.; Das Sarma, S. *Phys. Rev. Lett.* **2004**, *92*, 117201.

[178] Noda, Y.; Ishikawa, Y. *J. Phys. Soc. Jpn.* **1976**, *40*, 690.